Au Nanoparticle-PDMS composites and Pd Nanowire Gratings for applications in Nanotechnology

A Thesis submitted in partial fulfillment of the requirements of the degree of

MASTER OF SCIENCE

as a part of the

Integrated PhD programme (in Material Science)

BY

Ritu Gupta

Chemistry and Physics of Materials Unit

Jawaharlal Nehru Centre for Advanced Scientific Research (A deemed University)

BANGALORE, INDIA

(April 2010)

Dedicated in loving memory

To

My Grandmother

Declaration

I hereby declare that this thesis entitled **"Au Nanoparticle-PDMS composites and Pd nanowire gratings for applications in Nanotechnology"** is an authentic record of research work carried out by me under the supervision of Prof. G.U. Kulkarni at the Chemistry and Physics of Materials Unit, Jawaharlal Nehru Centre for Advanced Scientific Research, Bangalore, India.

In keeping with the general practice of reporting scientific observations, due acknowledgement has been made wherever the work described here has been based on the findings of the other investigators. Any oversight due to error of judgment is regretted. I authorize Jawaharlal Nehru Centre for Advanced Scientific Research to lend this thesis to other institutions or individuals for the purpose of scholarly research.

Date :

Bangalore, INDIA Ritu Gupta

Certificate

Certified that the work described in this thesis titled **"Au Nanoparticle-PDMS composites and Pd nanowire gratings for applications in Nanotechnology"** has been carried out by *Ms. Ritu Gupta* at the Chemistry and Physics of Materials Unit, Jawaharlal Nehru Centre for Advanced Scientific Research, Bangalore, India under my supervision and that it has not been submitted elsewhere for the award of any degree or diploma.

Date:
Bangalore, INDIA

Prof. G.U. Kulkarni
(Research Supervisor)

Table of Contents

Acknowledgements

I express my deep sense of gratitude and profound feeling of admiration to my mentor and thesis supervisor Prof. G. U. Kulkarni. I sincerely thank him for guiding me at this early stage of research. I am deeply grateful for his patience, words of advice and for sharing his own experiences with me. He has been caring and understanding like a guardian and friend. His style of working on various scientific problems, enthusiasm and creative thinking has influenced and always inspired me.

I thank Prof. C.N.R. Rao for his encouragement and introducing to the visitors. His mere presence is a source of inspiration.

It gives me pleasure to thank Dr. Adina Scott, Purdue University with whom, I collaborated. It had been a great learning experience while working with her.

I also thank Dr. Rajesh Ganpathy (ICMS, JNCASR) with whom I got an opportunity to work on rheology and Mansa for doing rheological measurements. I thank Prof. Tapas Kundu, Selvi and Yogesh (MBGU, JNCASR) for bio-related experiments and useful discussions.

I thank Prof. Sundareshan and Nitesh for trying out magnetic measurement. I also thank Prof. Hemlatabalram and Sonia for antibacterial activity related experiments.

I thank all the faculty members of JNCASR: Prof. Chandrabhas, Dr. Eswaramoorthy, Prof. K.S.Narayan, Prof. Shivaprasad, Dr. Sundareshan, Dr. Tapas Maji, Dr. Subi George, Dr. Govindraju, Dr. Govindraj, Prof. U. Waghmare, Dr. S.K. Pati, Dr. Balasubhramaniam and Prof. S. Narashiman for the courses that have been extremely beneficial.

Special thanks to Prof. Ranganathan for sharing his views and ideas on historical science along with course work.

I am grateful to my present lab mates Radha, Narendra, Dr. Abhay, Mallikarjun and Gangaiah for their cooperation, help in experiments, useful discussions and cheerful company. I had a chance of interacting with my past labmates for short period: Dr. Reji, Dr. Ved, Dr. Karthick, Dr. Vijay and Dr. Bhuvana. I thank them for their help in experiments, words of encouragment and sharing their past experiences. I also thank Dr. Angappane for his friendly advices and help.

I thank Mr. Srinath, Mr. Srinivas and Mr. Srinivas Rao for the technical assistance. I acknowledge Ms. Vanita, Sunil and Moorthy for timely help and friendly attitude.

I am very thankful to Selvi (SEM), Mrs.Usha (TEM), Dr. Basavaraja (AFM), Mr. Anil (XRD) and Mr.Vasu (UV and PL) for their constant help.

I thank the staff of academic and administrative section in JNCASR for their assistance. I also thank the library staff for their help. I am thankful to the computer lab staff. I thank DST for financial assistance.

Int. Phd batchmates: Soumik, Piyush, Bivas, Abhay, Nitesh, Shekhar, Nisha, Urmi, and Vini, I thank all for enjoyable company in and outside classroom, useful discussions, assignments, birthday treats and many more fun-filled moments. I also thank all other friends in JNC including Dhiraj, Dinesh and Sandeep for joyous company. I also thank my friend, Gaurav for being most understanding and daily sending me papers from literature.

I wish to convey my heartiest thanks to Dr. Subba Rao, Dr. Archana, Dr. Yogesh (IISc) and Dr. Dharmpal (Ramaiah Hospital) who helped me immensely. Special thanks to Mr. Suresh, Shibu and Parvati aunty in hostel for helping me in daily activities during my hand fracture.

I also express my gratitude to Dr. Rakesh, Dr. Pragati and Eishu, without their support I would have not been able to come in this field. They always shared my problems, happiness and encouraged me to do well.

I am grateful to Mrs. Kulkarni for providing me homely atmosphere, warmth and care.

I also thank Teju and Poorna for bringing some happy moments, fun and laughter.

I would like to conclude by extending my deepest gratitude to my mother. Without her unconditional love and support, I would have not been able to complete this degree. I owe a lot to my father, brother, sister and family.

Synopsis

The thesis titled **'Au Nanoparticle-PDMS composites and Pd nanowire gratings for applications in Nanotechnology'** is divided in 2 broad parts.

Part 1 consists of synthesis, characterisation, properties and applications of Au nanoparticle-poly(dimethylsiloxane) (AuNPs-PDMS) composite. It is divided into sections.

Section 1.1 deals with synthesis and characterization of AuNPs-PDMS composite in different forms namely gels, films and foams. The particle size of the nanoparticles and distribution can be varied depending on the synthesis condition.

In Section 1.2, the rheology of AuNPs-PDMS composite gel is studied to understand its linear viscoelastic properties. For this purpose, AuNPs-PDMS gels were prepared by varying the concentration of precursor and temperature condition while synthesis.

Section 1.3 deals with the use of AuNPs-PDMS composite in the form of film and foam for waste water treatment particularly, for the removal of organic solvents and odorous contaminants. The material is tested for efficiency as well as reusability from thioanisole as model example.

Section 1.4 is focussed on biological application of the composite for cell adhesion and drug delivery. The cellular interaction of the AuNPs-PDMS composite is studied along with the possibility of releasing molecular species (R6G) held on Au nanoparticles surface in PDMS matrix.

Section 1.5 involves metallization of PDMS by further growth of Au nanoparticles with connected granular film.

Section 1.6 covers synthesis and characterization of AgNPs-PDMS systems and provides an insight into possible applications.

Part 2 is a study of metal nanowire gratings for optical diffraction based sensing applications. The Pd nanowires are fabricated by micromolding technique using Pd hexadecyl thiolate as organic precursor. The grating height and width is optimized by electroless deposition of Cu on Pd to achieve high diffraction efficiency.

List of Abbreviations

AuNPs	Au Nanoparticles
AuNPs-PDMS	Au nanoparticles-poly(dimethyl siloxane)
AFM	Atomic Force Microscopy
CD	Compact Disc
DE	Diffraction Efficiency
DMEM	Dulbecco's modified Eagle medium
DMSO	Dimethyl sulfoxide
ED	Electron Diffraction
FESEM	Field Emission Scanning Electron Microscopy
FTIR	Fourier Transform Infrared
G’	Storage Modulus(Pa)
G’’	Loss Modulus (Pa)
G*	Complex Modulus
HRTEM	High Resolution Transmission Electron Microscopy
HDT	Hexadecanethiol
LB	Lysogeny broth (media for bacterial growth)
MCL	Maximum Concentration Limit
OP	Optical Profilometry
PBS	Phosphate Buffer Solution
PDMS	Poly(dimethylsiloxane)
PL	Photoluminescence
R6G	Rhodamine 6G
SEM	Scanning Electron Microscopy
STEM	Scanning Tunneling Electron Microscopy
THF	Tetrahydrofuran
XRD	X-Ray Diffraction

List of figures

Figure 1.2.6 Amplitude sweep for plain PDMS before crosslinking.

Figure 1.2.7 (a) The strain amplitude sweep at constant frequency of 10 rad/s for strain varying from 0.01% to 1000% for gel samples **A** and **D** as examples.(b) The storage and loss moduli of different gel samples (**A, B, C, and D**).

Figure 1.2.8 (a) The strain amplitude sweep at constant frequency of 10 rad/s for strain varying from 0.01% to 100% for different gel samples.(b) The storage and loss moduli of the AuNPs-PDMS gels prepared at different temperatures.

Figure 1.3.1 (a) Optical photographs of AuNPs-PDMS as such (above) and after swelling with toluene (below). (b) Deswelling behavior of AuNPs-PDMS foam, PDMS foam and PDMS film in toluene with time.

Figure 1.3.2 Deswelling of PDMS and AuNPs-PDMS foams with time for (a) DMSO and (b) THF.

Figure 1.3.3 (a) The calibration curve for toluene. (b) UV-visible spectra for solutions of different concentrations of toluene in water.

Figure 1.3.4 UV-visible spectra for removal of toluene from water by varying amount of (a) PDMS and (b) AuNPs-PDMS composite.

Figure 1.3.5 (a) UV-visible spectra of contaminated water (500 ppm toluene) showing reduction in intensity of toluene modes after treatment with 200 mg of PDMS and AuNPs-PDMS foam. The spectra of treated water samples are multiplied by factor of 10 for clarity. (b) Concentration of saturated and 100 ppm (inset) toluene in water after treatment as a function of amount of AuNPs-PDMS foam and PDMS foam used.

Figure 1.3.6 UV-visible spectra of (a) Na_2S solution in water (0.6 mM) (c) thiophenol (0.128 mM) and (e) Thioanisole (0.10 mM)) recorded after different time intervals. The inset in each plot shows the decrease in absorbance with time for treated samples along with blank solution absorption taken after 12 hrs. UV-Visible spectra from AuNPs-PDMS films dipped in (b) Na_2S and (d) thiophenol and (f) thioanisole show the interaction of these chemicals with the nanocomposite.

Figure 1.3.7 (a) Removal of thioanisole from water by AuNPs-PDMS composite after repeated cycles. (b) Average removal efficiency of 23.5% by thioanisole removal of water in 1 hr from 100 ml of 85 μM thioanisole using 0.9 g of AuNPs-PDMS film for 7 different cycles.

Figure 1.3.8 Schematic illustration of how the AuNPs-PDMS composite material works. A certain mass of AuNPs-PDMS composite is stirred in the contaminated water. The organic molecules are absorbed by AuNPs-PDMS composite and released by heating for repeated cycles.

Figure 1.4.1 (a) Schematic illustrating synthesis procedure for AuNPs-PDMS film. (b) UV-visible spectra corresponding to two different samples.

Figure 1.4.2 STEM images of AuNPs-PDMS gel synthesized with (a) 2 mM and (c) 0.2 mM of $KAuCl_4$ .The corresponding SEM images in (b) and (d) respectively.

Figure 1.4.3 The optical Images of HeLa cells taken 24 hrs after incubation at 37 ºC, 5% CO_2 environment, DMEM medium. (a) poly-L-lysine, (b) PDMS, (c) and (d) AuNPs-PDMS

composite layers prepared with 0.2 and 2 mM of Au precursor respectively. Inset (right) in all images shows the magnified image of the morphology of cells.

Figure 1.4.4 Bright field (left), dark field (middle) and fluorescence (right) microscopy images of cells seeded on different layers for 24 hrs, (a) poly-L-lysine, (b) PDMS, (c) and (d) AuNPs-PDMS composite layers prepared with 0.2 and 2 mM of Au precursor respectively.

Figure 1.4.5 Bright field (left), dark field (middle) and fluorescence (right) microscopy images of cells seeded on different layers for 48 hrs, (a) poly-L-lysine, (b) PDMS, (c) and (d) AuNPs-PDMS composite layers prepared with 0.2 and 2 mM of Au precursor respectively.

Figure 1.4.6 (a) Trypan blue cell viability assay of HeLa cells incubated with PDMS and AuNPs–PDMS composite of different AuNPs loading. Assay is done after 24 and 48 hrs and the cells were counted using neubauer's chamber. Data are averages plus standard deviations for two independent experiments.

Figure 1.4.7 Schematic of R6G incorporation in AuNPs-PDMS nanocomposite and release using HDT.

Figure 1.4.8 (a) UV-visible absorption and (b) PL emission spectra from AuNPs-PDMS and plain PDMS films upon adsorption R6G.

Figure 1.4.9 (a) UV-visible absorption and (b) PL emission (at 490 nm excitation wavelength) from HDT solution in toluene on release of R6G. Both UV-visible and PL spectra are multiplied by 7 and 2 respectively, relative to Figure 1.4.8 for clarity.

Figure 1.5.1 (a) Synthesis of Au-PDMS metallised film, (b) the metallised bottom, surface**.** (c) the top surface resembling pristine AuNPs-PDMS composite.

Figure 1.5.2 (a) The optical microscope image showing different regions of partially folded flexible Au-PDMS metallised film transferred on glass from top surface of aq. media. (b) The optical profilometric measurement for thickness determination.

Figure 1.5.3 SEM image of (a) the metallised surface with magnified view in the inset and (b) the pristine surface of the film.

Figure 1.5.4 XRD pattern from the metallised face of PDMS corresponds to polycrystalline Au.

Figure 1.5.5 The I-V characteristics from the metallised surface.

Figure 1.5.6 The UV-visible spectra of Au/PDMS film (a) in the transmission mode (b) in the reflectance mode.

Figure 1.5.7 The contact angle of a water droplet (10 µl) placed over (a) pristine surface and (b) metallised surface.

Figure 1.5.8 (a) Schematic procedure for patterning of metallised AuNPs-PDMS film. (b) The optical microscope image of the patterned surface at 100X magnification.

Figure 1.6.1 UV-visible spectra of the Ag-PDMS gel prepared with aq. $AgNO_3$ solution at room temperature by stirring at different temperatures.

Part 1

AuNPs-PDMS Composites: Synthesis, Properties & Applications*

Summary

The synthesis and characterization of Au nanoparticles-poly(dimethylsiloxane) (AuNPs-PDMS) nanocomposites is presented. The nanocomposite is prepared in different forms - gels, foams, and films with distinct properties. The synthesis is a simple in-situ process, carried out entirely in the aqueous medium and therefore it is a green process. $KAuCl_4$ is used as the Au precursor. PDMS acts as both reducing and stabilizing agent. The process offered a facile control over loading of Au nanoparticles with size in the range of 5-50 nm. The mechanical properties could be controlled by choosing appropriate temperature and stirring conditions. A study of the rheological properties of the nanocomposites has also been carried out. The nanocomposites prepared this way, exhibit novel properties due to the nanoscale size of the Au particles coupled with the solid-solution nature of the PDMS matrix. Extensive use is made of the size and environment-dependent optical properties of Au nanoparticles to study the behavior of the composite in different chemical environments. It is seen that the nanoparticles are held robustly within the PDMS while still being chemically accessible to molecules with high solubility in PDMS. The potential applications of the nanocomposites in water treatment, cell adhesion and drug delivery, have also been investigated. The study was extended to Ag nanoparticles containing nanocomposites as well.

*A paper based on this study is accepted for publication in Journal of Macromolecular Physics and Chemistry (2010).

1.1 Synthesis and Characterization of AuNPs-PDMS composites

1.1.1 Introduction

A composite is made of two or more constituent materials with significantly different physical or chemical properties which remain separate and distinct. A nanocomposite[1] is one where grain/domain size of constituent material is in nanometric range.The nanocomposite differs from conventional composite material in that the constituents are thoroughly mixed down to nanometric range with very high surface to volume ratio.[2] Thus, effective area of the interface between the two constituents is typically at least an order of magnitude greater. Importantly, the interface is usually endowed with new properties foreign to either of the components. The nanocomposites with different combinations of nanomaterials-nanoparticles, silica and clay particles, fullerenes, carbon nanotubes, graphene, polymers etc. are well known.[3] Some of these composites such as AuNPs-graphene,[4,5] CNT-polymers,[6] Ag nanoparticles with PVP[7] etc. have recently been studied. Among these, nanocomposites with polymers as matrix have been popular.[8] In polymer nanocomposites, properties related to local chemistry, polymer chain mobility, conformation, degree of chain ordering or crystallinity can be made to vary significantly.

Noble metal nanoparticle embedded polymer composites are of great interest because the advantageous properties of the nanoparticles can be exploited for a wide variety of applications while the polymer matrix holds and stabilizes the nanoparticles.[9] Using this strategy, it is possible to develop new materials with fine control over properties.[2,10] There are many reports of metal nanoparticle-polymer composites which make use of the unique optical properties of nanoparticles to obtain effects such as wavelength-tunable light attenuation, chemically-tunable luminescence, surface plasmon resonance and lasing.[3-6] Besides playing a stabilizing role, polymers in many cases impart additional desirable properties to the nanocomposite. Opto-mechanical actuators and opto-thermal devices which utilize the photothermal properties of Au nanoparticles coupled with the elastic and thermal properties of polymers have been demonstrated.[11,12] Conductive nanoscale patterns have been formed using Ag/polystyrene nanocomposite as an electron beam resist and conductive micron scale features have been patterned directly from metal powder-loaded polymer.[13,14]

Polymeric nanocomposite materials with novel electrical properties such as the tunable dielectric function and tunable conductivity can be engineered by the controlled inclusion of nanoparticles.[15,16] Cell adhesion and patterning, bio-electrochemical sensing, and antimicrobial materials combine specific metal nanoparticle properties with the bio-compatible nature of polymers, leading to advanced bio-functional materials.[17-19]

The choice of polymer thus plays an important role in determining the functionality of the nanocomposite. In this context, PDMS which consists of $-Si(OCH_3)$ repeating units, is an attractive polymeric matrix due to its many favorable properties[20] such as chemical inertness, biocompatibility, mechanical flexibility and stability, high dielectric constant and breakdown field, optical clarity in the visible and ultraviolet region and importantly, the ease of processing. It has applications in many fields including microfluidics,[21] biomedical implants and devices,[22,23] chemical separation,[24] and microstructure fabrication.[25] Another important feature of PDMS is its solid solution nature and high sorption ability for a range of organic molecules.[26]

The Au nanoparticle system is a good candidate for nanocomposite formation. The literature on Au nanoparticles is rich and abound with examples relating interesting properties to potential applications.[27,28] Au nanoparticles are of interest for electronic, optical, biomedical, and sensing applications because they have size and shape-tunable optical properties, their surfaces are not easily oxidized, and they are easily functionalized by a variety of methods to achieve chemical or biological specificity. The tendency of Au nanoparticles to form assemblies with different ligands such as thiols,[29] ability to conjugate with biomolecular systems, optical and photothermal properties[30] associated with surface plasmon resonance enables it to exhibit several promising applications. Thus, the classical examples include Au nanoparticles for cancer treatment,[31] drug delivery, bioimaging and cellular imaging,[32] biosensing and catalysis.[33,34] The Au nanoparticle-oligonucleotide complexes are used as intracellular gene regulation agents to control the protein expression in cells.[35] Only a few recent examples can be found in literature on the synthesis of AuNPs-PDMS composite inspite of their individual interesting properties and applications discussed above. During the last year, in-situ synthesis of Au nanoparticles in PDMS leading to nanocomposites has been realised. Chen et al.[36] first reported the preparation of AuNPs-PDMS films where the curing agent itself acts as the reducing agent. In this case, $HAuCl_4$ is reduced at the surface of cured PDMS in aqueous medium in multistep over a period of several hours to days. Ajayan and

co-workers[37] synthesized Au, Ag, and Pt nanoparticle-PDMS composite films by introducing the metal salt in organic solvents with the uncured PDMS and allowing the nanoparticles to reduce during curing. The Au nanoparticles formed on the surface of PDMS surface showed a broad plasmon peak. The resulting material shows enhanced Young's modulus and exhibit antibacterial properties.

1.1.2 Scope of the Investigation

There are many possible ways for the preparation of nanoparticle based composites.[38] The most common approach involves dispersion of premade nanoparticles inside the polymer.[39] Another technique involves polymerizing the matrix around a metal nanocore by using chemically compatible ligands or polymeric structures. The simplest approach is the in-situ preparation of metal nanoparticles within the polymer matrix by the reduction of a metal salt solution. However, one of the aspects which remain still challenging is the homogeneous dispersion and stability of metal nanoparticles in the matrix. Secondly, the capping agent used to prevent agglomeration of nanoparticles can affect the polymer matrix adversely. Therefore, efforts are in progress in search of new methods which can stabilize metal nanoparticles inside the polymer matrix while attending to such issues. The methods followed in recent literature are novel but still has certain drawbacks. Chen et al.[36] first polymerized the PDMS matrix followed by the synthesis of Au nanoparticles over the surface by reduction of metal salt solution in aqueous medium involving several days. The Au plasmon peak was observed to be weak and broad. Ajayan et al.[37] followed in-situ preparation method for synthesis of Au nanoparticles PDMS composite but the reaction required an organic media.

In this study, a single step in-situ reduction method is developed which uses only plain water as the medium. The method offers a good control over the particle size and loading. In addition, the nanocomposite may be obtained in the form of a gel, foam, or a patterned flexible thin film.

1.1.3 Experimental

Materials

A commercially available PDMS kit (Dow Corning, Sylgard 184), $KAuCl_4$ (Aldrich, 98%), double distilled water and sulfur-free toluene (99%) were used in the synthesis.

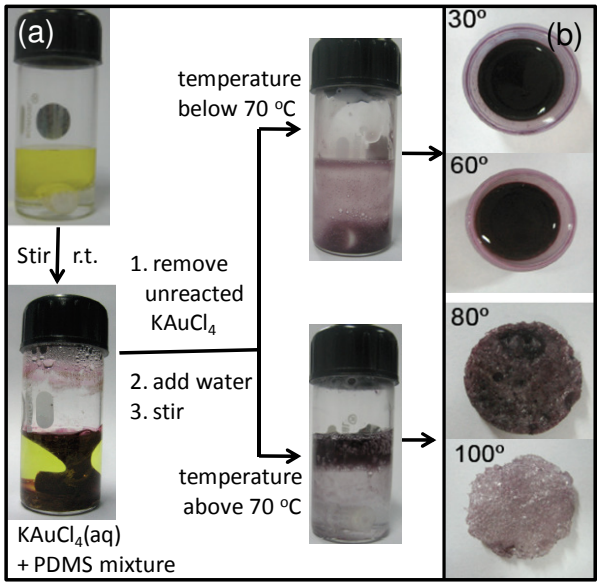

Figure 1.1.1 AuNPs-PDMS nanocomposites: (a) Optical photographs of the vial containing PDMS mixture in $KAuCl_4$ (aq., 20 mM) before (above) and after stirring (below) at room temperature for 30 min. Optical photographs of the vials following gel (above) or foam (below) formation. (b) Optical photographs of gels formed at 30 °C and 60 °C and foams formed at 80 °C and 100 °C.

Synthesis of Au nanoparticles-PDMS composite

The AuNPs-PDMS composite can be synthesized into versatile forms such as gel, film and foam. The procedure for synthesis is illustrated in **Figure 1.1.1**. An uncured PDMS mixture was prepared by mixing thoroughly the pre-polymer and the curing agent in a 10:1 volume ratio. The mixture was taken in a glass vial containing 20 mM aqueous $KAuCl_4$ solution in a 200:1 (m/v) ratio and stirred below 70 ºC for 2 hrs to form gel. At lower temperatures, the curing of the elastomer is extremely slow resulting in gel formation. Thus formed gel can be cast into a mould or coated as a film and cured. The air bubbles are removed by exposing to vacuum and subsequently heating at 100 ºC for 48 hrs. Foam can be synthesized using a similar process by stirring PDMS and $KAuCl_4$ (aq.) below 70 ºC for up to 45 min and

arresting the reaction by decanting off the unreacted $KAuCl_4$ solution and rinsing the remaining AuNPs-PDMS mixture with copious amounts of water. When the mixture is further stirred and heated in plain water at temperatures above 70 ºC, curing of the elastomer is possible. The AuNPs-PDMS mixture in this case floats at the aqueous surface and cures into a sponge-like phase as seen from the bottom part of **Figure 1.1.1**. Instead of loading Au at lower temperatures and further heating in plain water, foams can also be realized by directly heating the PDMS and $KAuCl_4$ between 70 ºC and 100 ºC while stirring.

Characterization Techniques and Methods

Several spectroscopic and microscopic techniques have been used to characterize the prepared samples reported in this thesis. In the following paragraphs, the details of instruments used and the sample preparation methods are described.

UV-visible absorption measurements were carried out at room temperature with a Perkin Elmer model Lambda 900 UV/vis/NIR spectrometer. The AuNPs-PDMS films were directly pasted with the help of double sided tape. The UV-visible spectra corresponding to foams were obtained by clamping it in between two pieces of glass slides. The absorption spectra from AuNPs-PDMS gel samples were recorded by dissolving it in toluene.

SEM images were recorded with a FEI Nova NanoSEM 600. STEM (scanning transmission electron microscopy) and low vacuum imaging were performed on the same instrument using a STEM and helix detectors respectively. The samples for STEM were prepared by drop-casting the solution of the gel dissolved in toluene on a carbon-coated grid.

Transmission electron microscopy (TEM) measurements were carried out with a JEOL-3010 instrument operating at 300 kV (λ = 0.0196 Å) and electron diffraction (ED) patterns were collected at a camera length 20 cm (calibrated with respect to the standard polycrystalline Au thin film).The samples prepared for STEM were also used for transmission electron microscopy .

1.1.4 Results and Discussion

AuNPs-PDMS composite foam

Foam can be characterized by the degree of compressiblity. In **Figure 1.1.2a**, an example is shown AuNPs-PDMS nanocomposite foam between two glass slides. Compression is achieved using metal clips to apply a nominal force. The foam shown in **Figure 1.1.2a** was characterized using optical microscopy and SEM. We have observed that the foam contained large open pores in the size range, 100 µm-1 mm which are interconnected across the entire volume of the sample. One such pore is shown in the optical image in **Figure 1.1.2b**. The SEM image of the foam in **Figure 1.1.2c** clearly reveals the presence of smaller pit-like structures, typically in the range, 10-100 µm all over the surface. Unlike the large open pores, these pits are essentially closed pores.

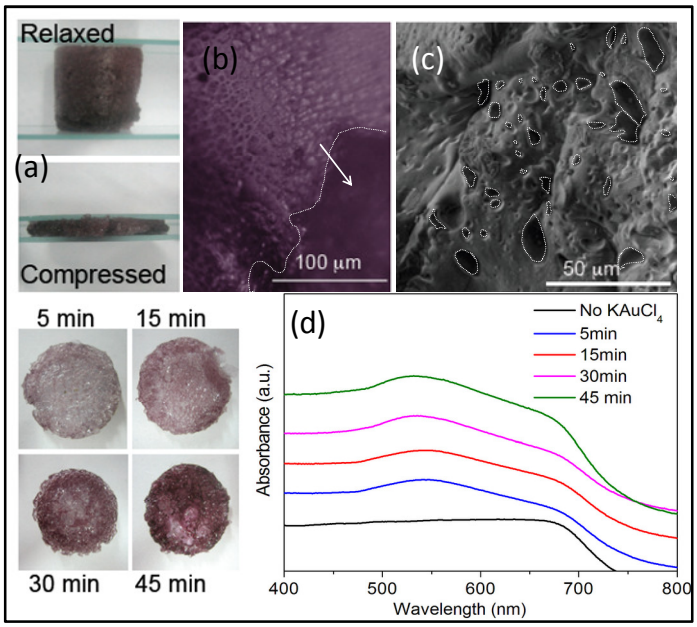

Figure 1.1.2 (a) Optical photographs depicting a cylindrical foam between two glass slides, compressed using metal clips. (b) high resolution (false color) optical micrograph and (c) SEM micrograph illustrating microporous nature of the foam prepared by 20 mM $KAuCl_4$ at 70 °C. (d) Optical photographs of AuNPs-PDMS foams formed by varying the pre-stirring time with 20 mM $KAuCl_4$. The corresponding UV-visible spectra obtained in the reflectance mode. The spectra are laterally shifted for clarity.

Thus the foam exhibits two different microstructures which are relevant for adsorption. In addition, the embedded Au nanoparticles themselves offer another active interface. In the

case of foams (**Figure 1.1.2d**), the visible intensity of the foam colour and the measured intensity of the Au plasmon peak at 534 nm in the UV-visible spectrum increase with increasing stirring time during synthesis (**Figure 1.1.2d**). This implies that Au nanoparticle loading in the foam increases with increasing stirring time. However, high resolution imaging to examine the particle morphology and loading was not possible because of difficulty in sample preparation for imaging. Foams obtained directly from the Au precursor solution (with plain water and no heating) are found to have a non-uniform distribution of nanoparticles with an excess of Au particles at the surface because $KAuCl_4$ continues to reduce at the surface even after the PDMS curing process almost ended. The nanoparticle concentration can be controlled by varying the temperature. At higher temperatures, the PDMS cures into a solid very quickly and does not allow much Au incorporation whereas at lower temperatures, there is more time for Au to reduce and get into the matrix.

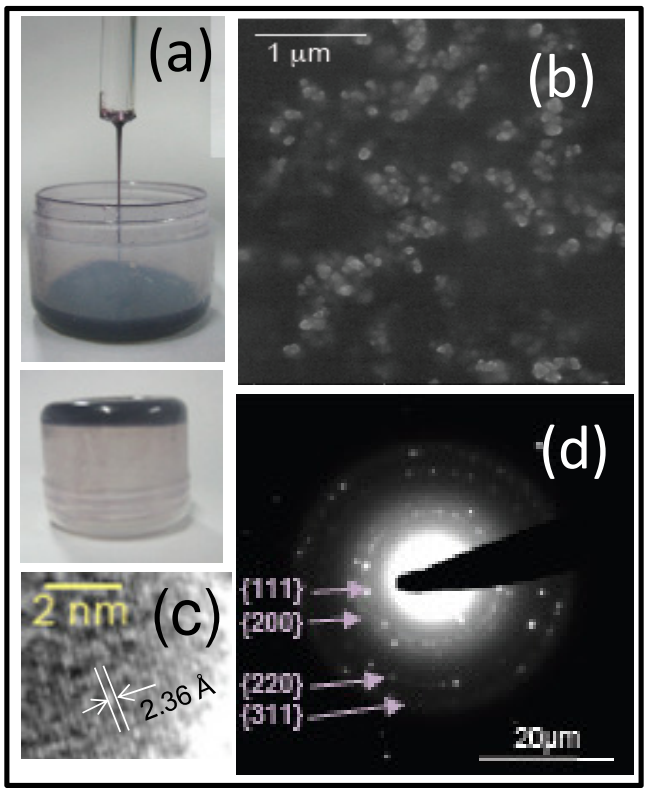

Figure 1.1.3 (a) Optical photographs illustrating the viscous nature of the AuNPs-PDMS gel. AuNPs-PDMS gel dissolved in toluene characterized using (b) STEM (c) HRTEM and (d) ED. The line spacing in (c) corresponds to d (111) of Au.

AuNPs-PDMS composite gel

AuNPs-PDMS gels were characterized using a variety of microscopic techniques (**Figure 1.1.3**).The STEM image shows that the particles are polydisperse with a size range of 5-50 nm as shown in **Figure 1.1.3b**. Lattice fringes in the HRTEM as shown in **Figure 1.1.3c** and the ED pattern in **Figure 1.1.3d** confirm the crystalline nature of the nanoparticles. The particles are seen in the size range of 20-50 nm and the particle density was calculated to be ~ 630 ± 10 μm^{-2} from the STEM image. In the case of gels, the particle loading can be controlled by varying either temperature, concentration of the precursor or the stirring time.

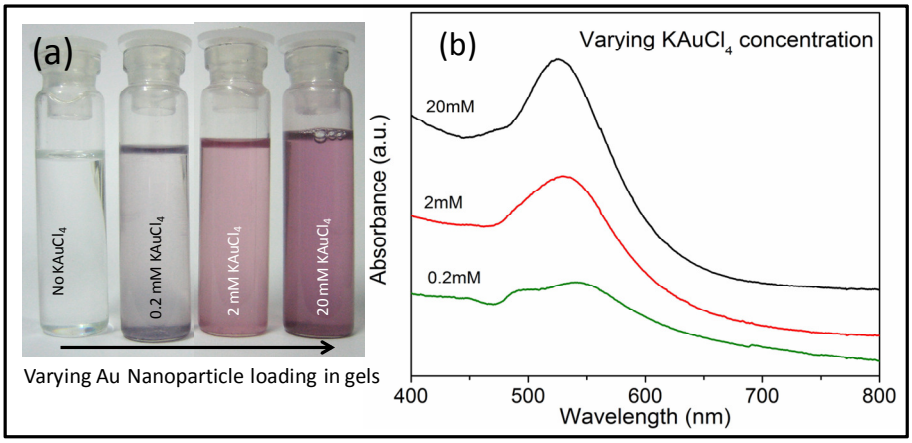

Figure 1.1.4 (a) Optical photographs of vials containing AuNPs-PDMS gel solutions in toluene (10mg/mL) obtained with different concentrations of $KAuCl_4$.(b) The corresponding UV-visible spectra (recorded in transmission mode) are also shown.

Variation in the concentration of $KAuCl_4$

The gels of different type are prepared by varying the concentration of $KAuCl_4$ precursor during synthesis keeping a constant stirring time of 2 hrs at room temperature. Higher precursor concentrations attribute more intense color to the resulting gel and hence to its solution as well (**Figure 1.1.4a**). The UV-visible spectrum from the 20 mM preparation exhibits a distinct peak around 534 nm due to Au surface plasmon absorption. This observation corroborates well with particle size obtained from electron microscopy (see **Figure 1.1.3b**). For lower precursor concentrations, not only the absorption peak intensity is diminishing and its position slightly red-shifted (see **Figure 1.1.4b**) but also is seen a

shoulder feature at ~ 500 nm. These spectral features can be explained as due to the changes in the local environment, size or shape of the nanoparticles.[28]

The AuNPs-PDMS gel synthesis has also been tried with $HAuCl_4$ (**Figure 1.1.5)** in place of $KAuCl_4$ under similar heating and stirring conditions**.** The gel obtained exhibits somewhat different color. The plasmon peak showed a red shift of ~ 4 nm (538 nm) as shown in **Figure 1.1.5a**. The Au nanoparticles are polydisperse in nature with size between 2-80 nm (**Figure 1.1.5b**). The lattice fringes are faintly visible in the HRTEM image as seen in **Figure 1.1.5c**. The ED pattern shows that particles are crystalline in nature with fcc structure (**Figure 1.1.5d**).

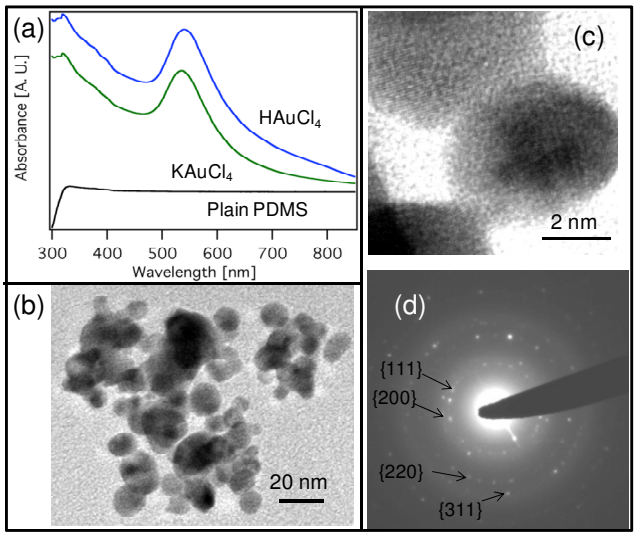

Figure 1.1.5 (a) UV- visible spectra of AuNPs-PDMS gels synthesized using 20 mM aq. $HAuCl_4$ and aq. $KAuCl_4$ solutions at 55 ºC. (b) TEM and (c) HRTEM image along with (d) ED pattern corresponding to AuNPs in PDMS.

Variation in temperature

Instead of preparing at room temperature, the gels have also been obtained by stirring PDMS mixture with the metal salt solution at different temperatures, 36 ºC, 46 ºC and 56 ºC, respectively. The size and loading of AuNPs is therefore varied (**Figure 1.1.6).** The UV-visible absorption spectra of the different gels are shown in **Figure 1.1.6a**. At room temperature of 26 ºC, the particles are seen uniformly distributed over the PDMS matrix with size of particles in the range of 6-10 nm as seen in STEM image in **Figure 1.1.6b**. The

particle size increased with increasing temperature of synthesis. The particles are found to be 30-50 nm in size for the gel sample prepared at 56 ºC (see **Figure 1.1.6c**).

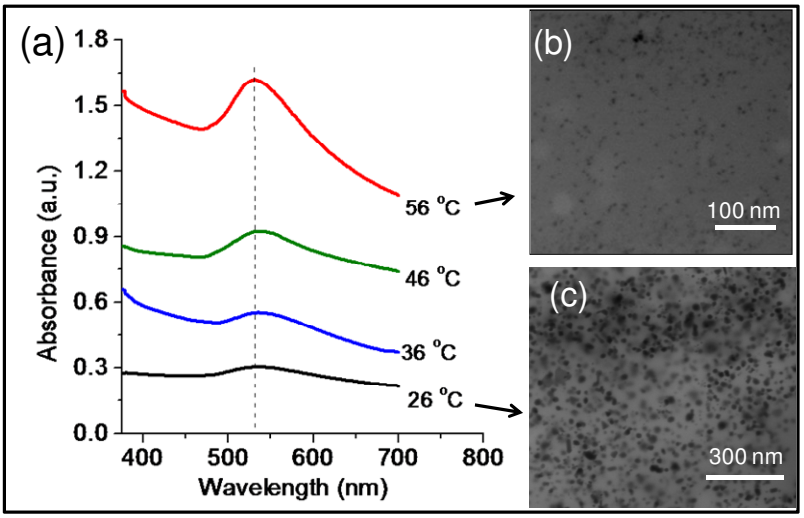

Figure 1.1.6 (a) UV-visible spectra of the AuNPs-PDMS gel samples prepared at different temperatures of 26 °C, 36 °C, 46 °C and 56 °C with 1 mM $KAuCl_4$ precursor. The STEM image corresponding to sample prepared at (b) 26 °C and (c) 56 °C.

AuNPs-PDMS films

The gel can be cross-linked by heating in air to 60 ºC for 6 hrs resulting in a flexible film. In **Figure 1.1.7**, is shown a SEM image of a cured film patterned by molding using a compact disk (CD) as master. As seen from the figure, the patterned film is optically diffracting in the transmission mode while at the same time, flexible.

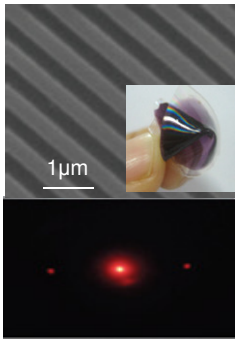

Figure 1.1.7 SEM image of a patterned AuNPs-PDMS film. A photograph of a patterned film hand twisted to bring out the diffracting colors. Below is the optical diffraction pattern obtained in the transmission mode using a 650 nm diode laser.

The AuNPs-PDMS films were tested for stability after high temperature treatment and robustness in different chemical environments as shown in **Figure 1.1.8**.

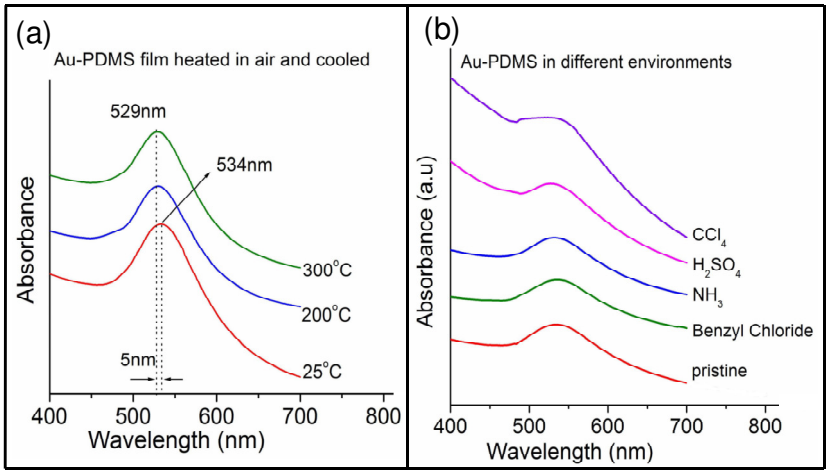

Figure 1.1.8 UV-visible spectra of AuNPs-PDMS films after (a) heating to different temperatures for 1 hr and cooling back to room temperature and (b) exposure to various concentrated acids, bases and chlorocarbons.

When a AuNPs-PDMS film is heated upto 300 °C in air, the surface plasmon peak position remains nearly unaltered (blue shifted by ~ 5 nm) (**Figure 1.1.8a**). PDMS itself is known to be minimally affected at such temperatures. In **Figure 1.1.8b**, the plasmon peak remains nearly the same following treatment with acids, bases and chlorocarbons. The near constancy in the plasmon peak intensity and position also implies that the particles are prevented from leaching into the media.

1.1.5 Conclusions

In conclusion, we have presented a simple, novel, green route for the synthesis of various AuNPs-PDMS composite materials. This technique involves in-situ reduction under mild conditions: stirring aqueous $KAuCl_4$ along with PDMS mixture at room temperature. The left over precursor is reusable in subsequent preparations as there is no other undesired product. The method offers a good control over loading of Au nanoparticles with size in the range of 5-50 nm. Gels, foams and thin films with controlled nanoparticle concentration can be formed using this one-pot method by simple variation in process parameters such as precursor concentration, reaction temperature and time.

1.2 Rheological Properties of AuNPs-PDMS gel

1.2.1 Introduction

PDMS consists of siloxane repeating units, $-Si(OCH_3)_n$, that undergo crosslinking process aided by the curing agent resulting in an elastomer.[20] The process of formation is shown in **Figure 1.2.1**. The curing agent contains Si−H bonds which participate in the crosslinking process. The cross condensation reaction takes place across the vinyl groups present in the prepolymer.

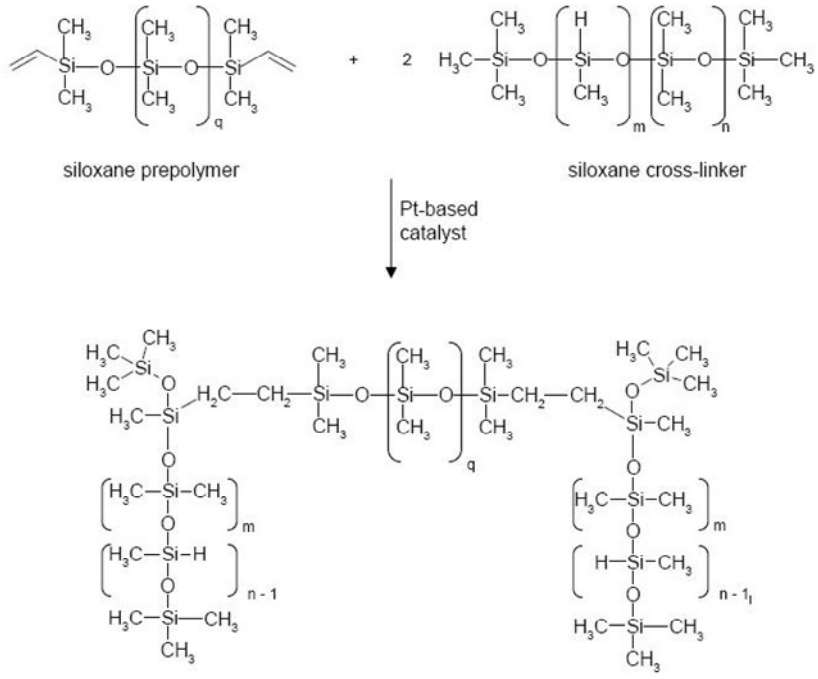

Figure 1.2.1 The crosslinking reaction between PDMS prepolymer and curing agent as crosslinker.[40]

In the Si−O−Si backbone, each Si carries two methyl groups. These chains are highly flexible due to relatively long skeletal bonds (1.64 Å), large bond angles and low torsional barrier about the Si−O bonds.[41] A single PDMS strand has a molecular weight of nearly 1,200 Daltons (amu). The molecular weight for PDMS can be a few hundred Daltons to several hundreds of thousands depending on the degree of crosslinking.[42] PDMS polymer matrix

possesses a low glass transition temperature of -127 ºC with excellent thermal stability. Thus, PDMS should form an interesting rheological system.

Rheology[43] is the study of flow and deformation of materials. A material can be either solid or fluid. A material is purely elastic, if deformation strain increases linearly with increasing applied stress. This is the feature of an ideal solid. When any form of shear strain is applied on the sample, the shear stress responds instantly and is proportional to strain as:

$$\sigma = G\gamma \qquad \text{..... (1)}$$

where σ is the stress due to applied strain γ and G is shear modulus

On the other hand, for a purely viscous material, the strain is proportional to the shear strain rate as:

$$\sigma = \eta \dot{\gamma} \qquad \text{..... (2)}$$

where η is the shear viscosity.

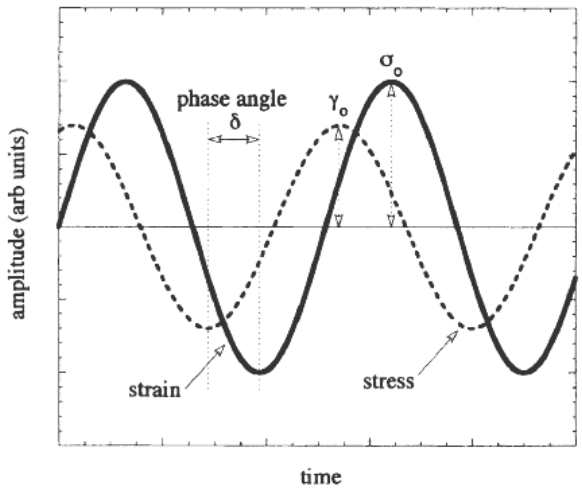

Figure 1.2.2 An oscillating strain and the stress response for a viscoelastic material.[44]

This is the feature of a fluid. However, certain types of materials like gels, dark chocolates, cells etc. that we come across have elastic as well as viscous contributions both in them. Such materials are called as viscoelastic materials, PDMS being an example. Considering the combination of viscous and elastic behaviours, the general form of the equation that governs the response is:

$$\sigma = G\gamma + \eta \dot{\gamma} \qquad \text{.....(3)}$$

Linear rheology probes the response of a viscoelastic material for small strain. There are two standard types of rheology measurements to investigate the viscoelastic properties. One is the amplitude sweep, where the strain amplitude is varied and the frequency is kept constant and the other, the frequency sweep where the frequency is varied and the strain amplitude is kept constant. The former probes the linear response regime and the latter probes the relaxation time of the sample for small (~ kbT) applied stress. **Figure 1.2.2** shows the response of a typical viscoelastic material to the applied stress. For an ideal solid, the strain response should be in phase with the stress response and therefore, the phase difference, δ is zero. For purely viscous material, the shear stress is out of phase by 90º as given by Newton's law. For a viscoelastic material, the phase difference, δ, lies in between 0 and 90º. This means that for a viscoelastic material, some energy is stored which is in phase with the applied strain while some energy is dissipated which is out of phase. The measure of how much energy is stored in a material is given by G'. After the load is removed, this energy is completely available and acts as a driving force for reformation. G'' is the loss modulus which is the measure of deformation or energy loss during shear. This energy is either used up during the process by changes in the sample structure or dissipated to the surroundings as heat. The complex modulus measures the visco-elastic character of the material and is given as sum of G' and G'' as

$$G^* = G' + iG''$$

$$|G^*| = \sqrt{(G')^2 + (G'')^2} \qquad \text{.....(4)}$$

The ratio of G' and G" gives tanδ which is known as the damping factor.

Conventionally, the swollen networks with low degree of crosslinking are referred to as gels. Rheology measurement for a nanocomposite sample is an indirect yet powerful technique to probe the state of dispersion and the nature of particle/polymer and particle/particle interactions. Moreover, studying rheological properties of such systems is fundamental to improving the processability of these materials, which is of primary importance in industry.

1.2.2 Scope of the Investigation

The incorporation of nanoparticles,[45,46] filler particles[42,47] or other polymers with PDMS can bring out significant changes in its rheological properties. The viscoelastic response for silica and clay nanoparticle-PDMS composites[48-50] have already been studied because of their nanometric size and large active surface thus improving mechanical, thermal, dimensional and barrier properties compared to pure PDMS polymer. The dispersed nanoparticles generally swell the linear chains present and cause increase in polymer radius of gyration with respect to nanoparticle volume fraction.[51] But, the dispersion of nanoparticles traditionally faces difficulty due to phase seperation and agglomeration. Despite its wide applicability, there are only few reports in the literature for PDMS nanocomposites with different kinds of filler particles. As presented in **Figure 1.1.3b** of **Section 1.1.3**, the in-situ reduction of Au nanoparticles within the PDMS polymer matrix which results in its uniform dispersion, should serve as fine example of nanoparticle-polymer composites. Here, the curing agent present in the PDMS mixture is assumed to play a dual role. It contains Si-H bonds which not only are involved in the crosslinking reaction of PDMS but also act as reducing sites for Au nanoparticles. Depending on the preparation temperature, the crosslinker may get preferentially engaged in the polymerization process or in the nanoparticle reduction. This is precisely the reason why at lower preparation temperatures, the composite is in the form of a gel. The extent of crosslinking should control the mechanical/flow response of the final product.

Rheology measurements have been performed on different gel samples prepared at different concentrations of the Au precursor and at different temperatures. Both these variables are expected to alter the nanoparticle density or size and influence the PDMS crosslinking process. This study focuses mainly on the amplitude sweep to understand the linear response of the AuNPs-PDMS gel. The STEM imaging and FTIR spectroscopy have also been performed to get an insight into the structural details.

1.2.3 Experimental

The 8 different gel samples were prepared at different temperatures (26 ºC, 36 ºC, 46 ºC and 56 ºC) and concentrations of aq. $KAuCl_4$ solution (0.2, 0.5, 1, 2 mM) following the procedure

explained in **Section 1.1.3**. The samples were kept in dessicator for 2 hrs prior to rheological measurements to remove trapped air bubbles.

The **Table 1.2.1** lists the different gel samples.

Sample No.	Preparation conditions (constant stirring for 2 hrs)	
	Temperature (°C)	Conc. of precursor used (mM)
A	26	0.2
B	26	0.5
C	26	1
D	26	2
E	26	20
F	36	1
G	46	1
H	56	1

Table 1.2.1 Different gel samples prepared under different conditions.

Characterization

The FTIR spectra were recorded using a Bruker IFS66-V/S spectrometer. The samples were prepared by dissolving gel in toluene to make a dilute solution followed by drop coating on a NaCl crystal. The toluene was allowed to dry prior to the measurement.

Rheological measurements

A controlled stress rheometer (MCR 301-WESP) with a controlled strain option was utilized in the parallel plate geometry (diameter 25 mm) as shown in **Figure 1.2.3**. All measurements were performed at 25 ºC. The gel sample was placed accurately in the middle of the peltier plate and humid atmosphere was maintained by enclosing it with an ordinary sponge wetted with water. The strain sweeps were performed at a fixed frequency of 10 rad/s while varying strain from 0.01% to 1000 %.

Figure 1.2.3 Rheometer (MCR 301-WESP) used for the study of gel samples.

1.2.4 Results and Discussion

As mentioned before, the AuNPs-PDMS gels were prepared by varying the concentrations of the precursor solution and the temperature. The gel samples have been characterized by UV-visible spectroscopy (see **Figure 1.1.4** of **Section 1.1.3**). The Au plasmon peak intensity increases as the Au precursor increased from 0.2 mM (gel **A**) to 2 mM (gel **D**). It is clear that the Au reduction is more facile in gel **D** as compared to gel **A.** Similarly, in the case of gel samples prepared at different temperatures (**C**, **F**, **G** and **H**), it is observed that the Au plasmon peak is relatively more intense for samples prepared at higher temperatures (**Figure 1.1.6** from **Section 1.1.3**). The gel samples have been further characterized by STEM microscopy imaging. The Au nanoparticles are seen to be distributed uniformly throughout the polymer matrix, more dense in the case of samples prepared at higher temperatures. The nanoparticle size is also bigger (30-50 nm) for higher temperature samples as seen in **Figure 1.1.6** from **Section 1.1.3.** Similarly, the gel samples prepared with high precursor concentrations were more dense with the particle size of 5-10 nm. Samples **A**, **C**, **D** and **H** were taken for further measurements.

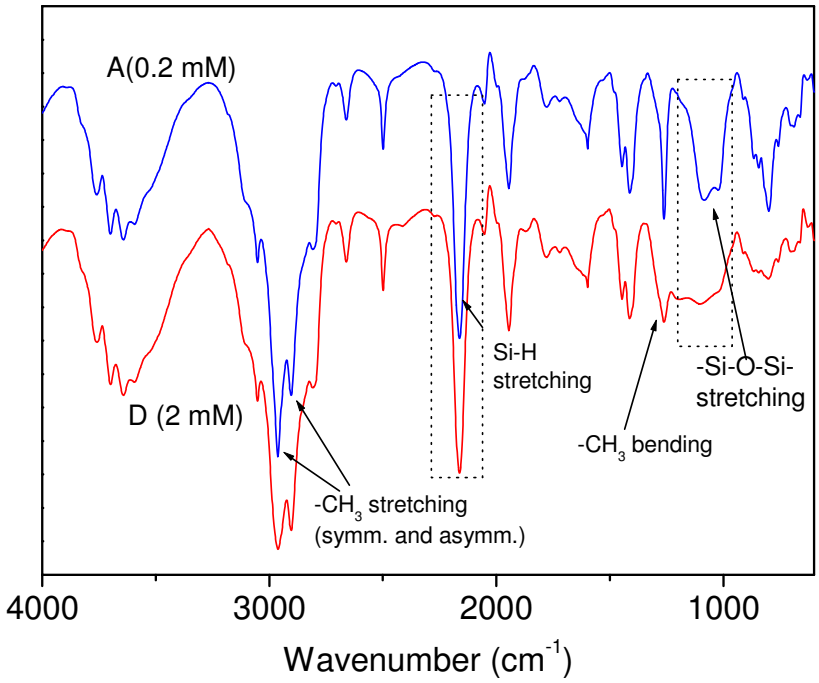

Figure 1.2.4 FTIR spectra of the AuNPs-PDMS gels prepared with different precursor concentrations. (Spectras are shifted laterally for clarity)

The degree of crosslinking was examined by FTIR spectroscopy. The infrared spectra of PDMS have been extensively reported in the literature thus enabling reliable assignment of transmittance peaks. PDMS shows following characteristic peaks:[52]

(1) the silanol peak around 3432.4 cm^{-1}, (2) the asymmetric and symmetric CH_3 stretching peaks centered at 2963.7 and 2904.5 cm^{-1}, (3) a strong peak indicating CH_3 bending modes at 1262.0 cm^{-1}, (4) a strong and broad peak at 1090.2 cm^{-1} assigned to asymmetric Si–O–Si stretching, and (5) a strong Si–C stretching and asymmetric CH_3 rocking peak at 801.5 cm^{-1}. The AuNPs-PDMS gel is seen to exhibit C−H stretching band at 2962 cm^{-1}, Si−O−Si asymmetric stretch at 1088 and 1020 cm^{-1}, Si−H stretching at 2165 cm^{-1} and C–H out of plane bending mode to explain the band at 800.3 cm^{-1} as shown in **Figure 1.2.4**. The intensity corresponding to CH_3 stretching, bending and rocking modes may vary according to the degree of crosslinking. An insight into Au nanoparticle formation in PDMS may be gained by examining the Si-H stretching and Si−O−Si stretching bands.[53] When the reduction of aq. $KAuCl_4$ takes place in the PDMS matrix, the Si−H sites present in the elastomeric chains get oxidized and convert to Si−O−Si linkages. Accordingly, for the sample prepared

with varying concentrations of the precursor solution, the Si−O−Si band intensity is found to be higher corresponding to sample (**A**) prepared with lower concentration (0.2 mM) of precursor as seen in **Figure 1.2.4**. This suggests that the curing of PDMS with lower Au nanoparticle concentration is more at room temperature as compared to the gel sample (**D**) prepared at a higher concentration (2 mM). For the gel sample, **H**, prepared at higher temperature shows an increase in the Si−O−Si peak intensity and a concomitant decrease in the Si − H band intensity (**Figure 1.2.5**). This observation implies that the polymer crosslinking is relatively less in presence of dense and big Au nanoparticles. The nanoparticles may cause increased hindrance for the cross linking process. In all, there are three factors which vary depending on the synthetic conditions directly influencing the viscoelastic properties. These are nanoparticle size, distribution and the degree of cross linking of PDMS polymer. The linear viscoelastic behaviour of gels is expected to get influenced by all the above factors.

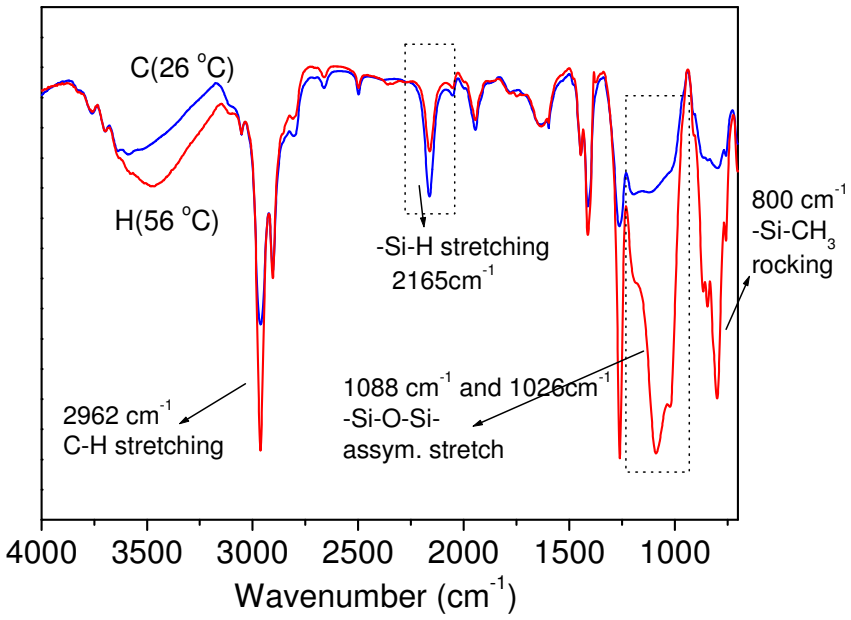

Figure 1.2.5 FTIR spectra of the AuNPs-PDMS gels (**C** and **H**) prepared at two different temperatures.

In general, for a typical particle-polymer gel, it has been observed that[54-57] at a constant frequency and varying strain, G' and G'':

1. decrease with increase in the particle size.
2. increase with increase in particle density or volume fraction of fillers.

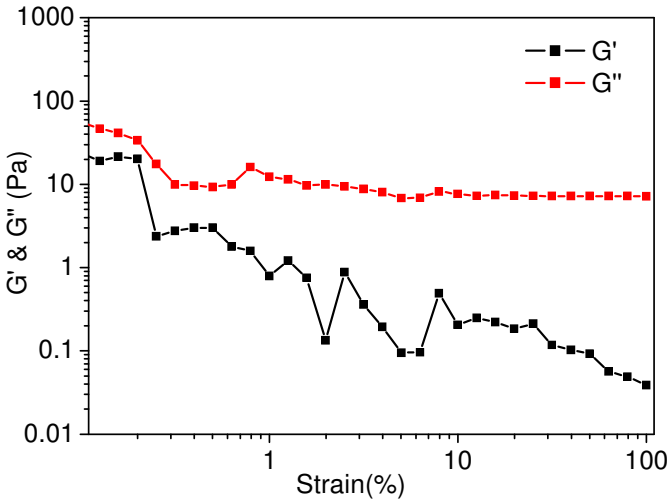

Figure 1.2.6 Amplitude sweep for plain PDMS before crosslinking.

In order to compare the effect of AuNPs on the crosslinking process, the strain-sweep experiment was first done for plain PDMS itself. As seen in (**Figure 1.2.6**), even a small strain (< 10%) brings lot of variations in G' and also G'', with no plateau, implying that crosslinking was too rapid for this measurement. The G'' decreased with increasing strain whereas G' showed dramatic fluctuations in the response curve because of which the linear viscoelastic behaviour could not be obtained.

Figure 1.2.7a shows the variation of G' and G'' for gels, **A** and **D**, versus the strain applied (at ω = 10 rad/s). G'' varies to a small extent as compared to G' in both cases. At strain less than 60%, G' of **D** is almost insensitive to the strain. This region called the linear viscoelastic region, is separated from the non-linear region by the critical strain amplitude (γ_L), also called as yield strain (see **Figure 1.2.7a**).[58] The γ_L values for gels, **A** and **D** are found to be 13% and 60% respectively. Gels **B** and **C** exhibited critical strain amplitude values close to **D.** In the non-linear region (above γ_L), the G' decreased significantly with increasing strain. Below the limiting value γ_L, the G' curve shows a constant plateau value which means that the material is in linear regime. Gel **A,** with fewer AuNPs, is expected to behave like the plain PDMS which is clearly not the case. The fact that the gels show linear viscoelastic regions means that the Au nanoparticles have a stabilizing effect on the gel.

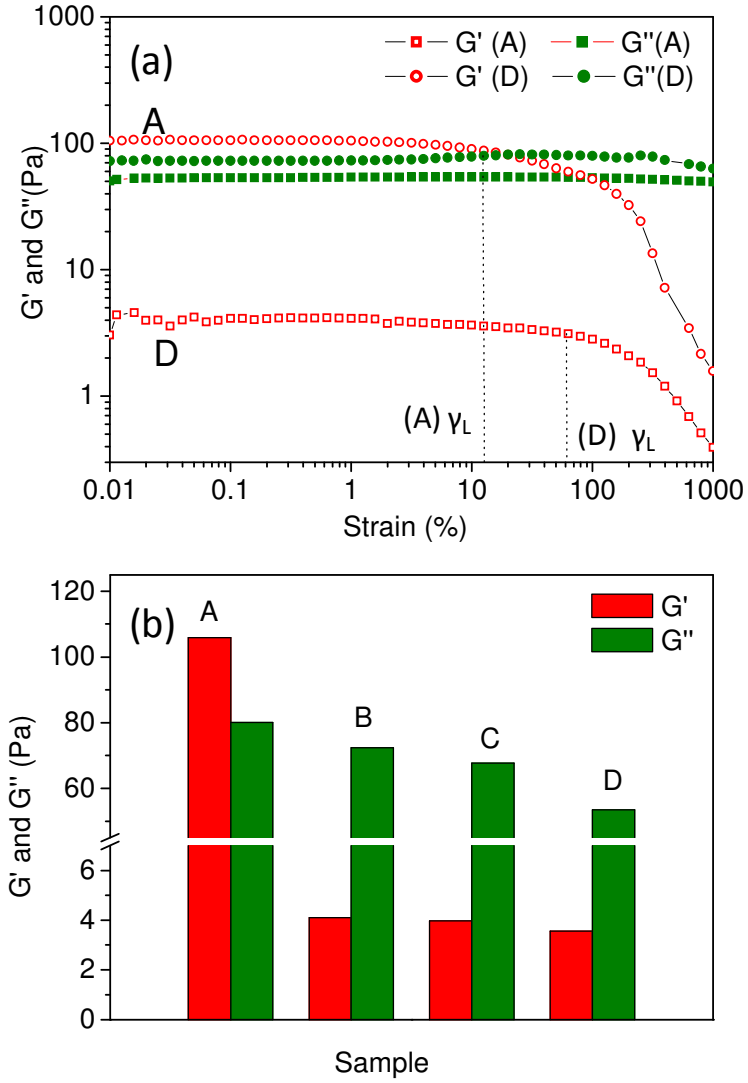

Figure 1.2.7 (a) The strain amplitude sweep at constant frequency of 10 rad/s for strain varying from 0.01% to 1000% for gel samples **A** and **D** as examples.(b) The storage and loss moduli of different gel samples (**A, B, C, and D**).

Secondly, there is an increase in the linear region for gel **D** with higher volume fraction of Au nanoparticles which is expected.[42] In gel **A**, in the linear viscoelastic region, the elastic behavior of the gel is dominating over the viscous behavior, since G' is greater than G''. However, G' of **D** is much less as compared to **A**, contrary to what is expected based on nanoparticle loading. Gels **B** and **C** also show significant decrease in G' and G'', the former being more sharp (**Figure 1.2.7b**). This means that AuNPs-PDMS gel undergoes a

transformation from being elastic to viscous on increasing the volume fraction of AuNPs in the PDMS matrix. This is in accordance with the FTIR data which shows lesser crosslinking with higher concentration of AuNPs (**Figure 1.2.4**). The reduced crosslinking affirms the fact that some part of curing agent is utilized in the reduction of Au precursor to AuNPs.

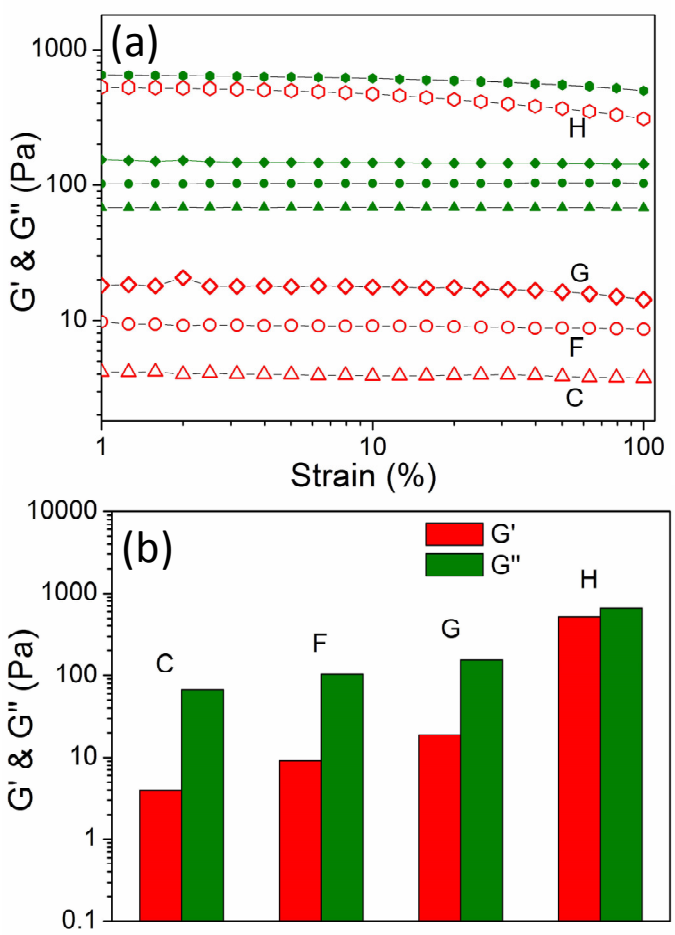

Figure 1.2.8 (a) The strain amplitude sweep at constant frequency of 10 rad/s for strain varying from 0.01% to 100% for gel samples **C, F, G** and **H** (b) The storage and loss moduli of different gels prepared at different temperatures.

The data with regard to gels **C**, **F**, **G** and **H** (prepared at different temperatures) are shown in **Figure 1.2.8.** As seen in **Figure 1.2.8**, the both G' and G'' values, increase gradually with the increasing temperature of the preparation due to which the gel **H** becomes more elastic as compared to gel **C,** the latter being more viscous. This effect is explainable on the basis of the extent of crosslinking taking place. For gel **C**, the curing agent utilized for the reduction

of AuNPs is relatively more than for crosslinking. On the other hand, the temperature accelerated the crosslinking process, resulting in an increase in the elasticity in the case of gels **F** and **G**. For gel **H,** the G' and G'' values become nearly equal which can be attributed to the equilibrium state between the curing of PDMS and formation of AuNPs.

Since the particle size and particle density usually have opposite influence on G' & G'', this may have a negligible effect due to both the parameters. The effective increase in G' and G'' may be attributed to the rate of crosslinking only.

The frequency response could not be studied for these gels, due to significant variation in the viscoelastic response due to aging.[59]

1.2.5 Conclusions

The higher density of AuNPs in the PDMS matrix of gels was obtained by increasing the concentration of precursor solution. The gels showed an unusual decrease in the G' and G'' values which is attributed to the crosslinking process which is accompanied with the in-situ particle formation. The increase in particle size and particle density resulted in higher values of G' and G''. The dispersion of nanoparticles, inter-nanoparticle interaction and the polymer-nanoparticle interaction strongly influence linear viscoelastic response; rheology consequently appeared to be a unique technique for the study of AuNPs-PDMS nanocomposites. The different rheology measurements and characterization techniques showed consistent results for gels prepared under different conditions.

1.3 Water treatment by removal of organics using AuNPs-PDMS composite

1.3.1 Introduction

Water purification is critical to our daily life. The removal of organic contaminants from water is an important industrial problem.[60] The contaminated water from industries usually contains large quantity of organic hydrocarbons with wide spread usage, toxicity and limited solubility such as toluene, benzene and xylene. These dissolved organic compounds cause bacterial growth, odour generation and biofouling with its limited reuse. Industrial discharges also contain pungent odor causing organosulphur compounds in the form of mercaptan, organic sulphides, thiols etc.

The recent flurry of activities in water treatment research aims at finding new, robust, low cost methods of purifying water with less energy while at the same time minimize the use of chemicals and impact on the environment.[61] The literature is bound with examples of materials such as zeolites with well defined porosity,[62,63] activated carbon with high surface area, cyclodextrins[64] with hydrophobic cavities for capture of organic molecules. Though activated carbon adsorption is still considered to be one of the best methodologies but the disposal of adsorbed contaminants along with the adsorbent is a major concern. Thus, the decomposition of the adsorbed organic contaminants and regeneration of the adsorbent is a critical step to the cost-effective use of porous adsorbents in waste water treatment. The challenging goal is to detect, decompose and remove contaminants present in low concentration despite potable constituents in high ratio as background.

With the advancement made in nanotechnology, nanomaterials have emerged out as potential candidates for water purification. Different forms of nanomaterials such as carbon nanotubes,[65,66] metal nanoparticles[67] and porous nanostructured materials with large surface areas have been recently employed for waste water treatment. For example, TiO_2/adsorbent nanocomposite[68] is used as photocatalytically active material for waste water treatment. Fan et al.[69] made nanocomplex of multi-walled carbon nanotubes with magnetic nanoparticles for catalytic oxidation and removal of phenols. Wu et al.[70] synthesized carbon nanotube sponges for removal of organic pollutants such as oils and solvents from the surface of water. Park et al.[71] developed silicone sponges for removal of BTEX and oil spills from water. The

chemistry of noble metal nanoparticles[72] has also been utilized for purification of water against halogenated organics, pesticides, heavy metals and microorganisms.

1.3.2 Scope of the Investigation

In this study, AuNPs-PDMS composites have been used for contaminated water treatment. The Au nanoparticles in PDMS can act as catalyst offering higher surface area for adsorption of molecules. PDMS has high affinity towards organic solvents such as toluene, benzene, ethyl acetate, amines etc.[73,74] It also has ability to form inclusion compounds with organic molecules due to its permeable and hydrophobic nature. The swelling behaviour of PDMS polymer in different solvents is generally determined by the solubility parameter which depends on dispersion forces, polarity forces and H-bonding. The solvents with solubility parameter different from that of PDMS do not swell PDMS whereas those having solubility comparable to PDMS cause swelling of the PDMS matrix. The property of swelling of the PDMS can be utilized for removal of organic solvents and thus can act as a potential adsorbent material. The AuNPs incorporated in PDMS matrix can be utilized for removal of odorous molecules such as thioanisole, thiophenol and Na_2S were used as model contaminated water. The levels of contamination by these organic compounds can be monitored using UV-visible spectrometry for simple and fast estimation.

1.3.3 Experimental

The AuNPs-PDMS and plain PDMS foam and films were synthesised as reported in **Section 1.1.2**. The plain PDMS foam and films (without AuNPs) were prepared in a similar way without adding the Au precursor during synthesis.

Swelling Tests of AuNPs-PDMS composites with different solvents

The swelling of AuNPs-PDMS composite was conducted in different solvents such as toluene, THF and DMSO. All solvents to be tested for swelling were taken in different vials. The pre-weighed sample of AuNPs-PDMS and plain PDMS in the form of foam as well as film were immersed in the respective solvents for 1 hr such that the sample weight reached a

constant value. The degree of swelling was determined by the ratio of sample weight before and after swelling.

Preparation of solution of toluene, thiophenol, thioanisole and Na_2S

Stock solutions of toluene (500 and 100 ppm), thiophenol (0.2 mM), thioanisole (0.2 mM) and Na_2S (0.6 mM) were prepared in water. The solutions were kept in tightly closed bottles to maintain uniform concentration over a period of time. Solutions are stirred in closed bottles for 24 hrs to equilibrate the dissolved organic component in water.

Sample preparation for toluene removal

The AuNPs-PDMS and PDMS foam and films of different amounts were weighed and 3 ml of stock solution (500 ppm and 100 ppm) was added to each taken in a vial and kept overnight after shaking thoroughly.

1.3.4 Results and Discussion

The mass change in differently swelled samples was monitored with time as the solvent evaporated under ambient conditions until each recovered to its original (deswelled) mass as shown in **Figure 1.3.1 and 1.3.2.**

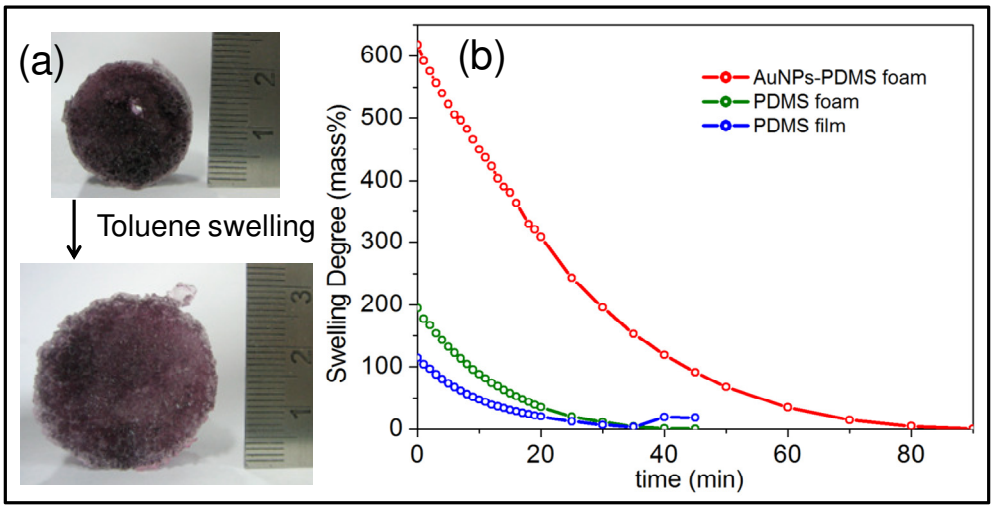

Figure 1.3.1 (a) Optical photographs of AuNPs-PDMS as such (above) and after swelling with toluene (below). (b) Deswelling behavior of AuNPs-PDMS foam, PDMS foam and PDMS film in toluene with time.

The solvent holding capacity of AuNPs-PDMS foam for toluene is remarkable. Indeed, volume expansion by toluene inclusion was vivid as shown in the photographs in **Figure 1.3.1a**. When plain PDMS in the form of foam as well as film, was dipped in toluene for 1 hr and taken out, its weight increased due to swelling to ~ 200% and 196% respectively (**Figure 1.3.1b**). These values may be compared with 131% reported for normally cured PDMS.[37] The toluene uptake is slightly more in the case of the foam due to the presence of large density of micropores. What is even more striking is that the AuNPs-PDMS foam was able to swell more than 600% times its mass (**Figure 1.3.1b**), which is attributable to large surface area made available by the embedded Au nanoparticles. As can be seen from the figure, AuNPs-PDMS is much slower in giving up toluene in evaporation. The exceptional ability of AuNPs-PDMS composite to take up and store toluene can be exploited for applications such as water purification.

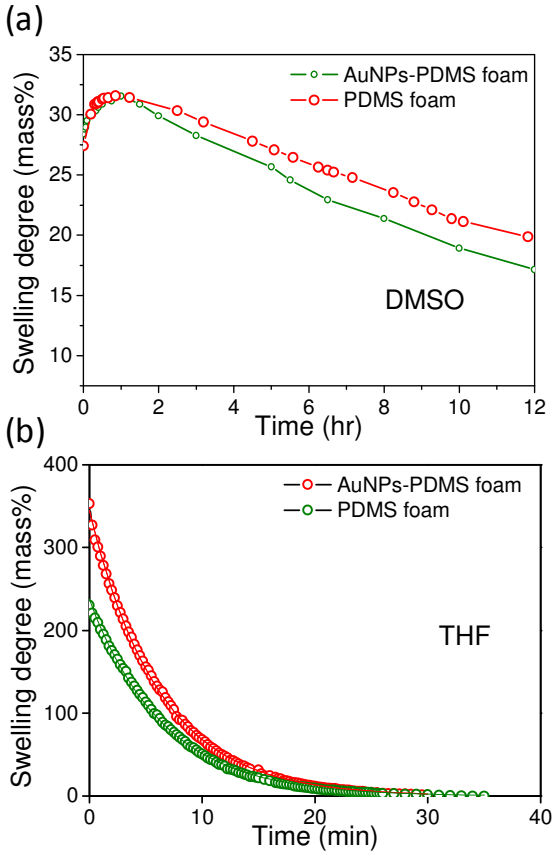

Figure 1.3.2 Deswelling of PDMS and AuNPs-PDMS foams with time for (a) DMSO and (b) THF.

DMSO resides only in the macro and microscopic pores and on the surface and do not cause much swelling of PDMS (**Figure 1.3.2a**). The THF is found to swell the AuNPs-PDMS matrix upto 350%. This shows that THF also behaves similarly to toluene in swelling of AuNPs-PDMS matrix.

Removal of organic solvents: a case study involving toluene contaminated water

The saturated solution (500 ppm) of toluene, was diluted to different known concentrations and corresponding UV-visible spectra were recorded (**Figure 1.3.3b**) to obtain the calibration curve (**Figure 1.3.3a**) for quantitative determination of toluene.

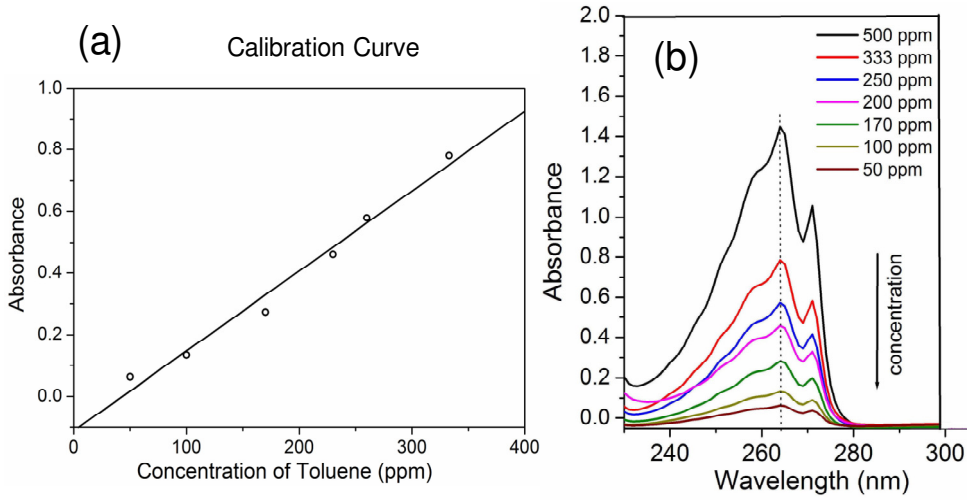

Figure 1.3.3 (a) The calibration curve for toluene. (b) UV-visible spectra for solutions of different concentrations of toluene in water.

The extent of toluene removed was monitored in terms of spectral changes as shown in the mass-normalized plots for PDMS and AuNPs-PDMS in **Figure 1.3.4a and b** respectively for 500 ppm and 100 ppm of toluene in water. Toluene has limited solubility in water, 500-627 ppm, but is a commonly occurring organic pollutant.[75,76]

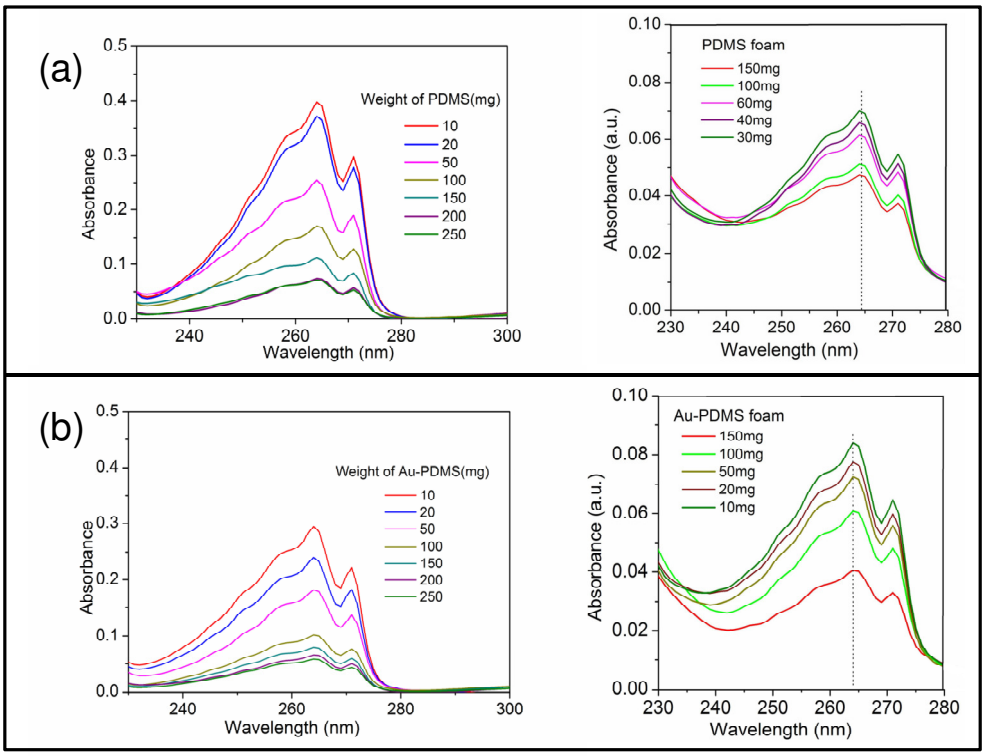

Figure 1.3.4 UV-visible spectra for removal of toluene from water by varying amount of (a) PDMS and (b) AuNPs-PDMS composite.

Figures 1.3.5a and b illustrate toluene removal from the contaminated water. Clearly, AuNPs-PDMS composite is more effective in removing toluene; a small quantity (10 mg) of the foam is good enough to bring down the contaminant from 500 to ~ 150 ppm within 8 hrs. Without Au nanoparticles, the latter value is ~186 ppm. The removal is more gradual thereafter for both the foam samples. Toluene or in general, organic removal from water is however increasingly difficult but more critical at lower concentrations, below 100 ppm as maximum contamination limit (MCL) is set to 7-10 ppm.[76] This region has been examined more carefully, using a 100 ppm solution of toluene in water as shown in inset of **Figure 1.3.5b**. Again, the AuNPs-PDMS foam is relatively more efficient to bring down the contamination to ~ 58 ppm with 100 mg of the nanocomposite.

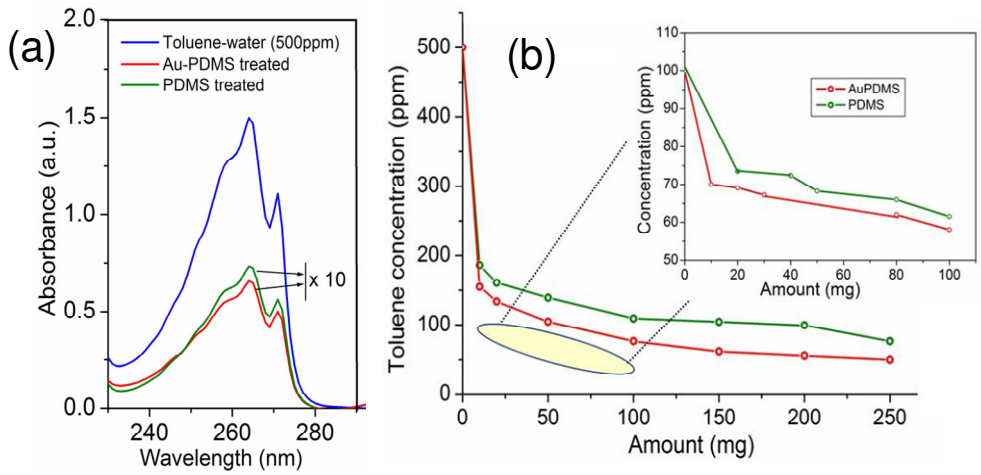

Figure 1.3.5 (a) UV-visible spectra of contaminated water (500 ppm toluene) showing reduction in intensity of toluene modes after treatment with 200 mg of PDMS and AuNPs-PDMS foam. The spectra of treated water samples are multiplied by factor of 10 for clarity. (b) Concentration of saturated and 100 ppm (inset) toluene in water after treatment as a function of amount of AuNPs-PDMS foam and PDMS foam used.

Removal of Odorous Compounds

The ability of AuNPs-PDMS composite for removal of odorous contaminants such as sulphides, thiophenol and thioether was examined.[77-79] These contaminants are present in waste water from crude oil and petroleum refineries, released from its manufacture sites, from use as pesticide, mosquito larvicide and use as pharmaceutical intermediate. These are highly toxic in nature. In particular, this study examines removal of Na_2S, thiophenol and thioanisole from water. Instead of foams, AuNPs-PDMS films have been used as the spectral changes of the composite could be monitored more accurately in this form.

Removal of Na_2S from water

The solution of Na_2S in water (0.60 mM) is basic (pH 10.26) because of its partial dissociation in water resulting in a high conductivity value of 63 μS cm^{-1}. The UV-visible spectra from a Na_2S solution in **Figure 1.3.6a** exhibits diminishing intensity of the peak around 233 nm when treated with the AuNPs-PDMS film which eventually vanishes after 12 hrs. The 233 nm peak corresponds to HS^- which forms when Na_2S is dissolved in water.[77] The variation in absorbance is shown in the inset. When it is treated with the AuNPs-PDMS film, the sulphide ions interact with Au specifically and get further reduced to bisulphide

ions. The bisulphide ion does not exhibit any feature in UV region, as seen in **Figure 1.3.6c**, but changes in Au-plasmon peak are observed. The decrease in pH of the solution to 7.34 can be related to the increase in hydrogen ion species on dissociation of sulphide to give bisulphide ions. Concomitantly, the conductance of water increased to 85 μS cm^{-1}.

Removal of thiophenol from water

The UV-visible spectra corresponding to uncharged form of thiophenol in water (0.1 mM) exhibits absorption maximum at 240 nm with a side shoulder at 265 nm corresponding to thiophenolate species[78] as seen in **Figure 1.3.6b**. When the solution was treated with a fresh AuNPs-PDMS film (**Figure 1.3.6d**), the thiophenolate became the predominant species. This was also evident from the pH change from 6.93 to 6.03 as solution turned acidic. The change in the spectral weight is clearly seen as the isosbestic point in the spectra. The variation is rapid (see inset). The conductivity of water changed from 20 to 117 μS cm^{-1} due to the ionization of thiophenol present.

Removal of thioanisole from water

The removal of thioanisole from water has been studied in detail. As thioanisole has an absorption peak at 250 nm,[78] its uptake from water by AuNPs-PDMS composite could be easily monitored by recording ultraviolet visible spectra of the contaminated water at different times during treatment. In **Figure 1.3.6e**, the 253 nm peak corresponding to thioanisole in water (0.1 mM) is seen to decrease to negligible intensity after 12 hrs of treatment with a fresh AuNPs-PDMS film. The variation is quite rapid as shown in the inset. Thioanisole is found to be chemisorbed on the surface of AuNPs-PDMS nanocomposite as seen from **Figure 1.3.6f**. The UV-visible spectra from films show that thioanisole chemisorb on Au nanoparticle surface resulting in a broad red shifted absorption at 257 nm. The pH change was minimal (6.5 to 6.3) while the conductivity increased from 8 to 82 μS cm^{-1}.

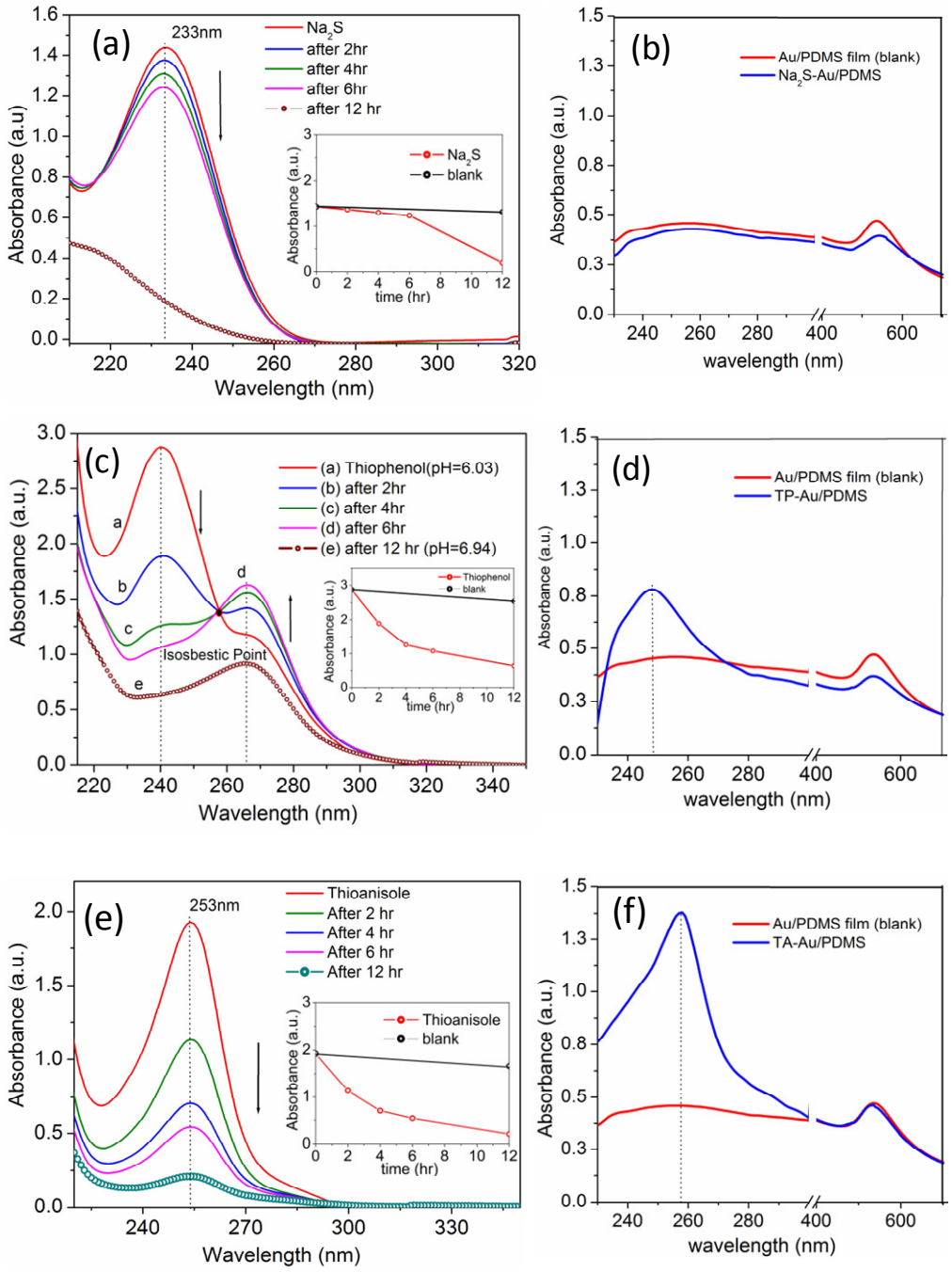

Figure 1.3.6 UV-visible spectra of (a) Na_2S solution in water (0.6 mM) (c) thiophenol (0.128 mM) and (e) thioanisole (0.10 mM)) recorded after different time intervals. The inset in each plot shows the decrease in absorbance with time for treated samples along with blank solution absorption taken after 12 hrs. UV-visible spectra from AuNPs-PDMS films dipped in (b) Na_2S and (d) thiophenol and (f) thioanisole show the interaction of these chemicals with the nanocomposite.

Reusability of AuNPs-PDMS composite for water treatment-The reusability of AuNPs-PDMS composite is an important issue for waste water treatment. Once the contaminants are absorbed by the material, release of contaminants from AuNPs surface and PDMS matrix is crucial. The easiest way of removing the volatile organic molecules can be performed through heating provided the material is robust enough to sustain high temperatures. When the sample was heated to a temperature upto 200 ºC for 1 hr, all thioanisole molecules absorbed by the sample got released from the composite. The heating was performed for prolonged to completely desorb thioanisole from AuNPs-PDMS composite and eventually levelling off. Once the AuNPs-PDMS composite is made free of thioanisole, then the material is again used for removal in repeated cycles.

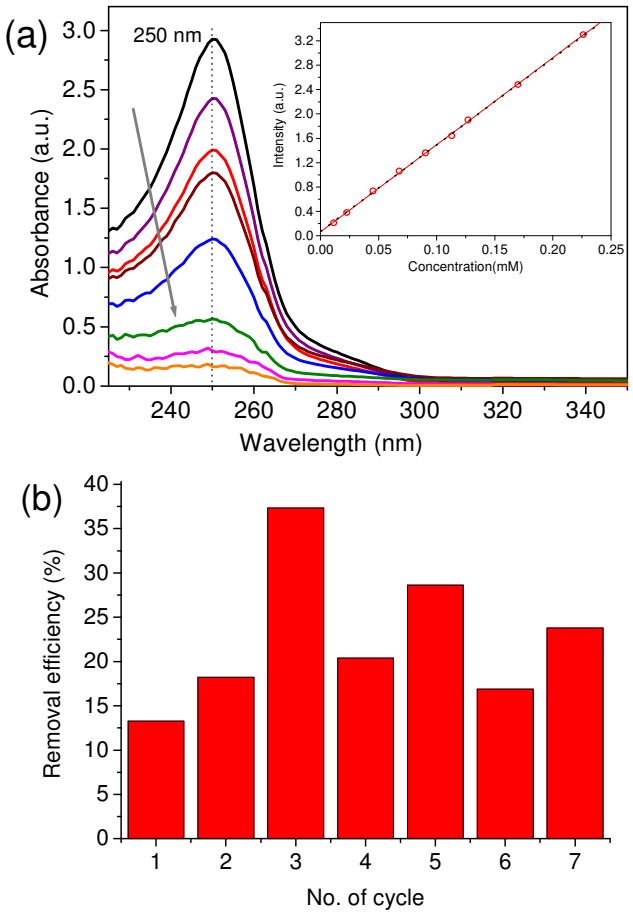

Figure 1.3.7 (a) Removal of thioanisole from water by AuNPs-PDMS composite after repeated cycles. (b) Average removal efficiency of 23.5% for a 0.9 g of AuNPs-PDMS film from 7 samples of contaminated water (100 ml of 85 µM, 1 hr each)

Figure 1.3.7 shows the successive removal of thioanisole by AuNPs-PDMS composite after release of thioanisole from the material after each step. By referring to a calibration curve for thioanisole in inset of **Figure 1.3.7a**, the exact concentration of thioanisole uptake by AuNPs-PDMS composite at different stirring times was determined. As shown by histogram in **Figure 1.3.7b**, we obtained nearly similar uptake and release of thioanisole for 7 samples of contaminated water (100 ml of 85 μM), each treated for 1 hr with the same nanocomposite sample.

This result not only shows the efficiency of the material but also confirms that the AuNPs encapsulated in PDMS matrix were not affected during the heating experiment.

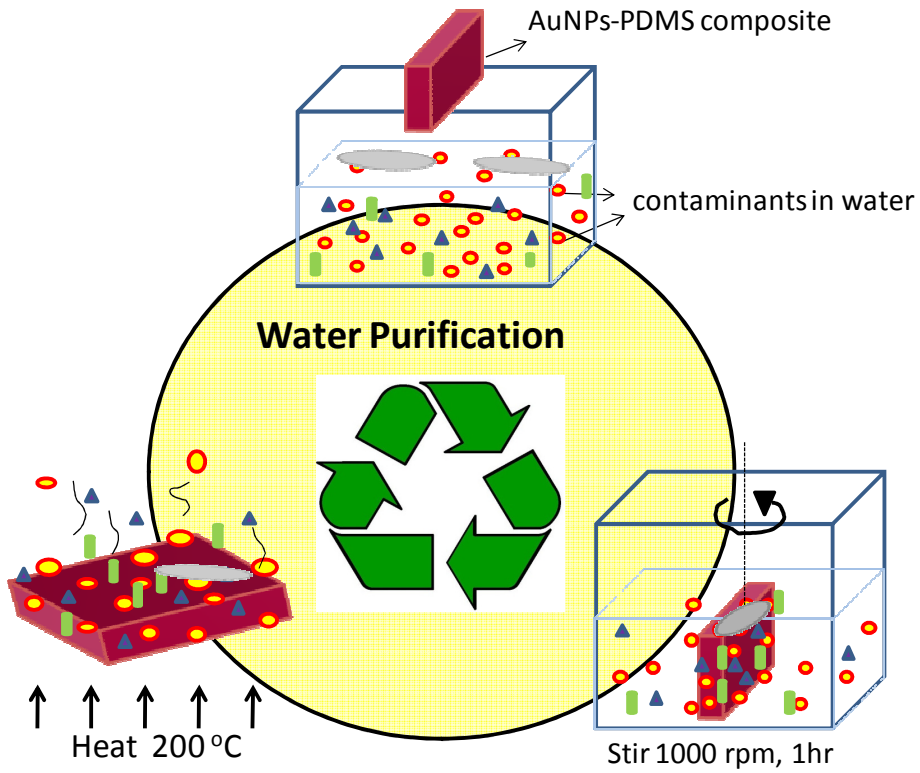

Figure 1.3.8 Schematic illustration of how the AuNPs-PDMS composite material works. A certain mass of AuNPs-PDMS composite is stirred in the contaminated water. The organic molecules get adsorbed inside the AuNPs-PDMS composite and released during heating. This can be repeated in cycles.

1.3.5 Conclusions

AuNPs-PDMS composite is identified as suitable, low cost, new alternative material for removal of organic contaminants in water. This unique combination of metal nanoparticles with polymer allows not only removal of contaminants through adsorption by PDMS network but also enables degradation by Au nanoparticles. The reusability of the composite material is demonstrated by releasing the absorbed contaminants by simply heating the composite material. The material can be used again and again with almost same efficiency over number of repeated cycles as shown by schematic in **Figure 1.3.8**.The significance of these results is that toxic and odorous organic contaminants may be reduced to few ppm levels in water with these nanocomposites as measured by UV-visible spectroscopy.

1.4 AuNPs-PDMS composite for Cell Imaging & Drug Delivery System

1.4.1 Introduction

Living cell and its substrate interaction is an important field of research with implications in microfluidics,[81] cell culture,[85] biomaterial implants etc.[82] Cell substrate adhesion is a multistep process including initial cell contact to the substrate, attachment, spreading and growth. The adhesion and proliferation of different types of cells on a biomaterial depends on many surface characteristics such as surface charge, wettability (hydrophobicity or hydrophilicity), microstructure, roughness and mechanical properties.[92] Hence, search for suitable matrices for cell growth is an important field in cell culture. The hydrophilic surfaces are generally believed to have lower protein adsorption than hydrophobic surfaces. The deterrence to cell adhesion takes place whenever there is resistance to protein adsorption.

PDMS is well exploited for variety of biological applications[32,80-83] because of its biocompatibility and low toxicity.[84,85] It is a commonly employed material for microfluidics as well. While using PDMS based microfluidic device in a bioapplication, one major hurdle is non-specific protein adsorption due to hydrophobic nature of the PDMS surface. This may induce clogging of cells along the fluid path making it difficult to reach specific locations.

Thus, chemical modification of the PDMS surface is an important area of research.[86,87] A number of strategies have been evolved to render the PDMS surface more hydrophilic. A straightforward method is O_2 plasma oxidation method which oxidizes $Si-CH_3$ group on PDMS surface to $Si-OH$.[88] However, the plasma treated PDMS undergoes 'hydrophobic recovery' after several hours due to the migration of low molar mass PDMS species from the bulk to the surface. This hinders its utilization in cell culture related applications. The surface modification of PDMS surface can be performed with biologically active molecules via different methods involving covalent linkage or adsorption processes. Often, additives such as poly(ethylene oxide) and poly(ethylene glycol) are deliberately introduced in PDMS to provide hydrophilic coatings for inhibiting protein and cell attachment.[89-91]

1.4.2 Scope of the Investigation

This study focuses on two main aspects, first is the use of AuNPs-PDMS composite for growth of cells. Mammalian Cells are considered to have an overall negative surface charge and hence poly-L-lysine coating is the most commonly used substrate.[85,93] Since the surface of PDMS gets modified with Au nanoparticles, AuNPs-PDMS composite surface is a candidate for the study the cellular interaction and cell adhesion. The PDMS matrix with Au nanoparticles can act like a carrier for a drug. This aspect has been examined using rhodamine 6G (R6G) as model system for drug delivery. Ideally, AuNPs should be made to carry a certain drug molecule and by external or internal trigger, the drug should be released to the cells hosted on the PDMS substrate. R6G is chosen because of its strong absorption in the visible region, high fluorescence yield and well characterized photo physical properties relevant in biological studies. It is also soluble in PDMS and is known to interact well with Au nanoparticles.[32,33] After the adsorption of R6G molecules, the release action can be carried out by using thiols as external stimuli. The external thiol molecules have capability to displace R6G molecules because of the strong Au-thiolate chemistry.

1.4.3 Experimental

Preparation of AuNPs-PDMS composite substrates

AuNPs-PDMS composite film substrates of high and low Au nanoparticles loading were prepared on cover slips following the previous method explained in **Section 1.1.2**. PDMS was made by mixing elastomer and curing agent in 10:1 ratio respectively. The aq. $KAuCl_4$ (10 ml) of 0.2 mM and 2 mM concentration was mixed in 2 vials taken separately with 2 g of PDMS mixture in each. The stirring was performed in both vials for 2 hrs at room temperature resulting in AuNPs embedded in PDMS gel. The AuNPs-PDMS gel was washed with water to stop further reaction, if any, and kept in vacuum for 1 hr to remove all bubbles. The gel was casted into films by heating at 60 ºC for 6 hrs and used for cell culture.

Mammalian Cell culture

HeLa cells were maintained at 37 ºC in Dulbecco's modified Eagle medium (DMEM), (Invitrogen) supplemented with 10% fetal bovine serum (Hyclone) and appropriate

antibiotics in 5% CO_2 incubator. 50,000 cells were seeded on different coated coverslips and after 24 and 48 hrs, respectively.The cells were processed for either cell viability assay or hoechst staining for visualization.

Cell viability assay by trypan blue

Trypan blue is the stain most commonly used to distinguish viable from nonviable cells. Viable cells exclude the dye and hence appear colourless, whereas the nonviable cells absorb the dye and appear blue. Based on this principle, a cell viability assay was performed and the cell count was taken as a measure of the viability. Since, trypan blue has high affinity for serum proteins, the cells were thoroughly rinsed with PBS before proceeding for the experiment. Cells that were seeded on different coatings, were trypsinized using 0.05% Trypsin EDTA solution (Invitrogen), after 24/48 hrs, and the cell suspension was mixed with 0.4% trypan blue solution in saline in equal volume. Following incubation at room temperature for 3 min, the above cell suspension was added to the haemocytometer and the cells were visually examined under the microscope. The viable and the nonviable cell count was performed individually and the final viability was represented as the fraction of viable cells by total number of cells/ml. The cell count was performed individually across the four different cell counting chambers and plotted separately. The experiment was performed as a replicate and the final data was plotted as the average viable cell count using microsoft excel sheet and the standard deviation was represented as the error bar.

Hoechst staining

Cells were grown on cover slips coated with poly-L-lysine, PDMS and AuNPs-PDMS (of low and high Au loading) at 37 °C in a 5% CO_2 incubator. After the indicated time point, cells were washed with PBS and fixed with 4% paraformaldehyde (in PBS) for 20 min at room temperature. Cells were then permeablized using 1% Triton X-100 (in PBS) for 10 min and subsequently washed with PBS for 10 min, 3 times. The nuclei were stained with Hoechst dye, (SIGMA) (1:10,000 dilution) for 20 min. Two times PBS washed cover slips were inverted on to a microscopic slide over 2 μL of 70% glycerol (in PBS) and visualized using fluorescence/confocal microscopy.

R6G absorption and release experiment

AuNPs-PDMS and pristine PDMS films were soaked in R6G solution in toluene (1 mM) for 6 hrs and washed with toluene to remove the excess R6G molecules from the film surface. For release, the R6G-incorporated films were soaked in a 2 mM solution of HDT in toluene for 8 hrs.

Characterization

In addition to UV-visible absorption measurements, photoluminescence measurements were also carried out with a (Perkin-Elmer LS50B) luminescence spectrometer. The emission spectra were recorded with an excitation wavelength of 490 nm.

1.4.4 Results and Discussion

The two samples with different loading of Au nanoparticles were prepared and characterized using UV-visible spectroscopy as shown in **Figure 1.4.1**.The synthesis procedure shown in **Figure 1.4.1a** is similar to that described in **Section 1.1.3.** The UV-visible spectra shown in **Figure 1.4.1b** shows plasmon peak centred at 536 nm for sample prepared with 2 mM Au precursor whereas broad and low intensity peak at 534 nm corresponds to sample prepared with 2 mM Au precursor solution.

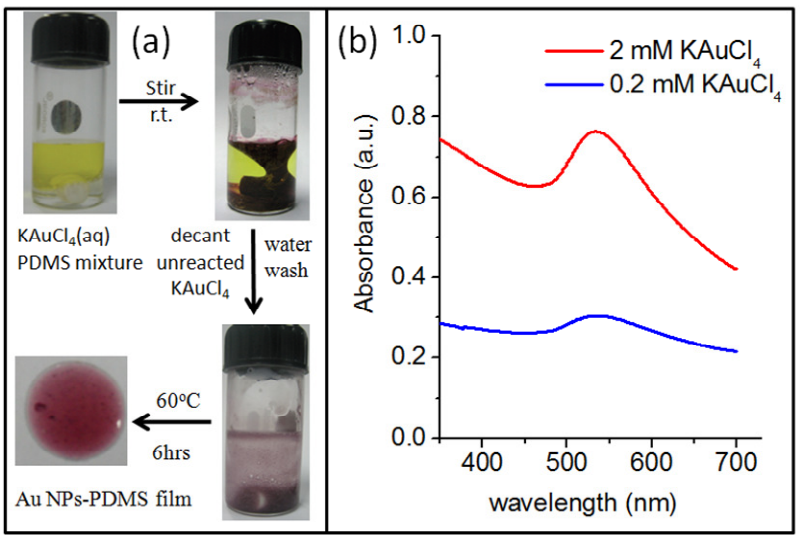

Figure 1.4.1 (a) Schematic illustrating synthesis procedure for AuNPs-PDMS film. (b) UV-visible spectra corresponding to two different samples.

The particle size was determined by STEM and SEM microscopy as shown in **Figure 1.4.2**. The sample prepared with 2 mM $KAuCl_4$ solution has higher nanoparticles density (~2200 ± 10 μm^{-2}) as compared to sample prepared with 0.2 mM with $KAuCl_4$ solution (~ 640 ± 10 μm^{-2}) with nearly similar particle size (~5-15 nm). The different loading of Au nanoparticles in the composite was carried out to see the effect of Au nanoparticles in modifying the surface of PDMS and thus the effect on cell growth.

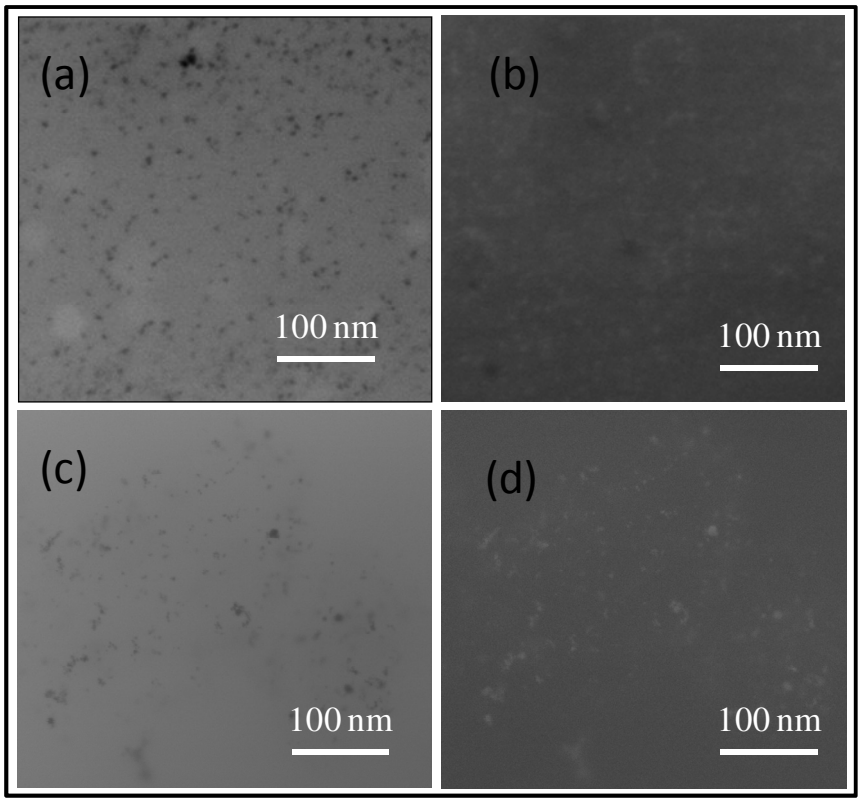

Figure 1.4.2 STEM images of AuNPs-PDMS gel synthesized with (a) 2 mM and (c) 0.2 mM of $KAuCl_4$ .The corresponding SEM images in (b) and (d) respectively.

From the microscopy images of HeLa cells in **Figure 1.4.3**, it can be seen that the cells incubated on PDMS surface (**Figure 1.4.3b**) were well attached and the cell morphology is somewhat elliptical as compared to that on the poly-L-lysine used as the control (**Figure 1.4.3a**). This still corroborates with the good biocompatibility of PDMS for the adhering

cells. On the AuNPs-PDMS surfaces, however, the cells were not able to attach and spread out properly even as compared to PDMS (see **Figure 1.4.3c** and **d**). The cells on the surface with low Au nanoparticle loading are seen to be spherical in shape as seen in **Figure1.4.3c** which shows that the cells tried to adhere to the surface. But, on the surface with high AuNPs loading, cells could be hardly seen in **Figure 1.4.3d**.

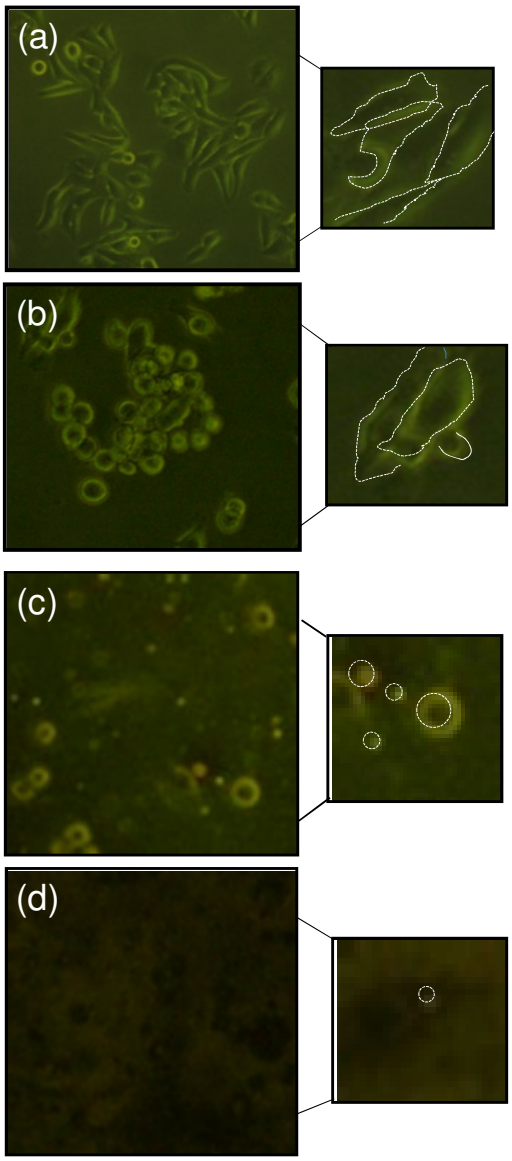

Figure 1.4.3 The optical Images of HeLa cells taken 24 hrs after incubation at 37 ^{o}C, 5% CO_2 environment, DMEM medium. (a) poly-L-lysine, (b) PDMS, (c) and (d) AuNPs-PDMS composite layers prepared with 0.2 and 2 mM of Au precursor respectively. Inset (right) in all images shows the magnified image of the morphology of cells.

The Hoechst stained images of HeLa cells (cervical cell line) indicate a differential adherence pattern with respect to different matrix coating. As expected, the commonly used poly-L-lysine coating shows maximum adherence of the cells which are well spread as seen in **Figure 1.4.4a** after 24 hrs. However, the hydrophobic PDMS coating seems to decrease the ability of the cells to adhere on the PDMS substrate as compared with positively charged lysine coating (**Figure 1.4.4b**).

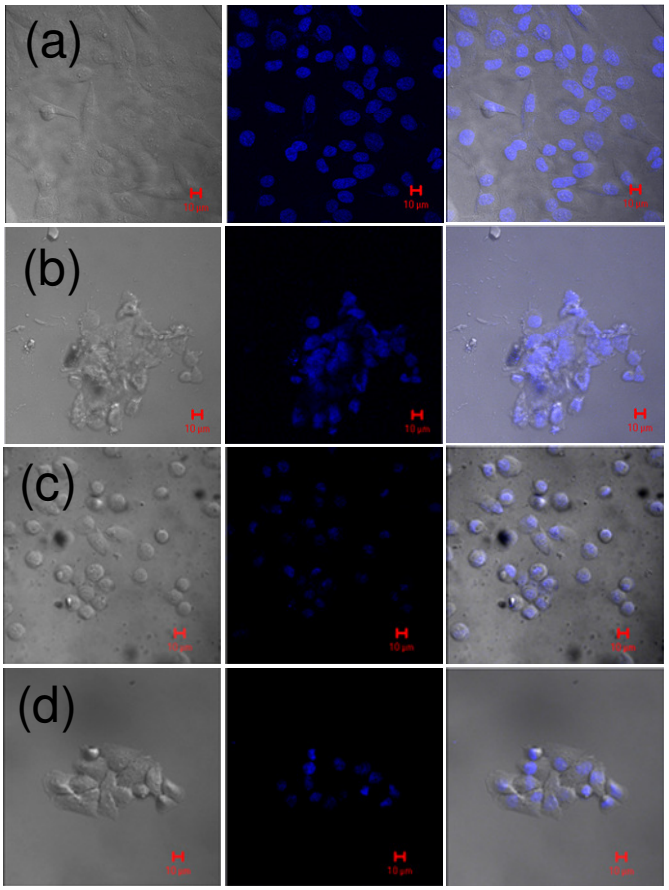

Figure 1.4.4 Bright field (left), dark field (middle) and fluorescence (right) microscopy images of cells seeded on different layers for 24 hrs, (a) poly-L-lysine, (b) PDMS, (c) and (d) AuNPs-PDMS composite layers prepared with 0.2 and 2 mM of Au precursor respectively.

Interestingly, the cells on the PDMS matrix were slightly shrunk indicating that the hydrophobic surface may not be favourable for cell growth as reported earlier.[86] This could

be because of the ability of the PDMS to adsorb serum proteins thus depriving the cells of growth factors. Surprisingly, the two Au nanoparticles loaded PDMS composited showed differences in both the cell number and the cell morphology. The number of cells adhering on AuNPs-PDMS surface with higher loading of AuNPs is less as compared to the AuNPs-PDMS with lower loading of AuNPs.

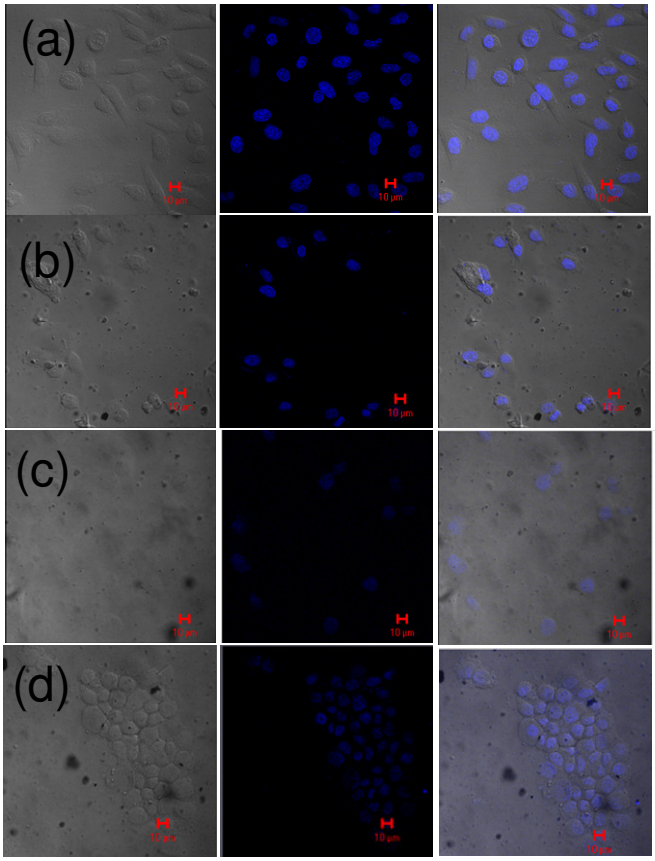

Figure 1.4.5 Bright field (left), dark field (middle) and fluorescence (right) microscopy images of cells seeded on different layers for 48 hrs, (a) poly-L-lysine, (b) PDMS, (c) and (d) AuNPs-PDMS composite layers prepared with 0.2 and 2 mM of Au precursor respectively.

In low AuNPs-PDMS, the cells were well spread out. However on the other surface with higher loading of Au nanoparticles, clumping of cells was observed. This could be also be due to non-uniformity of AuNPs in PDMS. The Hoechst stained images were examined again after 48 hrs. The number of adhering cells dropped down for the AuNPs-PDMS

substrate with low AuNPs decreased but the AuNPs-PDMS surface with higher AuNPs got multiplied as seen in **Figure 1.4.5**.

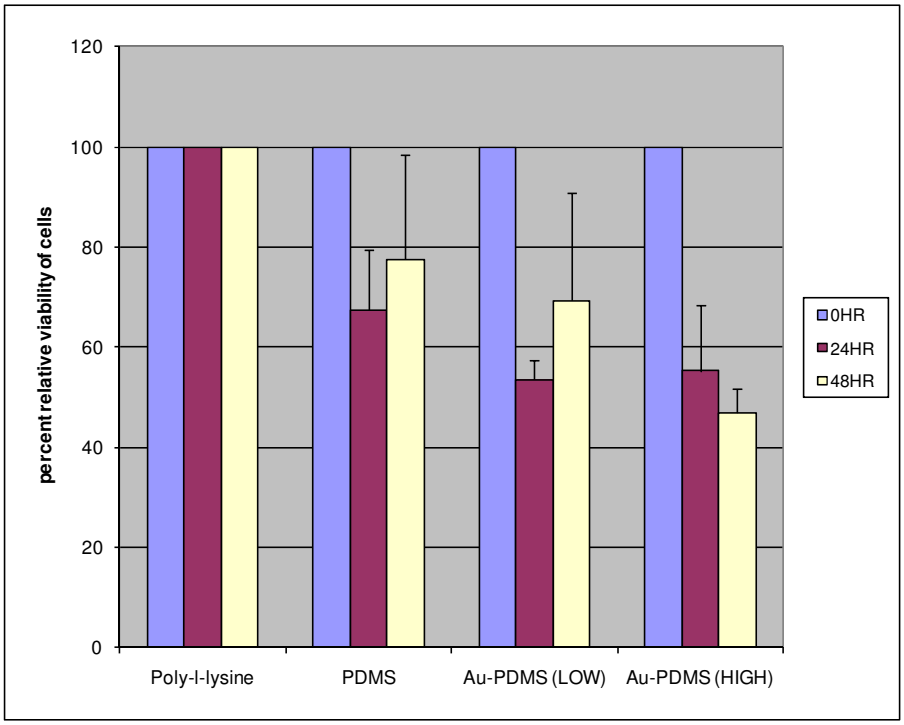

Figure 1.4.6 (a) Trypan blue cell viability assay of HeLa cells incubated with PDMS and AuNPs–PDMS composite of different Au NPs loading. Assay is done after 24 and 48 hrs and the cells were counted using neubauer's chamber. Data are averages plus standard deviations for two independent experiments.

Note: The cell clumping leads to less accessibility to medium/growth factors as well as space constraints which leads to lesser cell count in the AuNPs-PDMS with higher AuNPs loading.

The in vitro cell viability tests have been carried out to test the cytotoxicity of the AuNPs-PDMS composite. As seen in **Figure 1.4.6**, the cell count on PDMS and both types of AuNPs-PDMS surfaces decreases after 24 hrs. This can be attributed to the hydrophobicity of the surface. But after 48 hrs, the number of cells multiplied on PDMS as well as on the AuNPs-PDMS composite surface with low AuNPs loading, which shows good biocompatibility; this is an important prerequisite for biomedical applications. But over all,

there was a decrease in no. of cells for high loaded Au nanoparticle PDMS composite substrate which is contrary to as seen in hoechst stain images in **Figure 1.4.5c and d**.

This result shows a possibility for drug delivery applications using AuNPs-PDMS composite material. Drug delivery can be achieved if one can successfully bind drug molecules with the Au nanoparticles such that intracellular glutathione (GSH) mediated release can take place. For the implication of this concept, we have studied the interaction of R6G dye as a model system and release of R6G from AuNPs-PDMS composite through hexadecanethiol as external stimuli as shown by schematic in **Figure 1.4.7**.

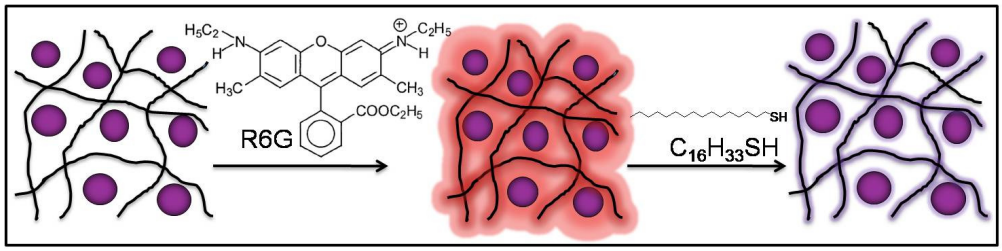

Figure 1.4.7 Schematic of R6G incorporation in AuNPs-PDMS nanocomposite and release using HDT.

Adsorption of R6G in AuNPs-PDMS composite

The interaction of rhodamine chloride (R6G), a fluorescent dye with AuNPs-PDMS composites using UV-visible spectroscopy was studied. As shown in **Figure 1.4.8**, the intensity of the characteristic R6G peaks at 508 and 543 nm is approximately 2 times greater for the AuNPs-PDMS composite than for plain PDMS, suggesting that the Au nanoparticles facilitate additional uptake of the dye. The absorption spectra in **Figure 1.4.8a** shows splitting of the broad absorption band of R6G into two peaks, the 508 nm peak attributes to molecular R6G while peak at 538 nm is due to chemisorbed species on the Au nanoparticle surface. [94] The absorption at 508 nm corresponds to dye aggregation band and 538 nm is the effect of Au surface plasmon.[94] A small peak at 714 nm arising from R6G far moved away from the main feature is also observed. Photoluminescence (PL) spectra of the samples obtained with an excitation wavelength of 490 nm are shown in **Figure 1.4.8b.**

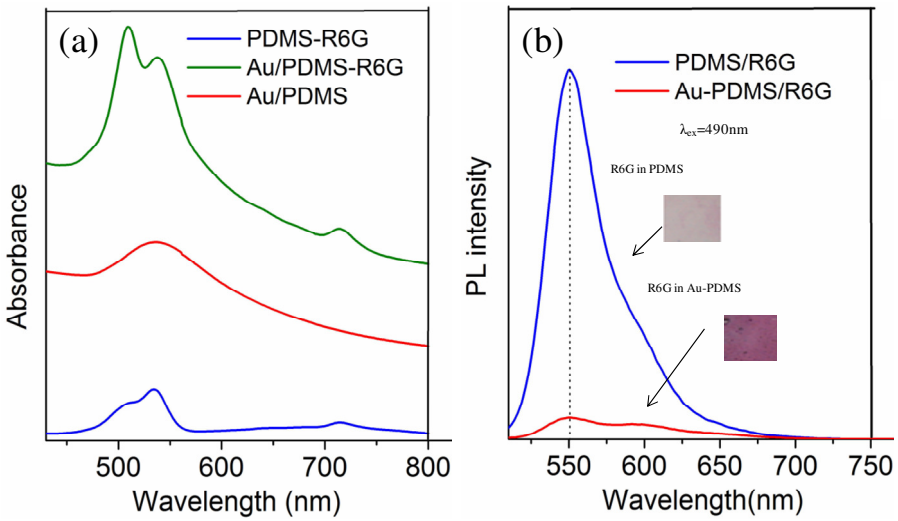

Figure 1.4.8 (a) UV-visible absorption and (b) PL emission spectra from AuNPs-PDMS and plain PDMS films upon adsorption R6G.

The relative PL intensity of the dye in the case of AuNPs-PDMS composite is 17 times less compared to plain PDMS, albeit having nearly double the amount of dye. The quenching of PL is due to the charge transfer interaction with the Au nanoparticle surface, which is consistent with the observations made in the literature.[94]

Release of R6G from AuNPs-PDMS composite

R6G was released from the nanocomposite using hexadecanethiol (HDT) as a chemical trigger. HDT has a strong affinity to Au due to the presence of the sulfur in the thiol groups, therefore it can displace the relatively weakly-interacting R6G from the nanoparticle surfaces and into the solvent medium, as shown schematically in step 2 of **Figure 1.4.7**. The relative release of R6G was characterized by performing PL on the resulting solutions. From the spectra in **Figure 1.4.9a and b**, it is clear that the amount of R6G released is much higher in the case of AuNPs-PDMS composite than plain PDMS. This is attributed to the higher capacity of the nanoparticle composite to hold the dye mediated by the chemical interaction between the dye molecules and the nanoparticle surface. The significantly higher R6G release into HDT solution relative to toluene is consistent with the proposed mechanism. Thus, R6G enabled us to probe the microenvironment of the composite.

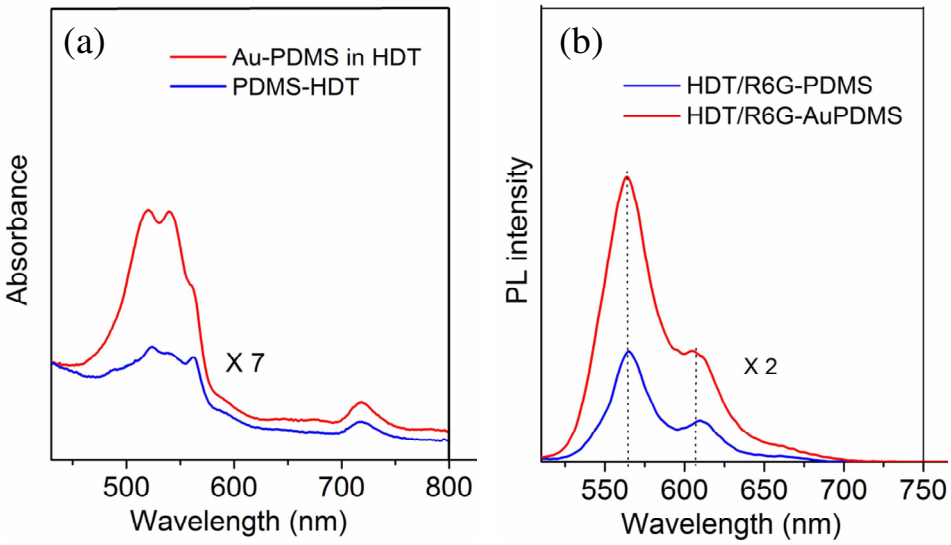

Figure 1.4.9 (a) UV-visible absorption and (b) PL emission (at 490 nm excitation wavelength) from HDT solution in toluene on release of R6G. Both UV-visible and PL spectra are multiplied by 7 and 2 respectively, relative to Figure 1.4.8 for clarity.

1.4.5 Conclusions

The PDMS surface as such is biocompatible and non-toxic. After incorporation of AuNPs in PDMS, the cell growth on PDMS does not take place easily. The cell adhesion decreases due to the surface modification by the incorporated AuNPs. Importantly, other properties of PDMS such as flexibility are well retained which are crucial in microfluidic device fabrication.

The ability of this composite to release the dye molecules in the presence of a specific chemical environment shows promise for storage and chemically-induced release of specific compounds, which can be applied for targeted drug delivery. The size of the AuNPs in the PDMS matrix can be tuned from 5-50 nm, and thus there is a possibility of varying the drug loading. These investigations not only provide an insight into the interaction of nanocomposite with biological systems but can also help in designing an efficient drug delivery system.

1.5 Metallisation of PDMS

1.5.1 Introduction

PDMS being flexible, stretchable, optically transparent, electrically insulating and biocompatible, is considered ideal as a substrate for futuristic devices.[95,96] An important difference from conventional electronics is that once metallised, PDMS can in principle, integrate well with living tissues to form circuit elements in epiretinal prosthetics,[97] electronic textiles etc.[98] PDMS can be metallised using Au overlayers, the choice of the metal owes much to its biocompatibility. Metal evaporation and sputtering have been the routine methods to deposit Au film on PDMS surfaces.[99] The Au film obtained from these methods however, suffers from poor adhesion and spontaneous buckling adding to undesired surface roughness. Further, such films have a tendency to develop cracks with compressive stress.[99] Metals adhere poorly to PDMS due to the low surface energy of PDMS.[99] To address this issue, several approaches using coupling agents have been reported to enhance chemical adhesion,[100] serial and selective etching to stack metal layers on PDMS[101] or manual injection and solidification of melted metals into PDMS microchannels.[102] Even with improved adhesion, the incompatibility between PDMS and metals often causes failure in fabrication processes. Thin metallic films tend to debond from flexible PDMS substrates, and thin layers have a potential cracking problem when bent or stressed,[101] which is undesirable in many flexible electronics applications.[103]

Several attempts have been made in the past for the fabrication of flexible metal or conductive electrodes. To avoid incompatibility issues, soft conductive materials have been utilized to embed conductive patterns in PDMS. Carbon nanotube is one of the common materials[104a] to be mixed with PDMS to form conductive composites that can be used to construct conductive and flexible micropatterns. The embedded conductive composite diffuses into the bulk PDMS polymer matrix, and therefore possible adhesion issues and cracking problems are eliminated. However, the use of carbon nanotubes in bioapplication is not much welcome due to its toxicity issues and limited control over functionalized-CNT behaviour.[104b] Recently, a few more approaches have been explored to form embedded conductive PDMS patterns. Bowden et al.[105] and Chen et al.[106] electrolessly prepared micro silver electrodes inside the PDMS channels by electroless plating based technique and more

recently Hao et al.[107] performed region selective electroless plating by combining the UV-induced poly(acrylic acid) grafting with electroless gold plating.

1.5.2 Scope of the Investigation

The advantageous properties of PDMS can be exploited only if one can circumvent the problems associated with the conventional deposition of Au film. The present work deals with metallization of PDMS via a chemical route. It relies on the growth of the Au nanoparticles to form a film starting with AuNPs-PDMS nanocomposites. Importantly, the method uses no adhesive layer in between. As PDMS is easily patternable by lithography procedures, this method opens up possibilities of patterning metallisation itself.

1.5.3 Experimental

Metallisation of AuNPs-PDMS film

A small portion of AuNPs-PDMS gel (**Section 1.1.3**, sample **E**) was dropped on the surface of aq. $KAuCl_4$ solution (0.1 mM). It was allowed to spread uniformly over the liquid surface and stand for 12 hrs. During this period, the bottom surface of the gel layer was in constant contact with the solution. As the gel was cured, the film was lifted gently from the solution using a glass slide.

Characterization

Film thickness measurement was done using a Wyko NT1100 (Veeco, USA) optical profiler (OP) as well as using a Stylus profiler Dektak 6M (Veeco, USA). In OP, the PSI mode was employed with a field of view and objective lens magnifications as 1X and 20X respectively. I-V measurements were carried out by making electrical contacts using conducting Ag paint. An external multimeter (Keithley 236) served as the source and measurement unit for current-voltage characteristics.

Powder X-ray diffraction measurement was done using Bruker diffractometer employing Cu Kα (λ = 1.5406 Å) radiation. Samples were prepared by transferring the film on glass slide followed by curing. The typical scan rate was 1 ° min^{-1}.

1.5.4 Results and Discussion

The process of metallisation of PDMS is shown in **Figure 1.5.1**. The AuNPs-PDMS gel spreads uniformly over the surface of aq. $KAuCl_4$ and forms a thin layer at the air-water interface as shown in **Figure 1.5.1a**. Upon lifting the layer after several hours using a glass slide, we readily observe that the surface exposed to the solution turned metallic shiny (**Figure 1.5.1b**), while the top surface turned slightly darker (**Figure 1.5.1c**). The metallised surface exhibits a mosaic structure with typical domain size of ~ 2 μm. Overall, the layer after this treatment is somewhat less jelly and shows a tendency to form a continuous film.

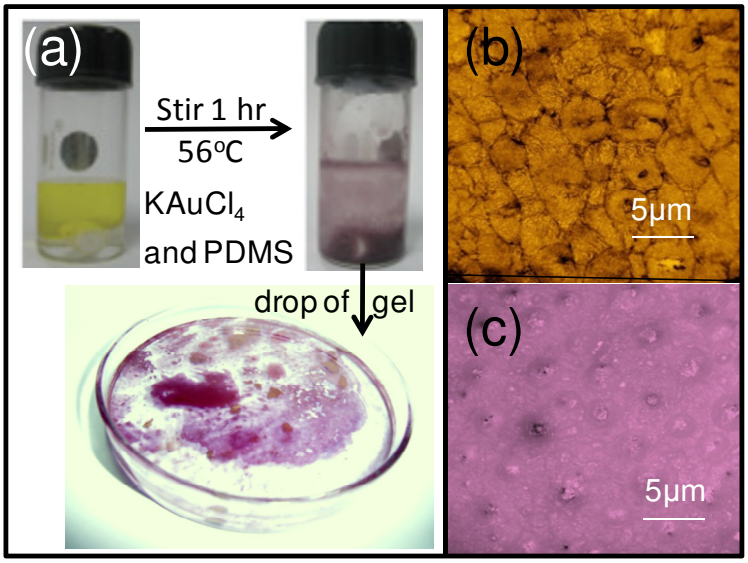

Figure 1.5.1 (a) Synthesis of Au-PDMS metallised film, (b) the metallised bottom surface. (c) the top surface resembling closely the pristine AuNPs-PDMS composite.

One such film transferred to a glass substrate, is shown in **Figure 1.5.2**. The film being fragile got folded while transferring. The line of fold can be clearly seen in the optical image shown in **Figure 1.5.2a**, demarking the pristine surface (reddish brown) and the folded golden portion from the bottom which was exposed to the solution. The thickness across the line of fold was found (see **Figure 1.5.2b)** to be 2.8 μm using the optical profiler. Half this value (1.4 μm) should correspond to the film thickness, assuming the film to be uniform.

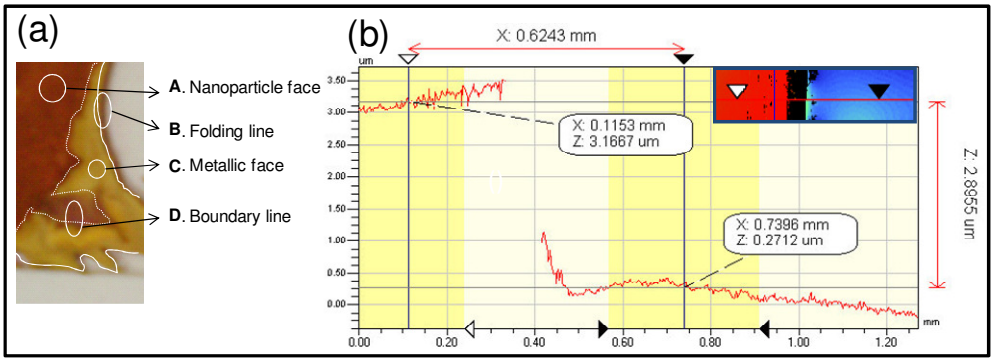

Figure 1.5.2 (a) The optical microscope image showing different regions of partially folded flexible Au-PDMS metallised film transferred on glass from top surface of aq. media. (b) The optical profilometric measurement for thickness determination.

The SEM imaging revealed further details (**Figure 1.5.3**). The golden side of the film showed aggregated network of the deposit (see **Figure 1.5.3a**) with irregularly shaped domains separated by cracks. A closer look at the surface (see inset) showed highly interconnected domains and cracks the latter being few nms to ~ 200 nms wide. The pristine surface shows nanoparticles closely spaced Au nanoparticles bigger in size (10-80 nm) as seen in **Figure 1.5.3b** compared to the gel (see **Figure 1.1.4**). During the deposition, the Au(III) solution seems to penetrate across the film thickness to cause further reduction and growth on the top surface of the gel layer.

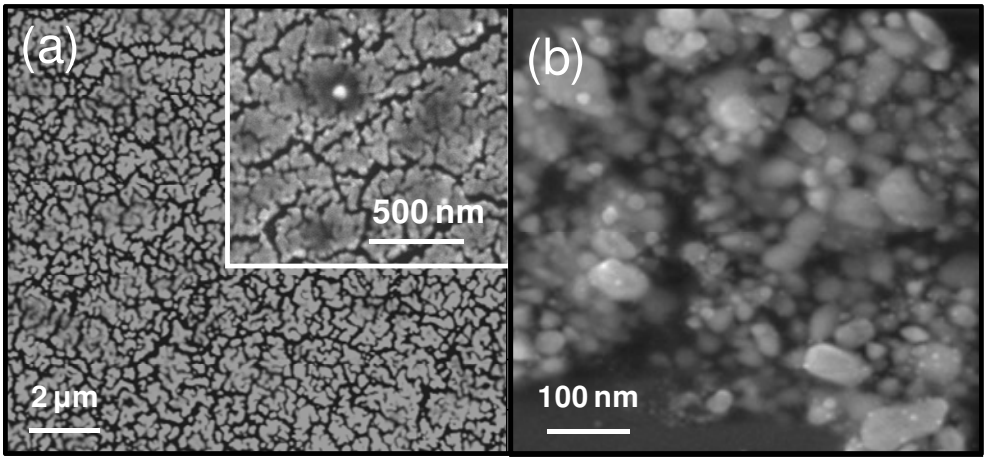

Figure 1.5.3 SEM image of (a) the metallised surface with magnified view in the inset and (b) the pristine surface of the film.

The golden surface was further characterized by XRD. The XRD pattern shown in **Figure 1.5.4**, is typical of a polycrystalline Au metal (JCPDS No. 040784).

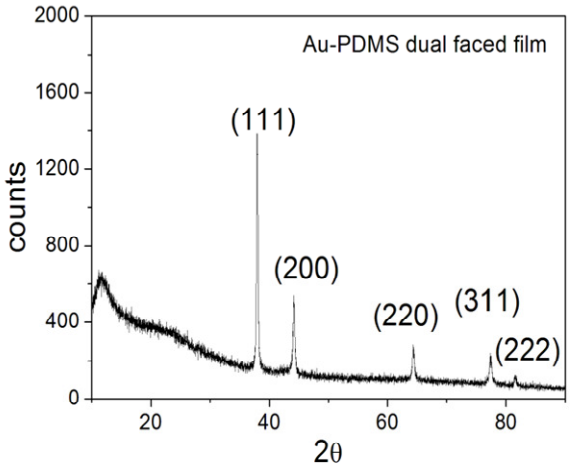

Figure 1.5.4 XRD pattern from the metallised face of PDMS corresponds to polycrystalline Au.

The metallised surface exhibited a linear I-V data (**Figure 1.5.5**) with a resistance of 22 Ω as calculated from its slope. The pristine surface was not electrically conducting. The resistance measured was beyond 10 GΩ.

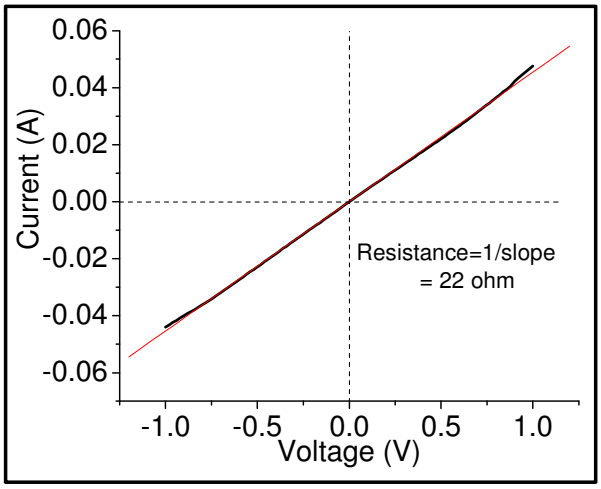

Figure 1.5.5 The I-V characteristics from the metallised surface.

The UV-visible spectra were recorded in both transmission and reflectance modes and are shown in **Figure 1.5.6**. In the transmission mode (**Figure 1.5.6a**), the plasmon peak appeared at 540 nm, irrespective of which surface faced the beam. On the other hand, the reflectance from the metallised surface was ~ 4 times higher compared to the pristine surface of the film (**Figure 1.5.6b**). Clearly, the metallisation process is effective.

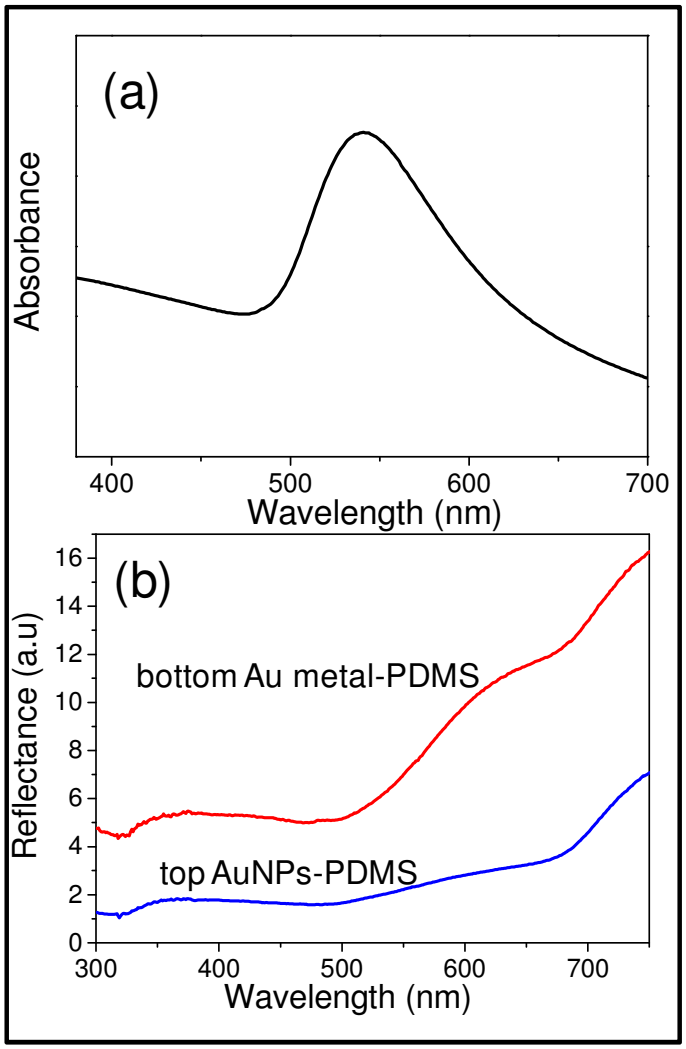

Figure 1.5.6 The UV-visible spectra of Au/PDMS film (a) in the transmission mode (b) in the reflectance mode.

For the projected use of the metallised PDMS in biomedical applications, it is important to know its wetting behavior. The contact angle was measured on either side of the film to

examine surface modification, if any, due to exposure to the Au(III) solution. The as-prepared film being quite fragile was cured by heating to 180 ºC for 12 hrs. The curing process made it sturdier. The contact angle on the metallic surface (**Figure 1.5.7**) was found to be 111º as seen in **Figure 1.5.7b** while the pristine surface on the other side of the film, gave an angle of 104° (**Figure 1.5.7a**), the literature values for PDMS range from 105º to 111º.[84] The metallisation has only a little effect on the wetting property of PDMS.

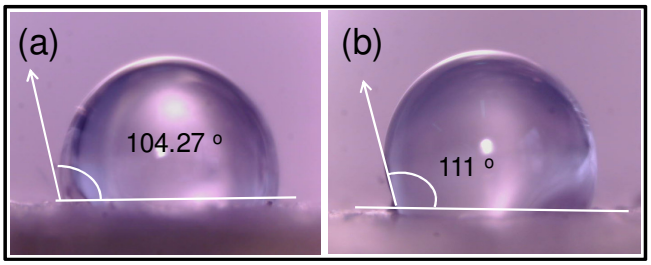

Figure 1.5.7 The contact angle of a water droplet (10 µl) placed over (a) pristine surface and (b) metallised surface.

The patterning of Au metallised PDMS layer was tried out using the microcontact printing technique as illustrated in **Figure 1.5.8.** The Au-PDMS film was transferred on a pre-patterned PDMS stamp. The stamp carrying the film was placed on the Si wafer and the dice was slowly heated to 180 ºC for 30 min (**Figure 1.5.8a**). The film gets partially cured and makes a good adhesion at regions in contact with the substrate. The stamp is then lifted up leaving the pattern on the Si substrate as shown in **Figure 1.5.8b**.

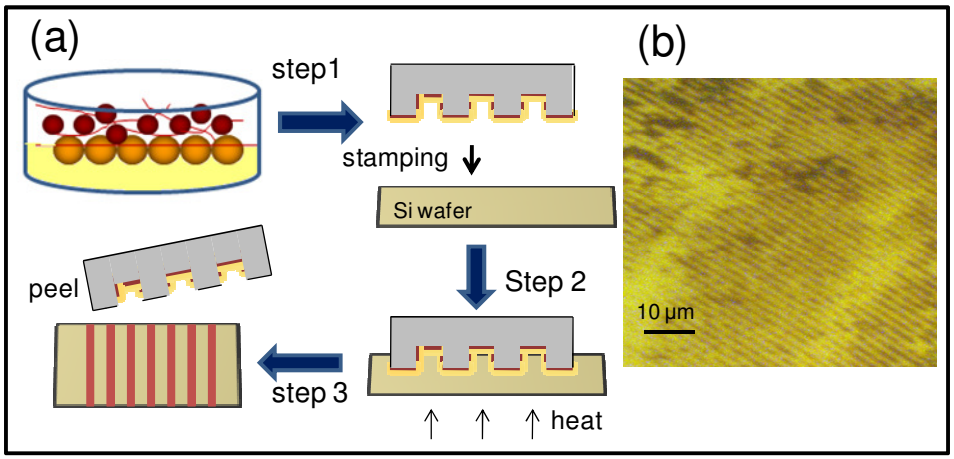

Figure 1.5.8 (a) the schematic procedure for patterning of metallised AuNPs-PDMS film. (b) The optical microscope image of the patterned surface at 100X magnification.

The AuNPs-PDMS gel offers as a system with right set of properties apt for preparing a flexible metallised film. It contains small Au particles which can potentially grow into big grains when exposed to a source of Au(III) ions. As the curing agent in the PDMS gel is not entirely used up, it can accelerate reduction of Au and growth of nanoparticles. Small polymeric chains being mobile across the layer volume can also contribute to the metallisation process. While the process reaches near completion, at the surface exposed to the solution, some growth at the top surface cannot be avoided, but does not harm in any way.

1.5.5 Conclusions

The metallisation of PDMS can be successfully done using this simple technique. This offers various applications in field of flexible electronics and optics. The process of metallisation in detail can be studied and possible applications including patterning can be explored further in future studies.

1.6 Ag nanoparticles–poly(dimethylsiloxane) composite

1.6.1 Introduction

Ag nanoparticle system (AgNPs) has attracted particular attention because of its optical properties,[108] broad efficacy against bacteria and relatively low toxicity to humans.[109] The synthesis of Ag nanoparticles has been reported in the literature by numerous methods.[110-113] The most popular method for Ag nanoparticles is the Lee–Meisel method[110] which produces a broad distribution of particle sizes. The most common method for the synthesis of nanosized Ag particles is the reduction of $AgNO_3$ with $NaBH_4$. The Creighton method[114] for synthesis generally yields ~10 nm particles of narrow size distribution. There are several other methods which employ capping agents such as self-assembled monolayers, surfactants, polymers, and dendrimers to protect the particles from aggregation. Three main steps in the preparation of nanoparticles that should be evaluated from a green chemistry perspective are the choice of the solvent medium used for the synthesis, the choice of an environmentally benign reducing agent, and the choice of a nontoxic material for the stabilization of the nanoparticles. There have been approaches reported for the synthesis of H_2O-soluble metal nanoparticles; however, to date there are only very few reports for a unified green chemistry approach to the overall process of nanoparticle production.[115]

1.6.2 Scope of the Investigation

The AgNPs-PDMS composite is prepared by following a green approach. The synthesis involves $AgNO_3$ as metal source precursor, PDMS (biodegradable and biocompatible) and water without need of extra stabilizing agent and reducing agent. The reaction can occur at room temperature without any energy inputs. Importantly, there are no side products in the reaction and the excess of precursor can be reused.

1.6.3 Experimental

The AgNPs-PDMS composite was synthesized in the form of foam, films and gels similar to AuNPs-PDMS nanocomposite (see **Section 1.1.3**) with the only difference that aq. $AgNO_3$ was used as a source of metal instead of using $KAuCl_4$.

1.6.4 Results and Discussion

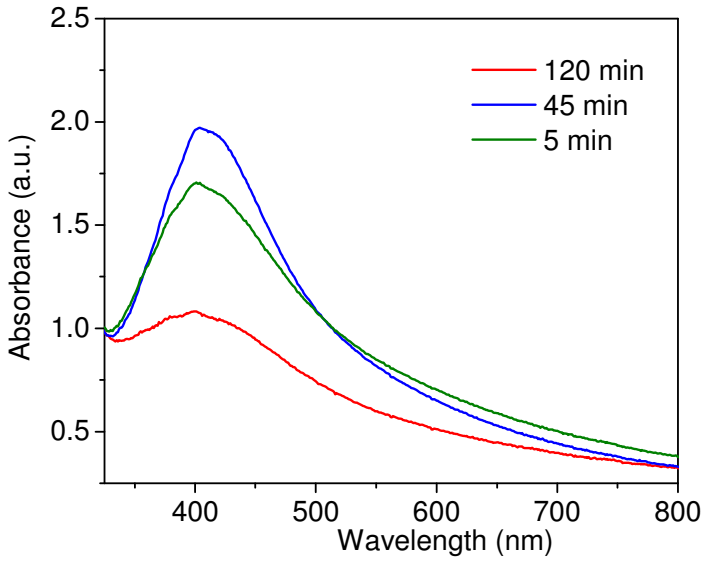

Figure 1.6.1 The UV-visible spectra of the Ag-PDMS gel prepared with aq. $AgNO_3$ solution at room temperature by stirring for different time intervals.

The formation of Ag nanoparticles in PDMS can be identified visually during synthesis. When the PDMS mixture consisting of elastomer and curing agent (in 10:1 ratio) is added to aq. Ag NO_3 solution, the white color of PDMS turns dirty-brown indicating the formation of AgNPs inside the PDMS matrix. **Figure 1.6.1** shows the UV-visible spectra of Ag-PDMS gel dissolved in toluene. The surface plasmon occurs at 405 nm with a broad absorption band.[114] The formation of Ag nanoparticles takes place very rapidly as seen from the absorption curve of low intensity after 5 minutes. The surface plasmon peak evolves more with increasing stirring time with highest absorption intensity after 2 hrs (**Figure 1.6.1**). The nanoparticles formed were visualized from TEM image as seen in **Figure 1.6.2**.

Figure 1.6.2a shows high magnification TEM image of the AgNPs-PDMS composite. It is seen that the particles are well defined, discrete and polydisperse in the PDMS matrix without any phase seperation. The contrast present in the image shows some particles are embedded inside the PDMS polymer matrix due to which these looks faint. The electron diffraction pattern in **Figure 1.6.2b** shows that the nanoparticles are crystalline and have a fcc structure. The size of nanoparticles varies between 5-20 nm.

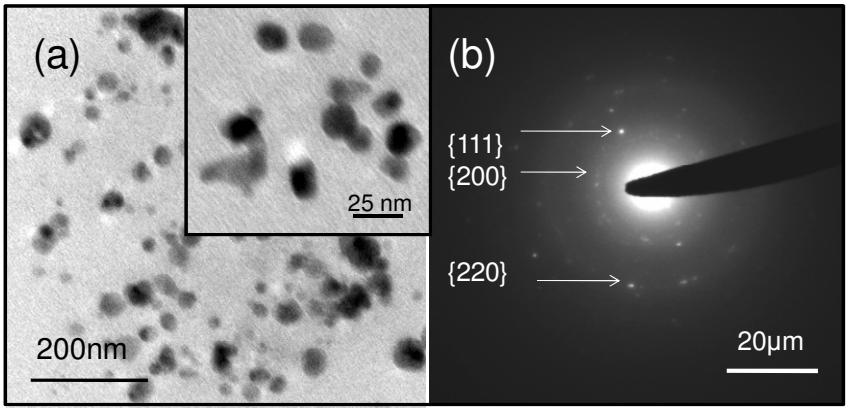

Figure 1.6.2 (a) TEM image of AgNPs-PDMS composite with magnified, high resolution image in the inset. **(b)** ED with lattice fringes marked.

The AgNPs-PDMS composite foams were also prepared by stirring mixture of PDMS with aq. $AgNO_3$ followed by heating above 60 ºC. The evolution of Ag plasmon peak with stirring time in case of foams prepared at 70 ºC can be seen in **Figure 1.6.3.** The plain PDMS foam also shows a broad absorption in the visible range. The intensity of absorption peak increased with stirring time. This may be due to higher loading of Ag nanoparticles with longer stirring. The different foams of AgNPs-PDMS composite were further tested for the antibacterial activity.

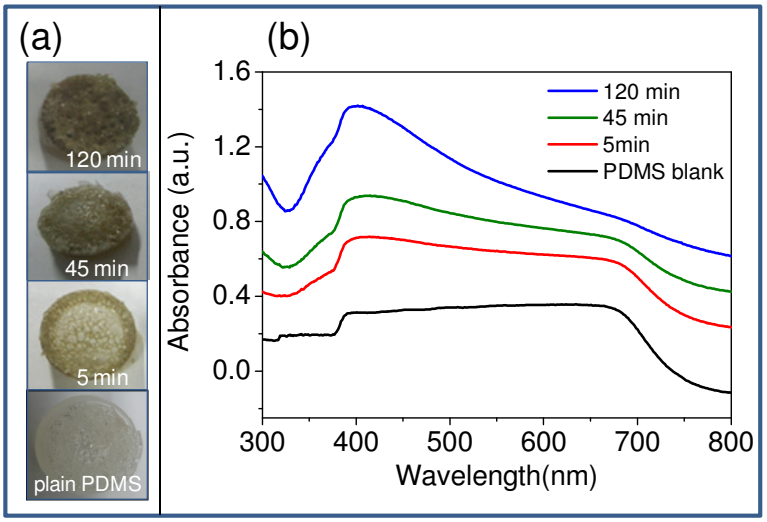

Figure 1.6.3 (a) Optical photographs of foams synthesized with different stirring time and corresponding (b) UV-visible spectra of foams.

Antibacterial Activity Test

Preliminary experiments have been carried out to check the antibacterial activity for varying amount of the AgNPs-PDMS composite foam. The AgNPs- PDMS foams were taken in different amounts and sterilized by autoclaving at 121 ºC for 30 min and then incubated overnight with microorganisms. Culture was diluted in the ratio 1:100 and was added to 5 test tubes (each 10µL) containing LB media. Ag PDMS foam (10, 30 and 50 mg) was added to the different test tubes. The LB media with 10ul culture and LB media with plain PDMS foam without Ag nanoparticles media were used as controls. Antimicrobial activity was tested on E. coli (strain DH5α, Gram negative) to evaluate antibacterial efficacy. The strains were grown on Luria-Bertani (LB) broth at 37 ºC while shaking. Bacterial growth was monitored in the presence of the foams. Growth of cells in suspensions was measured by Optical Density (OD) at 600 nm.

	Sample	OD_{600}
1.	C1(10 ml LB +10 µl Culture)	1.56
2.	C2 (plain PDMS+ 10 ml LB)	1.54
3.	10mg AgNPs-PDMS foam	1.55
4.	30mg AgNPs-PDMS foam	1.48
5.	50 mg AgNPs-PDMS foam	1.49

Table 1.6.1 The OD_{600} of different amount of AuNPs-PDMS foam along with controls.

The values of OD did not show much difference for AgNPs-PDMS foam as compared to the plain PDMS. Surprisingly, there is no antibacterial activity from the Ag nanoparticle containing nanocomposites.. This is in clear contrast to observations made in literature. It appears that a coating of PDMS covers the nanoparticles surface preventing them from interacting with the microbes. This observation clearly shows that the AgNPs-PDMS composite has potential to behave like an ideal system where Ag is not available for antimicrobial action though it is physically present. Further studies are required to access where such surfaces would be usefully applied.

1.6.5 Conclusions

The AgNPs-PDMS composites have been synthesized by an in-situ, single step green method in the form of foams, films as well as gels. The rheological property of AgNPs-PDMS gels is preserved for future studies. The uniqueness of AgNPs-PDMS composite can be realized only when the nature of the application is known.

References

1. Sepahvand, R.; Adeli, M.; Astinchap, B.; Kabiri, R., New nanocomposites containing metal nanoparticles, carbon nanotube and polymer. *J. Nanopar. Res.* **2008,** 10, 1309-1318.

2. Balazs, A. C.; Emrick, T.; Russel, T. P., Nanoparticle polymer composites: where two small worlds meet. *Science* **2006,** 315, 1107-1110.

3. Tamai, T.; Watanabe, M.; Hatanaka, Y.; Tsujiwaki, H.; Nishioka, N.; Matsukawa, K., Formation of metal nanoparticles on the surface of polymer particles incorporating polysilane by UV irradiation. *Langmuir* **2008,** 24, 14203-14208.

4. Muszynski, R.; Seger, B.; Kamat, P. V., Decorating Graphene Sheets with Gold Nanoparticles. *J. Phys. Chem. C* **2008,** 112, 5263-5266.

5. Hong, W.; Bai, H.; Xu, Y.; Yao, Z.; Gu, Z.; Shi, G., Preparation of Gold Nanoparticle/Graphene Composites with Controlled Weight Contents and Their Application in Biosensors. *J. Phys. Chem. C* ,**2009**,114, 1822-1826.

6. Peng, H., Aligned Carbon Nanotube/Polymer Composite Films with Robust Flexibility, High Transparency, and Excellent Conductivity. *J. Am. Chem. Soc.* **2007,** 130, 42-43.

7. Mbhele, Z. H.; Salemane, M. G.; van Sittert, C. G. C. E.; Nedeljkovic, J. M.; Djokovic, V.; Luyt, A. S., Fabrication and Characterization of Silver Polyvinyl Alcohol Nanocomposites. *Chem. Mater.* **2003,** 15, 5019-5024.

8. Prasad, K. E.; Das, B.; Maitra, U.; Ramamurty, U.; Rao, C. N. R., Extraordinary synergy in the mechanical properties of polymer matrix composites reinforced with 2 nanocarbons. *Proc. Nat. Acad. Sci.* **2009,** 106, 13186-13189.

9. Shan, J.; Tenhu, H., Recent advances in polymer protected gold nanoparticles: synthesis, properties, and applications. *Chem. Commun.* **2007**, 4580-4598.

10. Schmidt, G.; Malwitz, M. M., Properties of polymer-nanoparticle composites. *Curr. Op. Colloid Int. Sci.* **2003,** 8, 103-108.

11. Sershen, S. R.; Westcott, S. L.; Halas, N. J.; West, J. L., Independent optically addressable nanoparticle-polymer optomechanical composites. *Appl. Phys. Lett.* **2002,** 80, 4609-4611.

12. Govorov, A. O.; Zhang, W.; Skeini, T.; Richardson, H.; Lee, J.; Kotov, N. A., Gold nanoparticle ensembles as heaters and actuators: melting and collective plasmon resonances. *Nanoscale Res. Lett.* **2006,** 1, 84-90.

13. Bhuvana, T.; Subramaniam, C.; Pradeep, T.; Kulkarni, G. U., Conducting nanocrystal patterns using a silver organic complex blended with polystyrene as e-beam resist. *J. Phys.Chem. C* **2009,** 113, 7038-7043.

14. Niu, X.; Peng, S.; Liu, L.; Wen, W.; Sheng, P., Characterization and patterning of PDMS-based conducting composites. *Adv. Mater.* **2007,** 19, 2682-2686.

15. Basak, D.; Karan, S.; Mallik, B., Significant modifications in the electrical properties of poly(methyl methacrylate) thin films upon dispersion of silver nanoparticles. *Sol. Stat. Commun.* **2007,** 141, 483-487.

16. Kempa, T.; Carnahan, D.; Olek, M.; Correa, M.; Giersig, M.; Cross, M.; Benham, G.; Sennett, M.; Ren, Z.; Kempa, K., Dielectric media based on isolated metallic nanostructures. *J. Appl. Phys.* **2005,** 98, 034310.

17. Bai, H.-J.; Gou, H.-L.; Xu, J.-J.; Chen, H.-Y., Molding a silver nanoparticle template on polydimethylsiloxane to efficiently capture mammalian cells. *Langmuir* **2009,** 26, 2924

8. Zhao, W.; Sun, S.-X.; Xu, J.-J.; Chen, H.-Y.; Cao, X.-J.; Guan, X.-H., Electrochemical identification of the property of peripheral nerve fiber based on a biocompatible polymer film via in situ incorporating gold nanoparticles. *Anal. Chem.* **2008,** 80, 3769-3776.

19. Giuffrida, S.; Ventimiglia, G.; Sortino, S., Straightforward green synthesis of "naked" aqueous silver nanoparticles. *Chem. Commun.* **2009**, 7, 4055-4057.

20. Mark, J. E., Some interesting things about polysiloxanes. *Acc.Chem. Res.* **2004,** 37, 946-953.

21. Liu, C., Recent developments in polymer MEMS. *Adv. Mater.* **2007,** 19, 3783-3790.

22. Ratner, B. D.; Bryant, S. J., Biomaterials: Where we have been and where we are going In. *Annual Rev.Biomed. Engg.*, **2004**, 6, 41-75.

23. Prasad Shastri, V., Non-degradable biocompatible polymers in medicine: Past, present and future. *Curr. Pharma. Biotech.* **2003,** 4, 331-337.

24. Feng, X.; Huang, R. Y. M., Liquid separation by membrane pervaporation: a review. *Ind. Eng. Chem. Res.* **1997,** 36, 1048-1066.

25. Luo, C.; Fu, Q.; Li, H.; Xu, L.; Sun, M.; Ouyang, Q.; Chen, Y.; Ji, H., PDMS microfludic device for optical detection of protein immunoassay using gold nanoparticles. *Lab on a Chip - Miniaturisation for Chemistry and Biology* **2005,** 5, 726-729.

26. Lee, J. N.; Park, C.; Whitesides, G. M., Solvent Compatibility of Poly(dimethylsiloxane)-Based Microfluidic Devices. *Anal. Chem.,* **2003,** 75, 6544-6554.

27. Rao, C. N. R.; Thomas, P. J.; Kulkarni, G. U., *Nanocrystals : synthesis, properties and applications*. Springer: Berlin; New York, **2006**.

28. Daniel, M.-C.; Astruc, D., Gold nanoparticles: assembly, supramolecular chemistry, quantum-size-related properties, and applications toward biology, catalysis, and nanotechnology. *Chem. Rev.* **2004,** 104, 293-346.

29. Jadzinsky, P. D.; Calero, G.; Ackerson, C. J.; Bushnell, D. A.; Kornberg, R. D., Structure of a thiol monolayer-protected gold nanoparticle at 1.1 Å resolution. *Science* **2007,** 318, 430-433.

30. Huang, X.; Jain, P.; El-Sayed, I.; El-Sayed, M., Plasmonic photothermal therapy (PPTT) using gold nanoparticles. *Lasers in Medical Science* **2008,** 23, 217-228.

31. Jain, P. K.; ElSayed, I. H.; El-Sayed, M. A., Au nanoparticles target cancer. *Nano Today* **2007,** 2, 18-29.

32. Murphy, C. J.; Gole, A. M.; Stone, J. W.; Sisco, P. N.; Alkilany, A. M.; Goldsmith, E. C.; Baxter, S. C., Gold Nanoparticles in Biology: Beyond Toxicity to Cellular Imaging. *Acc. Chem. Res.* **2008,** 41, 1721-1730.

33. Juan , M. C.; Diego, L.; Rafael, L.; José , M. M.; Antonio , A. R., Sustainable Preparation of Supported Metal Nanoparticles and Their Applications in Catalysis. *Chem. Sus. Chem.* **2009,** 2, 18-45.

34. Haruta, M., Catalysis: Gold rush. *Nature* **2005,** 437, 1098-1099.

35. Rosi, N. L.; Giljohann, D. A.; Thaxton, C. S.; Lytton-Jean, A. K. R.; Han, M. S.; Mirkin, C. A., Oligonucleotide-modified gold nanoparticles for infracellular gene regulation. *Science* **2006,** 312, 1027-1030.

36. Zhang, Q.; Xu, J. J.; Liu, Y.; Chen, H. Y., In-situ synthesis of poly(dimethylsiloxane)-gold nanoparticles composite films and its application in microfluidic systems. *Lab on a Chip - Miniaturisation for Chemistry and Biology* **2008,** 8, 352-357.

37. Goyal, A.; Kumar, A.; Patra, P. K.; Mahendra, S.; Tabatabaei, S.; Alvarez, P. J. J.; John, G.; Ajayan, P. M., In situ synthesis of metal nanoparticle embedded free standing multifunctional PDMS films. *Macromol. Rap. Commun.* **2009,** 30, 1116-1122.

38. Walters, G.; Parkin, I. P., The incorporation of noble metal nanoparticles into host matrix thin films: synthesis, characterisation and applications. *J. Mater. Chem.* **2009,** 19, 574-590.

39. Yang, K.; Fan, H.; Malloy, K. J.; Brinker, C. J.; Sigmon, T. W., Optical and electrical properties of self-assembled, ordered gold nanocrystal/silica thin films prepared by sol-gel processing. *Thin Solid Films* **2005,** 491, 38-42.

40. Lisensky, G. C.; Campbell, D. J.; Beckman, K. J.; Calderon, C. E.; Doolan, P. W.; Rebecca, M. O.; Ellis, A. B., Replication and Compression of Surface Structures with Polydimethylsiloxane Elastomer. *J. Chem. Edu.,* **1999,** 76, 537.

41. James E. Mark, B. E., *Rubberlike Elasticity A molecular Primer*. Cambridge University Press: Cambridge, UK, **2007**.

42. Marceau, S.; Dubois, P.; Fulchiron, R.; Cassagnau, P., Viscoelasticity of Brownian Carbon Nanotubes in PDMS Semidilute Regime. *Macromolecules* **2009,** 42, 1433-1438.

43. Macosko, C. W., *RHEOLOGY: Principles, Measurements and Applications*. Wiley: **1994**.

44. Hughes, J. W. G. a. R. W., *Rheology for Chemists: An introduction*. 2nd ed.; The Royal Society of Chemistry. **2008**.

45. Nora, J. F.; Sabina, A.; Silvia, E. J.; Marta, E. D., Composites of polymeric gels and magnetic nanoparticles: Preparation and drug release behavior. *J. Appl. Polym. Sci.* **2007,** 105, 647-655.

46. Murugadoss, A.; Khan, A.; Chattopadhyay, A., Stabilizer specific interaction of gold nanoparticles with a thermosensitive polymer hydrogel, *J. Nanopar. Res.*, **2009**,11, 225.

47. Zhu, Z.; Thompson, T.; Wang, S.-Q.; von Meerwall, E. D.; Halasa, A., Investigating Linear and Nonlinear Viscoelastic Behavior Using Model Silica-Particle-Filled Polybutadiene. *Macromolecules* **2005,** 38, 8816-8824.

48. Paquien, J.-N.; Galy, J.; Gérard, J.-F.; Pouchelon, A., Rheological studies of fumed silica-polydimethylsiloxane suspensions. *Colloids and Surf. A: Physicochem. and Eng. Aspects* **2005,** 260, 165-172.

49. Jalili, K.; Abbasi, F.; Oskoee, S. S.; Alinejad, Z., Relationships between the morphology, swelling and mechanical properties of poly(dimethyl siloxane)/poly(acrylic acid) interpenetrating networks. *J. Mech. Behav. Biomed. Mater.* **2009,** 2, 534-541.

50. Jongkwan, K.; Riaz, A.; Seung Jong, L., Synthesis and linear viscoelastic behavior of poly(amic acid)-organoclay hybrid. *J. Appl. Poly. Sci.* **2001,** 80, 592-603.

51. Mackay, M. E.; Tuteja, A.; Duxbury, P. M.; Hawker, C. J.; Van Horn, B.; Guan, Z.; Chen, G.; Krishnan, R. S., General Strategies for Nanoparticle Dispersion. *Science* **2006,** 311, 1740-1743.

52. Zongming, G.; Julia Schulze, N.; James, E. M.; Adel, S., Poly(dimethylsiloxane) coatings for controlled drug release. I. Preparation and characterization of pharmaceutically acceptable materials. *J. Appl. Polym. Sci.* **2003,** 90, 658-666.

53. Zhang, Q.; Xu, J.-J.; Liu, Y.; Chen, H.-Y., In-situ synthesis of poly(dimethylsiloxane)-gold nanoparticles composite films and its application in microfluidic systems. *Lab on Chip* **2008,** 8, 352-357.

54. Mary, B.; Dubois, C.; Carreau, P.; Brousseau, P., Rheological properties of suspensions of polyethylene-coated aluminum nanoparticles. *Rheologica Acta* **2006,** 45, 561-573.

55. Pryamitsyn, V.; Ganesan, V., Origins of Linear Viscoelastic Behavior of Polymer Nanoparticle Composites. *Macromolecules* **2005,** 39, 844-856.

56. Olhero, S. M.; Ferreira, J. M. F., Influence of particle size distribution on rheology and particle packing of silica-based suspensions. *Powder Technology* **2004,** 139, 69-75.

57. Abraham, T. N.; Debdatta, R.; Siengchin, S.; Karger-Kocsis, J., Rheological and thermal properties of poly(ethylene oxide)/multiwall carbon nanotube composites. *J. App. Polym. Sci.,* **2008,** 110, 2094-2101.

58. Hu, B.; Fuchs, A.; Huseyin, S.; Gordaninejad, F.; Evrensel, C., Supramolecular magnetorheological polymer gels. *J. Appl. Polym. Sci.,* **2006,** 100, 2464-2479.

59. Seila, S.; Sarah, M. M.; Yue, H., Aging effects of precipitated silica in poly(dimethylsiloxane). *J. Rheo.* **2007,** 51, 325-340.

60. Cleaning up water. *Nat. Mater.,* **2008,** 7, 341-341.

61. Shannon, M. A.; Bohn, P. W.; Elimelech, M.; Georgiadis, J. G.; Marinas, B. J.; Mayes, A. M., Science and technology for water purification in the coming decades. *Nature* **2008,** 452, 301-310.

62. Metes, A.; Kovacevic, D.; Vujevic, D.; Papic, S., The role of zeolites in wastewater treatment of printing inks. *Water Res.,* 38, 3373-3381.

63. Natasa Zabukovec Logar, V. K., Nanoporous Materials: From Catalysis and Hydrogen Storage to Wastewater Treatment. *Acta Chim. Slov.,* **2006,** 53, 117-135.

64. DeQuan Li, M. M., Nanosponges for water purification. *Clean Products and Processes,* **2000,** 2, 112-116.

65. Pillay, K.; Cukrowska, E. M.; Coville, N. J., Multi-walled carbon nanotubes as adsorbents for the removal of parts per billion levels of hexavalent chromium from aqueous solution. *J. Hazard. Mater.,* **2009,** 166, 1067-1075.

66. Y. H. Li, Y. M. Z., W. B. Hu, I. Ahmad,Y. Q. Zhu, J. Peng,; Luan, Z. K., Carbon nanotubes - the promising adsorbent in wastewater treatment. *J. Phys.: Conf. Ser.,* **2007,** 61, 698-702.

67. Tiwari, D. K.; Behari, J.; Sen, P., Application of Nanoparticles in Waste Water Treatment, World. A. *Sci. J.* **2008,** 3, 417-433.

68. Xiwang, Z.; Tong, Z.; Jiawei, N.; Darren Delai, S., High-Performance Multifunctional TiO_2 Nanowire Ultrafiltration Membrane with a Hierarchical Layer Structure for Water Treatment. *Adv. Func. Mater. ,* **2009,** 19, 3731-3736.

69. Zuo, X.; Peng, C.; Huang, Q.; Song, S.; Wang, L.; Li, D.; Fan, C., Design of a carbon nanotube/magnetic nanoparticle-based peroxidase-like nanocomplex and its application for highly efficient catalytic oxidation of phenols. *Nano Res.,* **2009,** 2, 617-623.

70. Xuchun, G.; Jinquan, W.; Kunlin, W.; Anyuan, C.; Hongwei, Z.; Yi, J.; Qinke, S.; Dehai, W., Carbon Nanotube Sponges. *Adv. Mater.,* 22, 617-621.

71. Park, I., Efimenko, K., Sjablom, J., Genzer, J., Rapid Removal of Organics and Oil Spills from water using Silicone Rubber "Sponges". *J. Disp. Sci. and Tech.,* **2009,** 30, 318 - 327.

72. T. Pradeep, A., Noble metal nanoparticles for water purification: a critical review. *Thin Solid Films,* **2009,** 517,6441-64478

73. Lee, J. N.; Park, C.; Whitesides, G. M., Solvent compatibility of poly(dimethylsiloxane)-based microfluidic devices. *Anal. Chem.,* **2003,** 75, 6544-6554.

74. Gevers, L. E. M.; Vankelecom, I. F. J.; Jacobs, P. A., Solvent-resistant nanofiltration with filled polydimethylsiloxane (PDMS) membranes. *J. Memb. Sci.* **2006,** 278, 199-204.

75. Ichiura, H.; Kitaoka, T.; Tanaka, H., Removal of indoor pollutants under UV irradiation by a composite TiO_2-zeolite sheet prepared using a papermaking technique. *Chemosphere,* **2003,** 50, 79-83.

76. Gao, S.; Zhang, H.; Wang, X.; Yang, J.; Zhou, L.; Peng, C.; Sun, D.; Li, M., Unique gold sponges: Biopolymer-assisted hydrothermal synthesis and potential application as surface-enhanced Raman scattering substrates. *Nanotech.* **2005,** 16, 2530-2535.

77. Roig, B.; Chalmin, E.; Touraud, E.; Thomas, O., Spectroscopic study of dissolved organic sulfur (dos): A case study of mercaptans. *Talanta* **2002,** 56, 585-590.

78. Tobien, T.; Cooper, W. J.; Nickelsen, M. G.; Pernas, E.; O'Shea, K. E.; Asmus, K.-D., Odor Control in Wastewater Treatment: The Removal of Thioanisole from WaterA Model Case Study by Pulse Radiolysis and Electron Beam Treatment. *Environ. Sci. & Tech.* **2000,** 34, 1286-1291.

79. Pouly, F.; Touraud, E.; Buisson, J. F.; Thomas, O., An alternative method for the measurement of mineral sulphide in wastewater. *Talanta* **1999,** 50, (4), 737-742.

80. Ma, Z.; Mao, Z.; Gao, C., Surface modification and property analysis of biomedical polymers used for tissue engineering. *Colloids Surf. B: Biointerfaces.* **2007,** 60, 137-157.

81. Daniel, M.-C.; Astruc, D., Gold Nanoparticles: Assembly, Supramolecular Chemistry, Quantum-Size-Related Properties, and Applications toward Biology, Catalysis, and Nanotechnology. *Chem. Rev.,* **2003,** 104, 293-346.

82. Guo, R.; Zhang, L.; Qian, H.; Li, R.; Jiang, X.; Liu, B., Multifunctional Nanocarriers for Cell Imaging, Drug Delivery, and Near-IR Photothermal Therapy. *Langmuir* **2009,** 26, 5428-5434

83. Mrinmoy, D.; Partha, S. G.; Vincent, M. R., Applications of Nanoparticles in Biology. *Adv. Mater.* **2008,** 20, 4225-4241.

84. Wu, J.; Bai, H.-J.; Zhang, X.-B.; Xu, J.-J.; Chen, H.-Y., Thermal/Plasma-Driven Reversible Wettability Switching of a Bare Gold Film on a Poly(dimethylsiloxane) Surface by Electroless Plating. *Langmuir* **2009,** 26, 1191-1198.

85. Lee, J. N.; Jiang, X.; Ryan, D.; Whitesides, G. M., Compatibility of Mammalian Cells on Surfaces of Poly(dimethylsiloxane). *Langmuir* **2004,** 20, 11684-11691.

86. Hu, S.; Ren, X.; Bachman, M.; Sims, C. E.; Li, G. P.; Allbritton, N., Surface Modification of Poly(dimethylsiloxane) Microfluidic Devices by Ultraviolet Polymer Grafting. *Anal. Chem.,* **2002,** 74, 4117-4123.

87. Min-Hsien, W., Simple poly(dimethylsiloxane) surface modification to control cell adhesion. *Surf. and Inter. Anal.,* **2009,** 41, 11-16.

88. Kirill Efimenko, W. E. W., and Jan Genzer, Surface Modification of Sylgard-184 Poly(dimethyl siloxane) Networks by Ultraviolet and Ultraviolet/Ozone Treatment. *J. Colloid and Inter. Sci.* **2002,** 254, 9.

89. Valerie, A. L.; William, E. J.; Sangeeta, N. B., Engineering protein and cell adhesivity using PEO-terminated triblock polymers. *J. Biomed. Mater.Res.* **2002,** 60, 126-134.

90. Lee, J. H.; Ju, Y. M.; Kim, D. M., Platelet adhesion onto segmented polyurethane film surfaces modified by addition and crosslinking of PEO-containing block copolymers. *Biomaterials* **2000,** 21, 683-691.

91. Klasner, S. A.; Metto, E. C.; Roman, G. T.; Culbertson, C. T., Synthesis and Characterization of a Poly(dimethylsiloxane)-Poly(ethylene oxide) Block Copolymer for Fabrication of Amphiphilic Surfaces on Microfluidic Devices. *Langmuir* **2009,** 25, 10390-10396.

92. Alvaro, M.; Cynthia, B.; Aaron, J. F.; George, M.; Shuvo, R., Growth of connective tissue progenitor cells on microtextured polydimethylsiloxane surfaces. *J. Biomed. Mater. Res.* **2002,** 62,499-506.

93. Van Wachem, P. B.; Hogt, A. H.; Beugeling, T.; Feijen, J.; Bantjes, A.; Detmers, J. P.; van Aken, W. G., Adhesion of cultured human endothelial cells onto methacrylate polymers with varying surface wettability and charge. *Biomaterials* **1987,** 8, 323-328.

94. Chandrasekharan, N.; Kamat, P. V.; Hu, J.; Jones, G., Dye-Capped Gold Nanoclusters: Photoinduced Morphological Changes in Gold/Rhodamine 6G Nanoassemblies. *J. Phys. Chem. B* **2000,** 104, 11103-11109.

95. McDonald, J. C.; Whitesides, G. M., Poly(dimethylsiloxane) as a Material for Fabricating Microfluidic Devices. *Acc. Chem. Res.* **2002,** 35, 491-499.

96. Khang, D.-Y.; Jiang, H.; Huang, Y.; Rogers, J. A., A Stretchable Form of Single-Crystal Silicon for High-Performance Electronics on Rubber Substrates. *Science* **2006,** 311, 208-212.

97. Ko, H. C.; Stoykovich, M. P.; Song, J.; Malyarchuk, V.; Choi, W. M.; Yu, C.-J.; Geddes Iii, J. B.; Xiao, J.; Wang, S.; Huang, Y.; Rogers, J. A., A hemispherical electronic eye camera based on compressible silicon optoelectronics. *Nature* **2008,** 454, 748-753.

98. Choi, M.-C.; Kim, Y.; Ha, C.-S., Polymers for flexible displays: From material selection to device applications. *Prog. Polym. Sci.* **2008,** 33, 581-630.

99. Huck, W. T. S.; Bowden, N.; Onck, P.; Pardoen, T.; Hutchinson, J. W.; Whitesides, G. M., Ordering of Spontaneously Formed Buckles on Planar Surfaces. *Langmuir* **2000,** 16, 3497-3501.

100. Lee, K. J.; Fosser, K. A.; Nuzzo, R. G., Fabrication of Stable Metallic Patterns Embedded in Poly(dimethylsiloxane) and Model Applications in Non-Planar Electronic and Lab-on-a-Chip Device Patterning. *Adv. Func. Mater.,* **2005,** 15, 557-566.

101. Lim, K. S.; Chang, W.-J.; Koo, Y.-M.; Bashir, R., Reliable fabrication method of transferable micron scale metal pattern for poly(dimethylsiloxane) metallization. *Lab on a Chip* **2006,** 6, 578-580.

102. Siegel, A. C.; Bruzewicz, D. A.; Weibel, D. B.; Whitesides, G. M., Microsolidics: Fabrication of Three-Dimensional Metallic Microstructures in Poly(dimethylsiloxane). *Adv. Mater.,* **2007,** 19,727-733.

103. Tsuyoshi, S.; Takao, S., Stretchable, Large-area Organic Electronics. *Adv. Mater.,* **2010***,* NA.

104. Jung, Y. J.; Kar, S.; Talapatra, S.; Soldano, C.; Viswanathan, G.; Li, X.; Yao, Z.; Ou, F. S.; Avadhanula, A.; Vajtai, R.; Curran, S.; Nalamasu, O.; Ajayan, P. M., Aligned Carbon Nanotube Polymer Hybrid Architectures for Diverse Flexible Electronic Applications. *Nano Lett.* **2006,** 6, 413-418.

105. Bowden, N.; Brittain, S.; Evans, A. G.; Hutchinson, J. W.; Whitesides, G. M., Spontaneous formation of ordered structures in thin films of metals supported on an elastomeric polymer. *Nature* **1998,** 393, 146-149.

106. Zhang, Q.; Xu, J. J.; Liu, Y.; Chen, H. Y., *Lab Chip* **2008,** 8, 352.

107. Hao, Z.; Chen, H.; Ma, D., Preparation of Micro Gold Devices on Poly(dimethylsiloxane) Chips with Region-Selective Electroless Plating. *Anal.Chem.* **2009,** 81, 8649-8653.

108. David, D. E., Jr.; George, C., Synthesis and Optical Properties of Silver Nanoparticles and Arrays. *ChemPhysChem* **2005,** 6, 1221-1231.

109. Hollinger; M, A., *Toxicological aspects of topical silver pharmaceuticals*. Informa Healthcare: Colchester, ROYAUME-UNI, **1996**, 26, 255-260.

110. Rivas, L.; Sanchez-Cortes, S.; Garc-a-Ramos, J. V.; Morcillo, G., Growth of Silver Colloidal Particles Obtained by Citrate Reduction To Increase the Raman Enhancement Factor. *Langmuir* **2001,** 17, 574-577.

111. Sambhy, V.; MacBride, M. M.; Peterson, B. R.; Sen, A., Silver Bromide Nanoparticle/Polymer Composites: Dual Action Tunable Antimicrobial Materials. *J. Am. Chem. Soc.* **2006,** 128, 9798-9808.

112. Keskinen, H.; Mäkelä, J.; Aromaa, M.; Keskinen, J.; Areva, S.; Teixeira, C.; Rosenholm, J.; Pore, V.; Ritala, M.; Leskelä, M.; Raulio, M.; Salkinoja-Salonen, M.; Levänen, E.; Mäntylä, T., Titania and titania-silver nanoparticle deposits made by Liquid Flame Spray and their functionality as photocatalyst for organic- and biofilm removal. *Catal. Lett.* **2006,** 111, 127-132.

113. Eckelman, M. J.; Graedel, T. E., Silver Emissions and their Environmental Impacts: A Multilevel Assessment. *Environ. Sci. & Tech.* **2007,** 41, 6283-6289.

114. Pancek, A.; Kvtek, L.; Prucek, R.; Kol, M.; Vec, R.; Pizrov, N.; Sharma, V. K.; Nevcn, T. j.; Zbol, R., Silver Colloid Nanoparticles: Synthesis, Characterization, and Their Antibacterial Activity. *J. Phys. Chem. B* **2006,** 110,16248-16253.

115. Jyothish, K.; Vemula, P. K.; Jadhav, S. R.; Francesconi, L. C.; John, G., Self-standing, metal nanoparticle embedded transparent films from multi-armed cardanol conjugates through in situ synthesis. *Chem. Commun.* **2009**, 36, 5368-5370.

Part 2

Pd Nanowire Gratings for Optical Diffraction based Sensor*

Summary

Pd nanowire diffraction gratings of controllable thickness have been fabricated using micromolding in capillary lithographic technique. These metal nanostructures are not only robust and uniform over large areas but also give diffraction patterns with at least 1000 times better resolution than the conventional gratings. The grating parameters such as height and width have been optimized to give maximum diffraction intensity in transmission mode. The utility of the produced gratings as optical sensors is demonstrated by performing the electroless deposition of Cu on Pd nanowire diffraction gratings as a model study. The amount of Cu getting deposited electrolessly has been monitored by collecting optical diffraction signals and compared with results from SEM and EDS analysis. The changes in diffraction grating height influencing the diffraction efficiency have been estimated using AFM. This result clearly brings out the optical diffraction based sensing from the patterned grating structure.

*This work was presented in ICONSAT -2010 held at IIT-Bombay. It won the Best Poster Award.

2.1 Introduction

Optical diffraction based sensing has emerged out as one of the simplest as well as promising detection tool. Minute changes in the diffraction intensities can be used as a sensor signal for events taking place on grating surface. For instance, biochemical and chemical sensing[1] has been performed a decade ago by employing few tens of micron sized diffraction gratings for detection of cells[2] and biomolecules[3-5] with fairly good sensitivity. Hupp et al.[6-8] performed sensing of volatile compounds, electrochemically induced changes in polymers as well as DNA detection with chemoresponsive diffraction gratings. Goh et al.[5,9] demonstrated multiple analytes binding ability simultaneously as a function of time using diffraction based system. Using in-situ assembled diffraction gratings, Savran et al.[10-14] could carry out biomolecular studies of various diseases and bacterial cells. Recently, Corn et al.[15] has reported fabrication of ordered arrays of Au and Ni nanowire gratings on a transparent surface as sensor material. With increasing interest in 1D nanoparticle assemblies, CdSe nanocrystals have been patterned using microcontact molding for the fabrication of efficient transmission gratings for chemical sensor applications.[16]

The diffractometry set up is simplest in the transmission mode with 3 basic requirements: a laser source, sample grating and detector. An inexpensive laser source of power as low as 1mW and small photodiode as detector should suffice for this purpose. The nature of grating is highly varied- from simple grating (few microns to few hundred nm) to 2D gratings.[1,6,15,16] The diffraction intensity not only depends on the refractive index of the surrounding medium but also on the grating parameters such as the width, spacing and thickness of the diffractive optical element. The spacing between the optical elements directly influence the resolution of the diffraction pattern. The resolution (R) is equal to the product of the diffraction order (m) and the number of grating lines in the laser illuminated area.[17]

$$R = m\left(\frac{W}{d}\right) \qquad (1)$$

where W is the laser illuminated area and d is the spacing of diffractive optical element. This means that the resolution of diffraction pattern can be enhanced by decreasing the spacing of the diffractive optical element keeping the laser illuminated area and wavelength constant. The

width, w of diffractive optical element influences the intensity and position of the diffraction spots. The grating equation is generally given by

$$\sin\theta - \sin\gamma = m\frac{\lambda}{D} \qquad (m = \pm 1,\ \pm 2) \qquad (2)$$

where D is the grating period, m is the order of interference, λ is the wavelength of light used, θ is the incidence angle and γ is the diffraction angle. The smaller the value of grating period higher will be angular divergence of the diffraction orders thus enabling use of simple photodetectors instead of CCD camera or any other expensive instrumentation. For an ideal diffraction grating, the height or the thickness of grating of $\frac{\lambda}{8}$ brings the phase difference between land and ridge to $\frac{\pi}{2}$ resulting in interferometric detection with maximum linear sensitivity.[10,18,19]

The diffraction efficiency, DE (%) of the grating is calculated as:[10, 14]

$$DE = \frac{I_1}{I_0} \qquad (3)$$

where I_1 is the intensity of first order diffraction spot (± 1) and I_0 is the zeroth order mode. Note: It is thus reasonable to study the grating parameters that alter the intensity of diffraction spots for achieving higher diffraction efficiencies.

There is more impetus to fabricate gratings with optimized grating parameters for achieving higher sensitivities and miniaturization of the sensor device.[1] Cui et al. [20] used two beam interference method followed by dry etching process to fabricate 1D metal grating with width 400 nm, thickness of 25 nm, and a spacing of 230 nm for improving the plasmonic coupling efficiency.

The sophistication in grating structures thus calls for advanced lithography fabrication tools. Photolithography is routinely employed to make grating patterns.[2] Conventional soft lithographic methods such as microcontact printing,[21,22] have been most commonly used to fabricate low cost diffraction gratings. Multiple beam interference[12] and electron beam lithography[14] though have capability of patterning over large areas but are expensive techniques. It is found that the fabrication of efficient and optically transmitting diffraction grating is very limited and still challenging aspect. The problem has been high absorptivity and

diffusivity along with poor adhesion of molecular inks to the transparent substrate. Metal nanowire grating patterns have been found to be optically transparent for light transmission.[23]

2.2 Scope of the Investigation

A simple way of fabricating a metal grating structure based on a direct micromolding in capillaries is presented. Pd alkanethiolate is used as single precursor source for molding in the capillary type channels of a PDMS mold.[24] Thus created Pd nanowire grating has been tested as optical sensing element for electroless deposition of Cu. The Pd nanowires obtained acted as catalytic surface for electroless deposition of Cu. The extent of electroless deposition of Cu taking place over Pd surface is estimated by measuring the Diffraction efficiency (DE) of the patterned Pd nanowire grating. In addition, we have examined the Cu deposition by AFM, SEM and EDS and compared with the diffraction data.

2.3 Experimental

The process of fabrication of Pd nanowire grating is illustrated in **Figure 2.1a**.

Preparation of the mold

Elastomeric stamps were fabricated by replica molding of polydimethylsiloxane (PDMS) on a commercially available compact disk (Sony CD-R). PDMS was prepared by mixing Sylgard-184 elastomer and the curing agent (Dow Corning) in the ratio 10:1.The mixture was sonicated at room temperature to reduce the air bubbles and then degassed under vacuum for 1 hour. PDMS mixture was poured onto the master (CD) and then cured in an oven at 60 °C for 6 hours. PDMS stamps were cleaned using hexane and sonicated in ethanol to remove any uncured polymer. The resulting stamp hosted relief features of width 500 ± 5 nm with intermediate channels of 1000 ± 5 nm width.

Synthesis of Pd precursor

The precursor employed for patterning the nanowires was Pd hexadecylthiolate, $Pd(SC_{16}H_{33})_2$, in toluene.[25] The synthesis of precursor involves single step procedure. $Pd(OAc)_2$ (5.0 mmol) in 7 ml toluene was added to 5.0 mmol of hexadecylthiol in toluene (3 ml), and the resulting mixture was stirred vigorously overnight resulting in a yellow viscous color solution which further deepened to orange-yellow. The obtained thiolate was washed with methanol followed

by precipitation to remove excess thiol. The solid was redissolved to obtain a concentrated 40 mM solution.

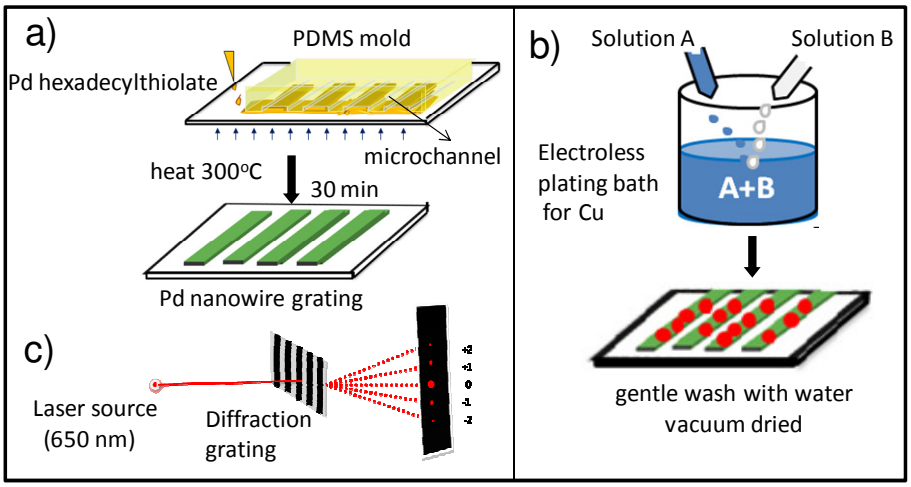

Figure 2.1 (a) Schematic illustration of the procedure used for fabricating Pd nanowire grating (b) electroless deposition of Cu on the Pd nanowire grating and (c) the diffraction set up.

Patterning of the grating

The glass slide used was cut into small pieces of 1 x 1 cm^2 and cleaned by sonicating in acetone and double-distilled water and dried under flowing argon. Approximately 30 µl of the precursor solution (20 mM in toluene) was dropped at one edge of the PDMS stamp kept on the substrate to fill the channels spontaneously by capillary action as seen in **Figure 2.1a**. The set up was gradually heated on a hot plate to reach 250 °C and was held for 30 min. Following cooling to room temperature, the stamp was removed leaving behind the patterns on the substrate.

Electroless Deposition of Cu

The deposition is initiated in an auto catalytic manner on the patterned Pd surface. The copper plating bath used for electroless Cu deposition[26] consisted of solution A (1.5 g of $CuSO_4$, 7 g of $KNaC_4H_4O_6 \cdot 4H_2O$ and 7 g of NaOH in 50 ml water) and solution B (37.2 wt% aqueous formaldehyde solution). The two solutions were taken in 10:1 (v/v) ratio and mixed together just before the electroless plating was performed as shown in **Figure 2.1b**. Each substrate was taken out after a predetermined time interval and immersed in a water bath to arrest the

reaction. The substrates were vacuum dried prior to diffraction experiments. The electroless bath was freshly prepared in each case to avoid the influence of aging.

Diffraction setup

A circular grating area slightly larger than the beam size (0.5 cm) was defined by scratching away rest of the patterned metal with a razor blade. The laser beam was aligned with respect to the designated circular area with help of a monocular eyepiece. The diffraction experiments were performed using a diode laser source (650 nm, 3 mW). The laser beam was focussed normal to the grating surface using a convex lens as shown in **Figure 2.1c**. The transmitted light after diffraction was measured using a photodiode (Thorlabs, DET 200) connected to digital oscilloscope (Hewlett Packard-54600B,100 MHz). The intensity of diffraction spots was measured from a fixed distance (3 cm) from the sample by placing the photodetector adjacent to screen position. In addition, the diffraction images were photographed using a digital camera.

Other characterisation

AFM measurements were performed using Veeco di Innova SPM in the tapping mode. Standard Si cantilevers were used for the normal topography imaging. The surface roughness was estimated from the AFM images using an offline software, Nanoscope v7.30. The patterned substrates were also examined under a Nova NanoSEM 600 instrument (FEI Co., The Netherlands). Energy-dispersive spectroscopy (EDS) analysis was performed with an EDAX Genesis instrument (Mahwah, NJ) attached to the SEM column.

2.4 Results and Discussion

Pd hexadecylthiolate was chosen as 'ink' for micromolding because it readily dissolves in organic solvents such as toluene with tunable viscosity and remains stable under ambient for longer time periods. Under the molding conditions at 250 ^{o}C, the 'ink' also undergoes thermolysis to give rise to Pd metal nanowire structures.[24] In order to achieve the desired nanowire height, the micromolding was performed with varying concentrations of the precursor solution viz., 2, 5 10, 15, 20 and 25 mM, keeping other molding conditions such as heating temperature, annealing rate etc. constant (see **Section 2.3**). The surface morphology of the patterns along with the height profiles obtained from AFM, is shown in **Figure 2.2a-f.**

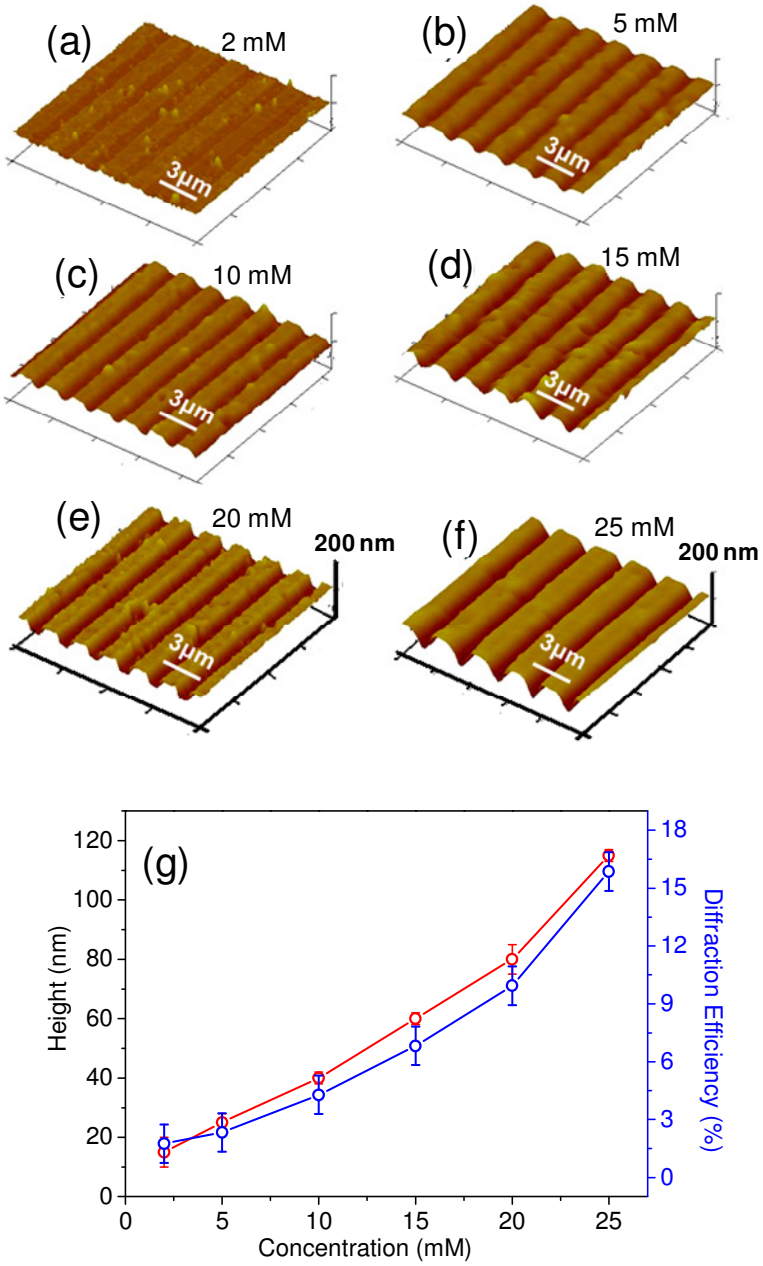

Figure 2.2 (a)-(f) AFM images of Pd nanowire gratings of different heights on glass substrates. The concentration of the precursor solution used is indicated in each case. (g) The variation in the grating height and diffraction efficiency with the precursor concentrations.

The grating structures are generally smooth (roughness, ~ 5-10 nm) with some protruding features perhaps arising while removing the stamp from the substrate. The height of the grating

was found to increase with increasing concentration of the precursor solution, from ~ 15 nm with 2 mM solution to ~ 115 nm with 25 mM. The variation is nearly linear up to 20 mM (**Figure 2.2g).** The diffraction efficiency from these grating structures is calculated and plotted as shown in **Figure 2.2g** (blue curve). It is observed to be varying in accordance with the grating height. The Pd nanowire grating with height of 82 nm (width 1043 nm and spacing of 490 nm), (**Figure2.2e**) was chosen for further diffraction studies and characterization. This grating was so chosen since it satisfies the quadrature condition where height of the grating is between 0 and λ/4 (λ = 650 nm) and results in diffraction pattern of high intensity and linear sensitivity for small height variations.[1, 2] The initial diffraction efficiency was calculated to be ~ 11% for this nanowire grating.

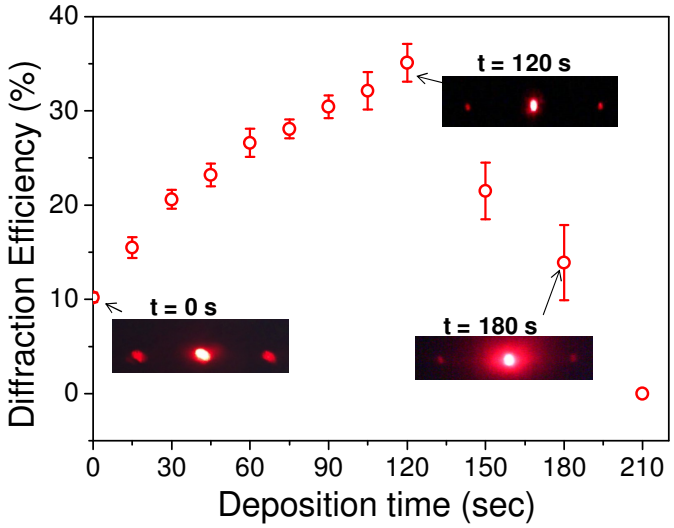

Figure 2.3 Variation in the diffraction efficiency (DE) with electroless plating time. Some of the diffraction patterns are shown alongside.

Figure 2.3 depicts the plot of diffraction efficiency as a function of Cu deposition time interval. The values of I_1 and I_o were calculated by taking average from minimum 7 different areas of the same sample for accuracy. The diffraction pattern obtained shows relatively sharp spots with high first order intensity upto 120 s of Cu deposited with increasing diffraction efficiency which gradually declined on Cu deposition beyond 120 s (see **inset**). Beyond 120 s, the diffraction efficiency values drop suddenly to reach near zero at 210 s. These changes are better understood based on further characterisation of the grating structures.

The SEM image shows that the Cu gets deposited in the form of small grains on Pd nanowires as seen after 90 s of electroless deposition in **Figure 2.4b** as compared to **Figure 2.4a** without any Cu. Interestingly, the growth of Cu on Pd takes place only at the regions wherever Pd is present and by this way, Cu deposition in any non-specific region is prevented. Based on Cu K EDS signals obtained from EDS analysis over 3 different areas, the respective atom percentage values was calculated. The amount of Cu deposition with respect to Pd is less in the beginning which shoots up after 120 s of dipping in electroless bath (**Figure 2.4c**).

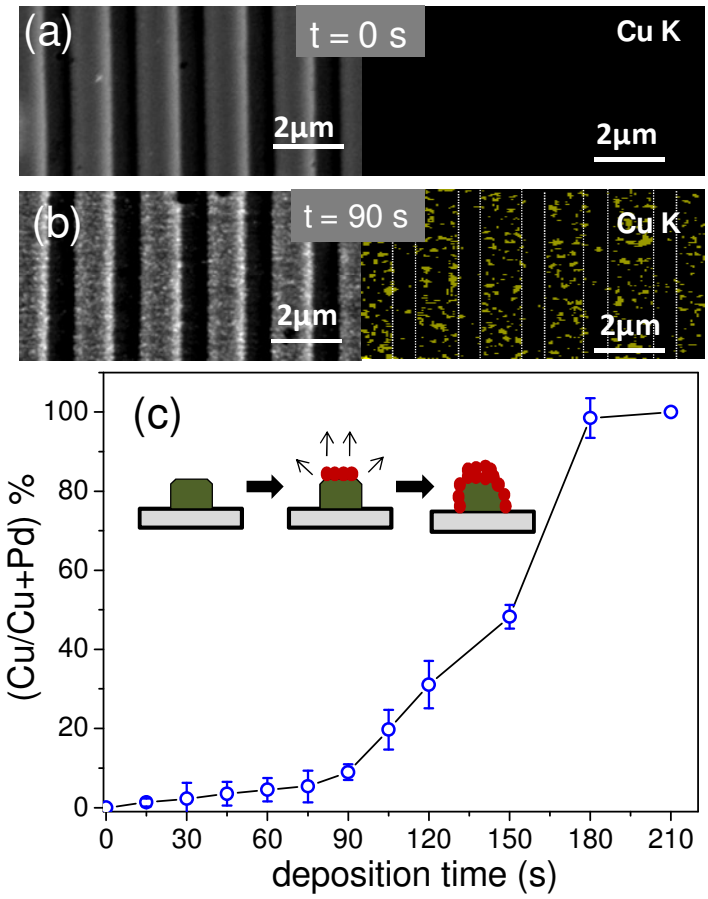

Figure 2.4 SEM micrograph (left) of Pd nanowire grating structure (a) before and (b) after dipping in Cu plating solution for 90 s and the corresponding EDS map (right) of Cu K indicating the electroless deposition of Cu onto Pd lines. (c) The atom percentage of Cu deposited over Pd with electroless plating time.

The AFM characterization was performed to study the variation in height and width of the grating after 60, 90, 120, 150 and 180 s of Cu deposition. The changes in grating parameters

such as height and width were calculated using the section profiles of each image an example of which can be seen in **Figure 2.5**. When the electroless deposition of Cu on Pd grating is carried out, Cu grains get homogeneously deposited on the patterned Pd nanowire. **Figure 2.5** shows AFM images of the surface changes that took place on Cu deposition over Pd nanowires with time. When the chosen Pd nanowire grating (shown in **Figure 2.2e**) is dipped in electroless plating bath for 60 s, deposition of copper takes place evenly all over Pd NW grating (**Figure 2.5a**). The height of grating increased by 15 ± 5 nm on depositing Cu for 90 s (**Figure 2.5b**). On further dipping into electroless plating bath, the Cu particles starts growing bigger in size and average height of the grating became 121 ± 10 nm at 120 s of Cu deposition (**Figure 2.5c**). When electroless deposition process is carried out beyond 180 s (**Figure 2.5d**), there was a dramatic increase in grating surface roughness making further AFM characterization difficult.

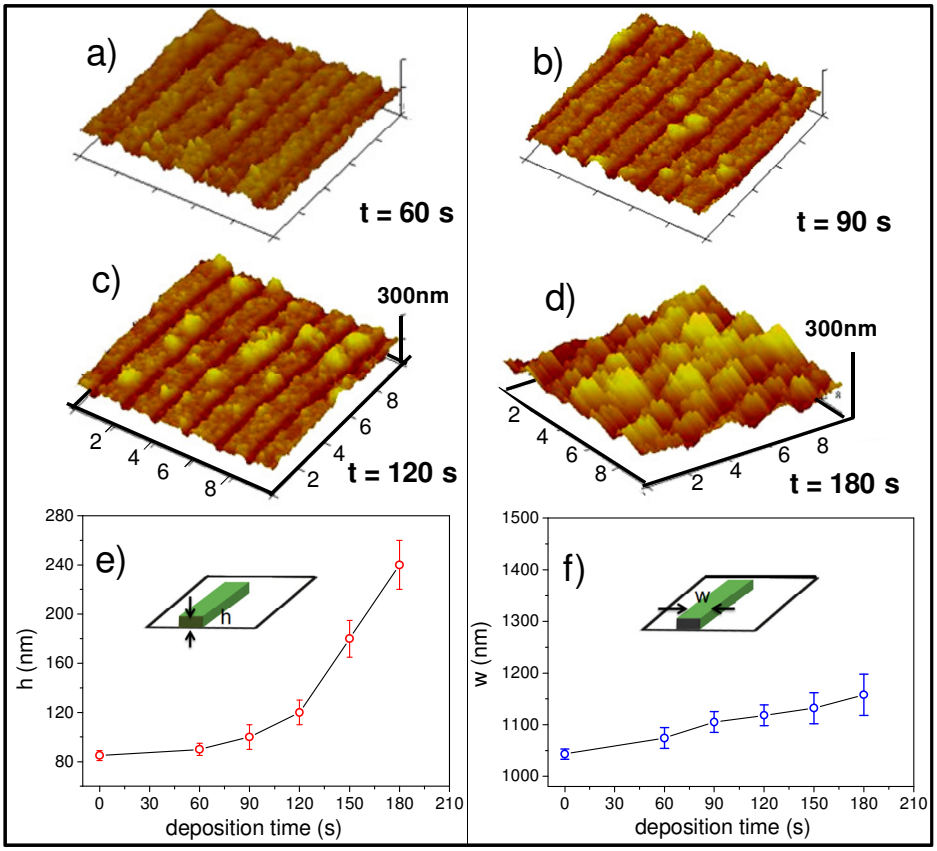

Figure 2.5 (a)-(d) AFM images of Pd nanowire gratings after dipping in Cu plating solution for varying time intervals of (a) 60 s (b) 90 s (c) 120 s and (d) 180 s. Variations in (e) height and (f) width of the nanowire grating with Cu deposition time

The surface roughness values were determined in terms of R_q by calculating the average from 7 different areas over the stripe region of pattern (from 10 µm x 10 µm) of AFM image. The surface roughness before Cu deposition and after 120 s of Cu deposition changed from 14.5 ± 2.9 nm to 60.3 ± 3.4 nm. The height of grating increases rapidly (**Figure 2.5e**) but the grating width has small effect due to Cu deposition for 120 s but beyond that the grating width changes considerably as shown in **Figure 2.5f.** The error for the grating height and width was determined as standard deviations of all the measurements calculated by average cross-section analysis from different areas of sample.

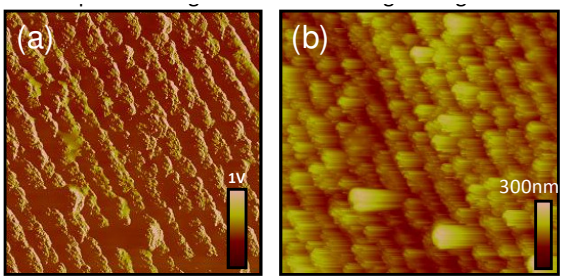

Figure 2.6 (a) Amplitude image and (b) height image corresponding to Pd with Cu deposited for 180 s.

Even after 180 s of Cu deposition, the grating features were somewhat preserved as seen in amplitude AFM image **Figure 2.6**. However, the surface roughness of the grating becomes so high (~ 350 nm), leading to diffused diffraction spots. The deposition of Cu for 210 s showed no visible diffraction pattern because of fusion of lines along with lower degree of adhesion of nanowires to the glass substrate.

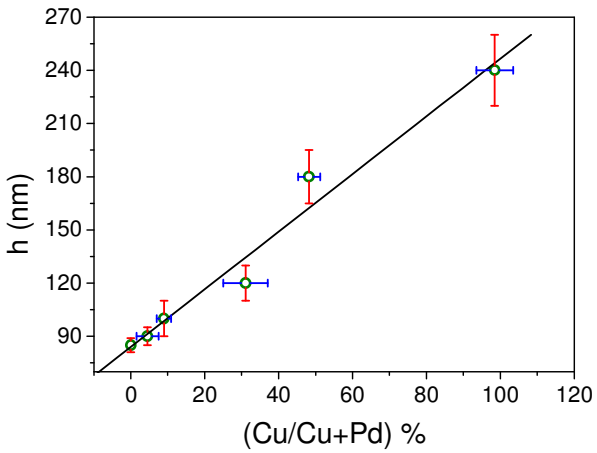

Figure 2.7 Variations in the grating height with atom percentage of Cu deposited on Pd nanowire gratings

The height of the grating as measured from AFM can be directly correlated to the amount of Cu deposited can be seen in **Figure 2.7.** It is observed that the height of grating increases proportionally with the increasing amount of Cu deposition upto 180 s (~ 50%). The intensity of light diffracted from gratings is influenced both by the height of grating which in turn depends on the amount of Cu deposition. The changes in diffraction efficiency is quite sharp as seen from **Figure 2.8a** at lower amounts of Cu deposition which proves the sensitivity of this technique employed. The variation in height of Pd nanowire grating on Cu deposition directly influences the diffraction efficiency. It has been found that with 8 nm increase in height on Cu deposition, the diffraction efficiency increases by 16.4% from initial diffraction of 10.2% with no Cu deposition (**Figure 2.8b**).

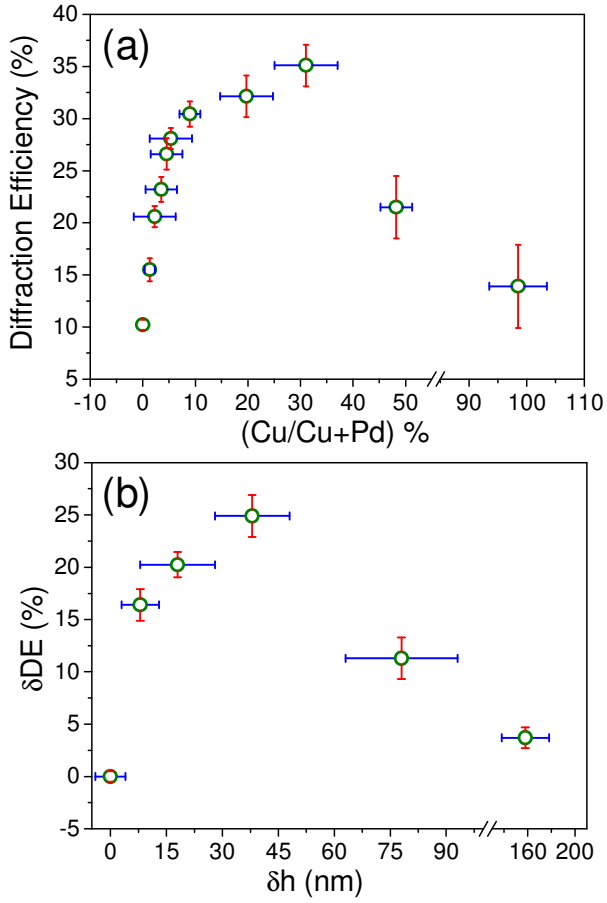

Figure 2.8 (a) Variation in the diffraction efficiency (DE) calculated from the measured intensities of diffraction spots with atom percentage of Cu on Pd nanowire grating and (b) changes in DE with increasing height of the grating.

2.5 Conclusions

The diffraction grating showed a 16% increase in the diffraction efficiency with 8 nm increase in grating height on Cu deposition over Pd NW gratings. This is in close agreement to the similar results in the literature.[16] The results obtained through the model study of Cu deposition on Pd NW affirms that optical diffraction based detection system is sensitive and one of the simplest sensing technique. It is already known to be responsive to biological interactions and chemical species but along with that it is found to be potential to compete with other known analytical techniques where sensitivity of detection is limited. Importantly, the gratings used in this study have been fabricated on a transparent substrate in a single step using a micromolding method.

Free standing Cu-Pd µ-ribbons*

The seed mediated growth of metal nanostructures on different kinds of surfaces such as glass, ITO, glassy carbon etc. has been well studied in the literature.[27,28] In this context, Pd is widely employed as a catalyst for electroless metallization of different metals such as Cu, Ni, Ag, Au etc. The electroless plating of Cu can be carried out very easily on any kind of surface by using Pd as seeds/catalyst. It involves an autocatalytic redox reaction in which metal salt such as $CuSO_4$ gets reduced at the surface of Pd as catalyst.[29,30]

Palladium is patterned on glass substrate by micromolding using soft lithography as explained in **Section 2.2**. But, the only difference in this case is that the Pd thiolate precursor was injected through the PDMS stamp in little excess such that it leaked inside the relief regions where PDMS makes conformal contact with the substrate. The substrate was heated slowly upto 250 ºC at a temperature ramp of 5 ºC per 10 min, followed by annealing at room temperature. The PDMS stamp was removed gently from the top and the patterned substrate was obtained. The surface was characterized by AFM and SEM imaging.

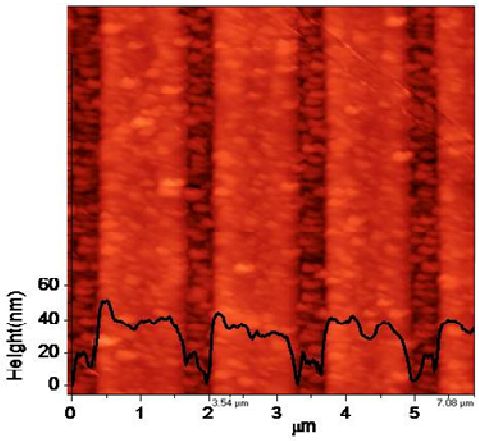

Figure 2.9 AFM image of the Pd patterned surface. The profile shows the height of ridge which is 40 ±5 nm and land 20 ±2 nm

*This part of the work has been submitted as a manuscript for the special issue of J. Nanosci. Nanotech., (INEC 2010).

The AFM image in **Figure 2.9** shows the Pd nanoparticles of the order of 20 nm size being formed in the 500 nm wide gaps. These nanoparticles also offer an active surface for Cu deposition.

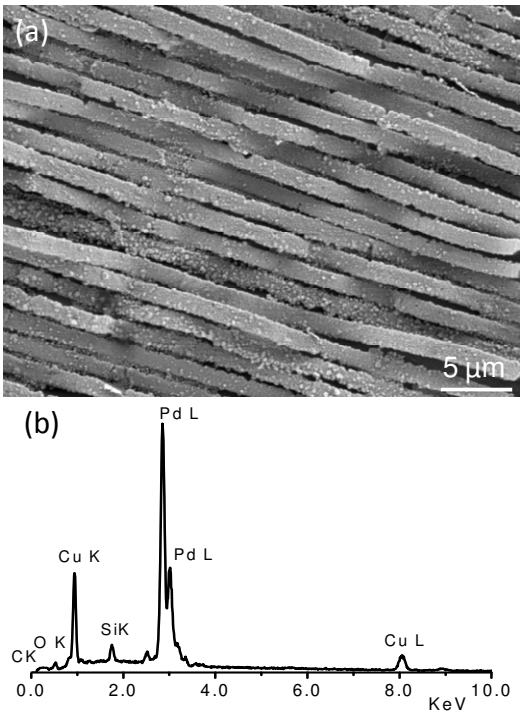

Figure 2.10 (a) SEM image of Cu-Pd ribbons which got delaminated from the surface; floating Cu-Pd ribbons were transferred onto a glass substrate for imaging. (b) EDS from the stripes showing the presence of Cu and Pd.

When electroless deposition of Cu is carried out with successively increasing time intervals, it was observed that the Pd lines with 1µm width got lifted off from the surface and float to the top of the solution. This may happen because of interplay between the force of adhesion of Cu-Pd layer to the surface and the internal stress of deposited Cu layer over Pd. When the thickness of deposited Cu increases, there comes a stage when the internal stress exceeds the adhesion force between the Pd stripe and the substrate, and Cu-Pd layer gets removed from the glass substrate.

In summary, free standing Cu-Pd stripes or µ-ribbons were produced by electrolessly depositing Cu on Pd patterned on glass.

References

1. Sarov, Y. E.; Capek, I.; Ivanov, T. B.; Ivanova, K. Z.; Sarova, V. A.; Rangelow, I. W., On Total Internal Reflection Investigation of Nanoparticles by Integrated Micro-Fluidic System. *Nano Lett.* **2007**, 8, 375-381.

2. Morhard, F.; Pipper, J.; Dahint, R.; Grunze, M., Immobilization of antibodies in micropatterns for cell detection by optical diffraction. *Sens. Actuators, B* **2000**, 70, 232-242.

3. Tsay, Y. G.; Lin, C. I.; Lee, J.; Gustafson, E. K.; Appelqvist, R.; Magginetti, P.; Norton, R.; Teng, N.; Charlton, D., Optical biosensor assay (OBA). *Clin. Chem.* **1991**, 37, 1502-1505.

4. St. John, P. M.; Davis, R.; Cady, N.; Czajka, J.; Batt, C. A.; Craighead, H. G., Diffraction-Based Cell Detection Using a Microcontact Printed Antibody Grating. *Anal. Chem.* **1998**, 70, 1108-1111.

5. Goh, J. B.; Loo, R. W.; McAloney, R. A.; Goh, M. C., Diffraction-based assay for detecting multiple analytes. *Anal. Bioanal. Chem.* **2002**, 374, 54-56.

6. Bailey, R. C.; Hupp, J. T., Micropatterned Polymeric Gratings as Chemoresponsive Volatile Organic Compound Sensors: Implications for Analyte Detection and Identification via Diffraction-Based Sensor Arrays. *Anal. Chem.* **2003**, 75, 2392-2398.

7. Massari, A. M.; Stevenson, K. J.; Hupp, J. T., Development and application of patterned conducting polymer thin films as chemoresponsive and electrochemically responsive optical diffraction gratings. *J. Electroanal. Chem.* **2001**, 500, 185-191.

8. Bailey, R. C.; Nam, J.-M.; Mirkin, C. A.; Hupp, J. T., Real-Time Multicolor DNA Detection with Chemoresponsive Diffraction Gratings and Nanoparticle Probes. *J. Am. Chem. Soc.* **2003**, 125, 13541-13547.

9. Goh, J. B.; Loo, R. W.; Goh, M. C., Label-free monitoring of multiple biomolecular binding interactions in real-time with diffraction-based sensing. *Sens. Actuators, B* **2005**, 106, 243-248.

10. Chang, C. L.; Acharya, G.; Savran, C. A., In situ assembled diffraction grating for biomolecular detection. *App. Phys. Lett.* **2007**, 90, 233901

11. Savran, C. A.; Low, P. S.; Henne, W. A.; Dooreweerd, D.; Lee, J. In Detection of cancer markers via nanoparticle-based mass enhancement,*Proc Annu. Conf. Expo. Exp. App. Mech.* **2006**, 1849-1856.

12. Acharya, G.; Chang, C. L.; Doorneweerd, D. D.; Vlashi, E.; Henne, W. A.; Hartmann, L. C.; Low, P. S.; Savran, C. A., Immunomagnetic diffractometry for detection of diagnostic serum markers. *J. Am. Chem. Soc.* **2007**, 129, 15824-15829.

13. Acharya, G.; Doorneweerd, D. D.; Chang, C. L.; Henne, W. A.; Low, P. S.; Savran, C. A., Label-free optical detection of anthrax-causing spores. *J. Am. Chem. Soc.* **2007**, 129, 732-733.

14. Acharya, G.; Chang, C. L.; Holland, D. P.; Thompson, D. H.; Savran, C. A., Rapid detection of S-adenosyl homocysteine using self-assembled optical diffraction gratings. *Angew. Chem. Int. Edit.* **2008**, 47, 1051-1053.

15. Halpern, A. R.; Nishi, N.; Wen, J.; Yang, F.; Xiang, C.; Penner, R. M.; Corn, R. M., Characterization of Electrodeposited Gold and Palladium Nanowire Gratings with Optical Diffraction Measurements. *Anal. Chem.* **2009**, 81, 5585-5592.

16. Shallcross, R. C.; Chawla, G. S.; Marikkar, F. S.; Tolbert, S.; Pyun, J.; Armstrong, N. R., Efficient CdSe Nanocrystal Diffraction Gratings Prepared by Microcontact Molding. *ACS Nano* **2009**, 3, 3629-3637.

17. Nakajima, F.; Hirakawa, Y.; Kaneta, T.; Imasaka, T., Diffractive optical chemical sensor based on light absorption. *Anal. Chem.* **1999**, 71, 2262-2265.

18. Varma, M. M.; Inerowicz, H. D.; Regnier, F. E.; Nolte, D. D., High-speed label-free detection by spinning-disk micro-interferometry. *Biosens. Bioelect.* **2004**, 19, 1371-1376.

19. Varma, M. M.; Nolte, D. D.; Inerowicz, H. D.; Regnier, F. E., Spinning-disk self-referencing interferometry of antigen-antibody recognition. *Opt. Lett.* **2004**, 29, (9), 950-952.

20. Xiaoqiang, C.; Keiko, T.; Kenji, K.; Junji, N., Enhanced Fluorescence Microscopic Imaging by Plasmonic Nanostructures: From a 1D Grating to a 2D Nanohole Array. *Adv. Func. Mater.*, **2010**, 20, 945-950

21. Xia, Y.; Whitesides, G. M., Soft lithography. *Annu. Rev. Mater. Sci.* **1998**, 28, 153-184.

22. Kane, R. S.; Takayama, S.; Ostuni, E.; Ingber, D. E.; Whitesides, G. M., Patterning proteins and cells using soft lithography. *Biomaterials,* **1999**, 20, 2363-2376.

23. Kang, M. G.; Kim, M. S.; Kim, J. S.; Guo, L. J., Organic Solar Cells Using Nanoimprinted Transparent Metal Electrodes. *Adv. Mater.,* **2008**, 20, 4408-4413.

24. Boya, R.; Giridhar, U. K., A Modified Micromolding Method for Sub-100-nm Direct Patterning of Pd Nanowires. *Small* **2009**, 5, (20), 2271-2275.

25. Bhuvana, T.; Kulkarni, G. U., Highly Conducting Patterned Pd Nanowires by Direct-Write Electron Beam Lithography. *ACS Nano* **2008**, 2, 457-462.

26. Hidber, P. C.; Helbig, W.; Kim, E.; Whitesides, G. M., Microcontact printing of palladium colloids: Micron-scale patterning by electroless deposition of copper. *Langmuir* **1996**, 12, 1375-1380.

27.Li, Y.; Chen, D.; Lu, Q.; Qian, X.; Zhu, Z.; Yin, J., Selective electroless deposition of copper on polyimide surface by microcontact printing. *App. Surf. Sci.* **2005**, 241, 471-476.
28.Wu, Z.; Ge, S.; Zhang, M.; Li, W.; Tao, K., Synthesis of nickel nanoparticles supported on metal oxides using electroless plating: Controlling the dispersion and size of nickel nanoparticles. *J. Colloid Inter. Sci.* **2009**, 330, 359-366.
29.Hidber, P. C.; Helbig, W.; Kim, E.; Whitesides, G. M., Microcontact Printing of Palladium Colloids: Micron-Scale Patterning by Electroless Deposition of Copper. *Langmuir* **1996**, 12, 1375-1380.
30.Kind, H.; Geissler, M.; Schmid, H.; Michel, B.; Kern, K.; Delamarche, E., Patterned Electroless Deposition of Copper by Microcontact Printing Palladium(II) Complexes on Titanium-Covered Surfaces. *Langmuir* **2000**, 16, 6367-6373.